REAL-VALUED COMPOSITE FILTERS FOR CORRELATION-BASED OPTICAL PATTERN RECOGNITION

Final Report
Contract No. NAG9-521

Submitted to

Lyndon B. Johnson Space Center
National Aeronautics and Space Administration
Houston, Texas

By

Dr. P. K. Rajan
and
Anushia Balendra

Center for Manufacturing Research
and
Technology Utilization
Tennessee Technological University
Cookeville, TN 38505

May 1992

ACKNOWLEDGEMENTS

The authors would like to express their appreciation to Dr. Richard D. Juday of NASA Johnson Space Center and Dr. Stanley E. Monroe, Jr., of Lockheed Engineering and Sciences Corporation for their consultations and advice given during the project.

The authors would like to thank the Lyndon B. Johnson Space Center, National Aeronautical and Space Administration (NASA), Houston, Texas for funding the research contract No. NAG9-521. The authors would also like to thank the Center for Manufacturing Research and Technology Utilization of Tennessee Technological University and the Department of Electrical Engineering, Tennessee Technological University for supporting this research.

This report was extracted with minor revisions from the thesis for M.S. degree in Electrical Engineering submitted Anushia Balendra to the Graduate School of Tennessee Technological University, comprising the research carried out under the supervision of Dr. P. K. Rajan.

ABSTRACT

Advances in the technology of optical devices such as spatial light modulators (SLMs) have influenced the research and growth of optical pattern recognition. In the research leading to this report, the design of real-valued composite filters that can be implemented using currently available SLMs for optical pattern recognition and classification was investigated.

The design of real-valued minimum average correlation energy (RMACE) filter was investigated. Proper selection of the phase of the output response was shown to reduce the correlation energy. The performance of the filter was evaluated using computer simulations and compared with the complex filters. It was found that the performance degraded only slightly.

Continuing the above investigation, the design of a real filter that minimizes the output correlation energy and the output variance due to noise was developed. Simulation studies showed that this filter had better tolerance to distortion and noise compared to that of the RMACE filter.

Finally, the space domain design of RMACE filter was developed and implemented on the computer. It was found that the sharpness of the correlation peak was slightly reduced but the filter design was more computationally efficient than the complex filter.

TABLE OF CONTENTS

Chapter Page

Chapter Page

LIST OF TABLES

Table Page

LIST OF FIGURES

Figure Page

CHAPTER 1

Introduction

Optical processors are attractive for many image processing applications such as machine vision systems. Because of their high speed, intrinsic real time parallel processing capacity, and high throughput rate, several signal processing operations such as Fourier Transform (FT), convolution, correlation, and spectral analysis, can be carried out using optical techniques more efficiently than with their electronic counterparts [1].

However, using only optical processors, it is still difficult to perform arithmetic computations and logic operations and extract information and obtain the interpretation of the data. So, for applications where real-time operations are necessary, a hybrid optical-digital system which makes use of the high speed operation of optics and the flexibility of digital computers would be ideal. Also, hybrid optical-digital systems give the optical system an increased flexibility by allowing the use of more sophisticated software algorithms. In such architectures, the digital computers are used to address the optical systems and give data and image features of various formats. Thus, the proper combinations of optical system operations and digital algorithms promise

practical systems for general applications in robotics and computer vision [2].

Optical processing can be broadly classified into two areas [3]: Optical signal processing and Optical image processing. In optical signal processing systems the signals are often one-dimensional quantitative data: range, velocity, acceleration, and so on, whereas in optical image processing systems the outputs are two-dimensional functions. Operations like FT and correlation are used in both signal and image processing systems. Applications in the first area include speech processing, biomedical signal processing, radar, and sonar [3]. Military and space vision systems are the applications in the optical image processing. This research is concerned with the development of algorithms for optical image processing in the field of pattern or object recognition. First, some basic principles of optical pattern recognition will briefly be reviewed.

1.1. Optical Pattern Recognition

Pattern recognition is the identification of a given pattern or an object, frequently visual data within a mass of extraneous signals/patterns. Considerable research has gone into developing optical pattern recognition (OPR) systems for military applications like identification of a target such as a tank in a terrain, guidance of missile systems, and reconnaissance [2]. Also, some limited success has been achieved in developing systems for commercial applications

such as autonomous robots, product inspection, computer vision, and automatic analysis of areal photographs [3].

As mentioned before, the most flexible type of OPR system combines optical devices and digital electronic computers into an optical-digital hybrid system. A general optical-digital architecture that includes digital preprocessing and postprocessing is shown in Figure 1.1. The electronic preprocessor operates on the input objects and produces filters that are used in the subsequent optical processing system. The optical system performs the correlation operation and the correlation plane output is processed by the digital postprocessor to recognize the presence of the reference object and determine its location in the scene.

There exists extensive literature describing many different automated pattern recognition techniques. Almost all of them fall into two broad categories: feature-based methods and correlation-based methods [4]. Optical feature extraction to pattern recognition is unique since it represents a fixed optical system, with no variable filters that can compute the features of any input object. The optical feature extractors compute certain properties of an input object, which are subsequently processed upon to determine the class of the input object. Feature extractors also provide the ability to determine the object's location, orientation, and scale [4]. Feature-based matching techniques

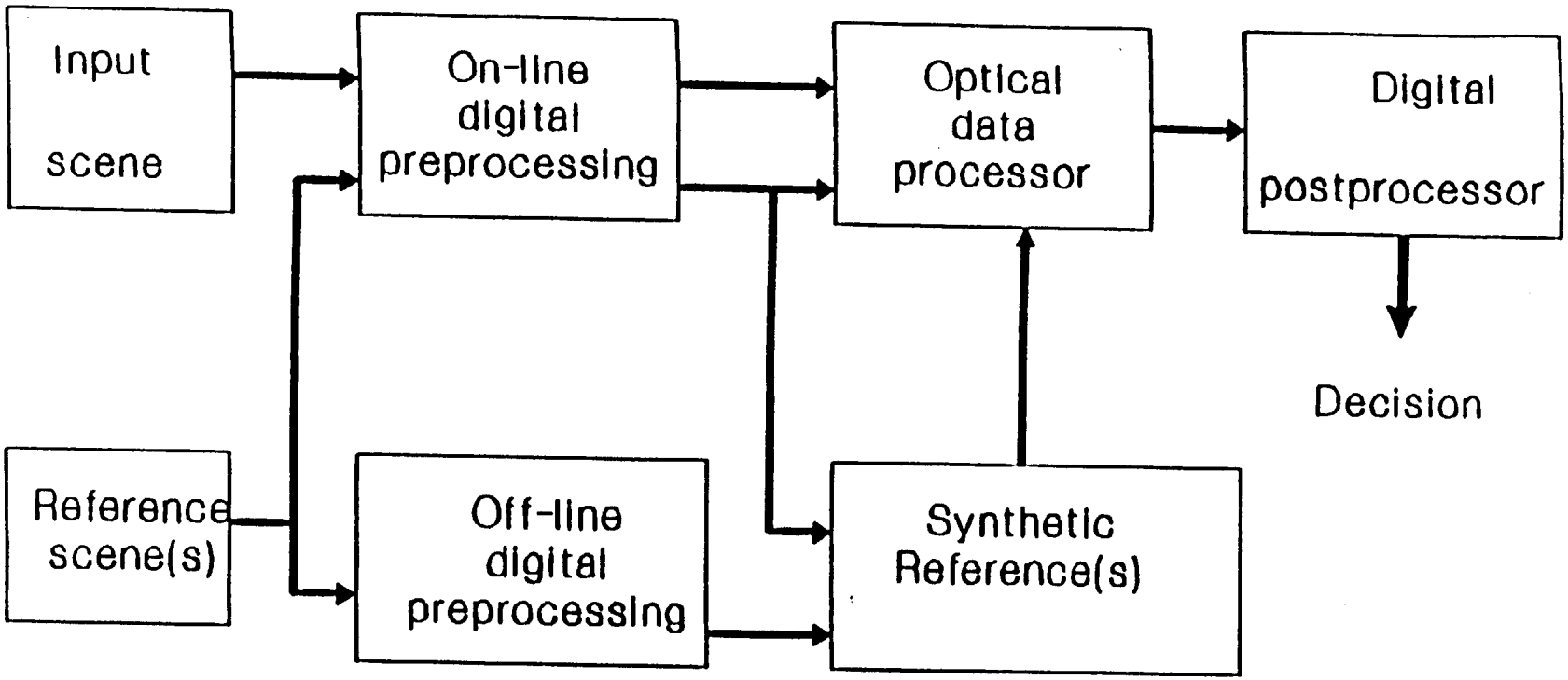

Figure 1.1. A Hybrid Optical-Digital System [2]

include various edge detection schemes and methods using artificial intelligence principles.

However, these feature extractors are susceptible to noise and also require segmentation before they can be effectively used. Hence, as an alternative to feature extraction, correlation-based pattern recognition techniques have been developed [5].

In the correlation-based algorithms the brightness data of the input object is directly compared with the brightness data of a library of objects for recognition. The invention of the holographic matched filter by VanderLugt [6] to perform optical correlation can be called a milestone in optical information processing. Also, the correlator represents a quite powerful pattern recognition processor possessing such desirable features as a large processing gain, the shift-invariance, and the ability to handle multiple objects simultaneously. This research is concerned with the design of correlation-based pattern recognition processors.

1.2. Need for the Study

During the last few years many efforts have been made to improve the correlation techniques to gain higher flexibility, less sensitivity to object modifications, better signal discrimination, and higher light efficiency. A correlation filter must possess the following characteristics:

1. It must reject the noise in the input.

2. It must produce sharp correlation peaks when the target is present so that the target in the scene can be recognized.
3. It must provide object orientation information.
4. It must be able to provide distortion-invariant pattern classification.
5. Of course, ease of implementation would also be desirable. Unfortunately, no single filter can provide all the above.

Optical correlators such as matched spatial filters (MSF) are extremely efficient in the sense that they provide the maximum output signal-to-noise ratio (SNR) in detecting a known reference signal in additive noise [6]. However, MSFs for optical pattern recognition have three major limitations:

- Geometrical differences between the input and reference objects degrade the performance of MSFs.
- MSFs are light-inefficient. That is, the ratio of the output light power to input light power is only about 44 percent [7].
- Most available spatial light modulators (SLM) cannot accommodate the complex frequency response of MSFs.

Light efficiency can be improved by using phase-only filters (POF) since the frequency plane filter will then pass all the incident light [8]. Real-time SLMs such as the magneto-optic SLM (MOSLM) can be employed in the filter plane, if the filters are binary phase-only filters (BPOF).

The emphasis of this study is, however, designing filters which are capable of providing distortion-invariant pattern recognition. Several methods have been suggested to introduce distortion tolerance in the optical correlators. These include mutually orthogonal correlation filters [9], Synthetic Discriminant Functions (SDF) [10]-[11], least square linear mapping techniques [12], and circular harmonic function-based filters [13].

The SDF, which is designed using a set of training images that span the distortion space of interest, achieves the distortion-invariance while retaining the process gain and the shift-invariance property of the correlator [11]. For each training image, the SDF filter is constrained to yield a user specified value at the origin of the correlation plane. Then the image to be classified is correlated with the filter, and the output correlation value at the origin of the two-dimensional correlation image is compared to the reference thresholds to classify the input image.

Traditionally, a SDF is designed from a linear combination of input training images with weights appropriately selected to satisfy the specified correlation values at the origin. Even though, this filter achieves distortion-invariance and shift-invariance, it cannot prevent large sidelobe levels from occurring in the correlation plane. Also, the design of these filters does not include the effects

of noise explicitly and hence, they often have poor noise performance.

In the recent past, several variations to SDFs have been proposed. Two among them have received considerable notice: the minimum variance synthetic discriminant function (MVSDF) [14] and minimum average correlation energy (MACE) filters [15]. The MVSDF is designed to minimize the effect of noise in the input on the output variance while the MACE filter is designed to minimize the average energy of the output correlation plane to yield a sharp correlation peak. Also, the design of MACE filter for the implementation in space domain (SMACE filter) has recently been reported [16].

One difficulty at present with the MACE, SMACE, and MVSDF filters is that they are complex in general, and hence, these filters cannot be easily implemented in the currently available SLMs. Purely real filters can overcome these problems associated with the optical implementation [17]. The design of a purely real MACE filter in the discrete frequency domain has recently been proposed [18]. However, in this method, the input objects and the output response are assumed to be real. Also, the properties of the real-valued filters, and the performance of these filters in noisy scene have not been studied.

The MACE filter which is designed to minimize the average correlation plane energy does not take the effect of noise into account [15]. The problem of noise has been addressed in

the design of MVSDF [14]; however, a sharp correlation peak is not guaranteed in this approach. An improved filter in the space domain which trades off between the noise performance and sharp correlation peak to facilitate the ease of detection has been reported [16]. No studies have so far been carried out on the real-valued frequency domain improved filters.

1.3. Objectives

In light of the above, the main objective of the research reported was to develop and study the real-valued composite filters for optical pattern recognition. More specifically, this research had the following objectives:

1. To develop a real-valued MACE filter in the discrete frequency domain and to evaluate its performance characteristics. The effect of additive noise on the performance of the filter were studied.
2. To develop a real MACE filter with a complex output constraint to reduce further the correlation plane energy.
3. To develop a real-valued MVSDF-MACE filter in the discrete frequency domain to produce a sharp correlation peak with a better noise performance than the MACE filter.
4. To develop a space domain real MACE filter and to study its performance.

The scope of this research was limited to the development of correlation-based composite filters. The purely real-

valued MACE filters were to be developed in both the discrete frequency and space domains. The performance was to be evaluated by using simulations on a digital computer. The signals used were restricted to be real ones. The performance of these filters were to be compared with that of the existing complex filters. Also, a study on the effect of additive stationary white, Gaussian noise on the performance of the filters was to be conducted. The actual optical implementation of these filters was not carried out.

1.4. Outline of the Report

The next chapter presents a brief historical background of the current state of research in this field and a general description of the algorithms being presently used. Chapter 3 discusses the development of the real-valued MACE filter. Also, Chapter 3 shows how the specification of complex output in the real-valued MACE filter can decrease the correlation plane energy. A comparison of this filter with the original complex MACE filter is also included. Chapter 4 presents the development and simulation studies of the real-valued MVSDF-MACE filter in the frequency domain. Finally, an alternative space domain methodology for designing real MACE filters is proposed and its performance studied in Chapter 5. Chapter 6 presents the conclusions of this research and recommendations for future work.

CHAPTER 2

Historical Background

As mentioned in Chapter 1, image processing is a major area of research in the field of optical information processing. It is an important technology with many potential applications in many systems such as space robotics, landmark identification, and missile guidance systems. Pattern recognition using optical techniques offer faster speed as compared with its electronic counterparts because of the massive parallelism of optics. Several methods of optical pattern recognition have been proposed in the past [2, 18-20]. In this chapter a brief review of previous works on correlation-based methods for pattern recognition is presented. First, the basic principles of an optical correlator will be discussed.

2.1. Optical Correlator

The realization of correlators using an optical system is well documented in Reference [21]. Many other optical information processing operations such as convolution can be interpreted as correlation. Correlation of two input functions $\bar{f}_1(x,y)$ and $\bar{f}_2(x,y)$ is given by

$$\overline{f_1}(x,y) \otimes \overline{f_2}(x,y) = \int\int \overline{f_1}(x',y')\ \overline{f_2^*}(x'-x,y'-y)\ dx'dy' \quad (2.1)$$

where the symbol $\otimes$ denotes the correlation operation and '*' denotes the conjugate operation and the limits of integration extend the whole of x'-y' plane. The overbar notation as $\bar{f}(x,y)$ is used for two-dimensional functions so that symbols without bar can be used later for one-dimensional functions and vectors. If the input functions are identical, then the operation is called auto-correlation. The Fourier transform (FT) of the correlation of two functions is the product of their transforms (the symbol F{} denotes the Fourier transform operation):

$$F\{\overline{f_1}(x,y) \otimes \overline{f_2}(x,y)\} = \overline{F_1}(u,v)\ \overline{F_2^*}(u,v) \quad (2.2)$$

where

$$\begin{aligned} \overline{F_1}(u,v) &= F\{\overline{f_1}(x,y)\} \\ \overline{F_2}(u,v) &= F\{\overline{f_2}(x,y)\} \end{aligned} \quad (2.3)$$

and

$$F\{\overline{f_1}(x,y) \otimes \overline{f_1}(x,y)\} = |\overline{F_1}(u,v)|^2. \quad (2.4)$$

For recognition applications usually either the correlation peak or the correlation value at (x = 0, y = 0) is measured. In this case the important fact to note is that the peak intensity of the normalized auto-correlation of a function is always higher than or equal to its normalized cross-correlation with any other function [4]. That is,

$$\frac{|\iint \overline{f_1}(x,y)\,\overline{f_1^*}(x,y)\,dxdy|^2}{\iint |\overline{f_1}(x,y)|^2\,dxdy} \geq \frac{|\iint \overline{f_2}(x,y)\,\overline{f_1^*}(x,y)\,dxdy|^2}{\iint |\overline{f_2}(x,y)^2|\,dxdy} . \quad (2.5)$$

Therefore in an optical correlation system the measured peak intensity can be directly used to recognize a specific input object.

In general, the implementation methods for the correlation operation may be classified into two categories [3]: processing in object space and processing in Fourier space. The object space version is shown in Figure 2.1. This scheme has many practical advantages due to the fact that the necessary filter masks or transparencies are directly given by the input and reference objects. However, the multiplication operation required in this scheme makes this very slow and impractical for many real time applications. Implementation by processing in Fourier space is based on Eq. (2.2). The ability of lenses to generate Fourier Transform (FT) of two-dimensional data at the speed of light allows for very compact optical correlation systems. Figure 2.2 shows the correlation operation in Fourier space.

The concept of coherent optical correlation using a matched spatial filter (MSF) also known as conjugate filter was first introduced by VanderLugt [6]. Mathematically, correlation and matched filtering under the assumption of white noise equivalent operations. Although matched filtering is the optimum detection scheme only for white noise, its

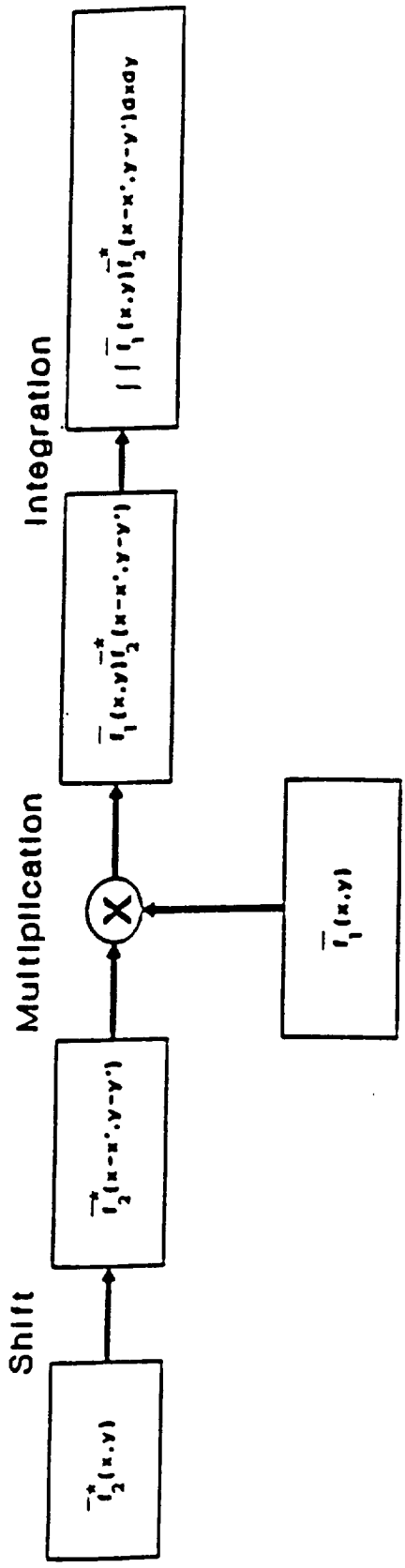

Figure 2.1. Basic Correlation Operation in Object Space

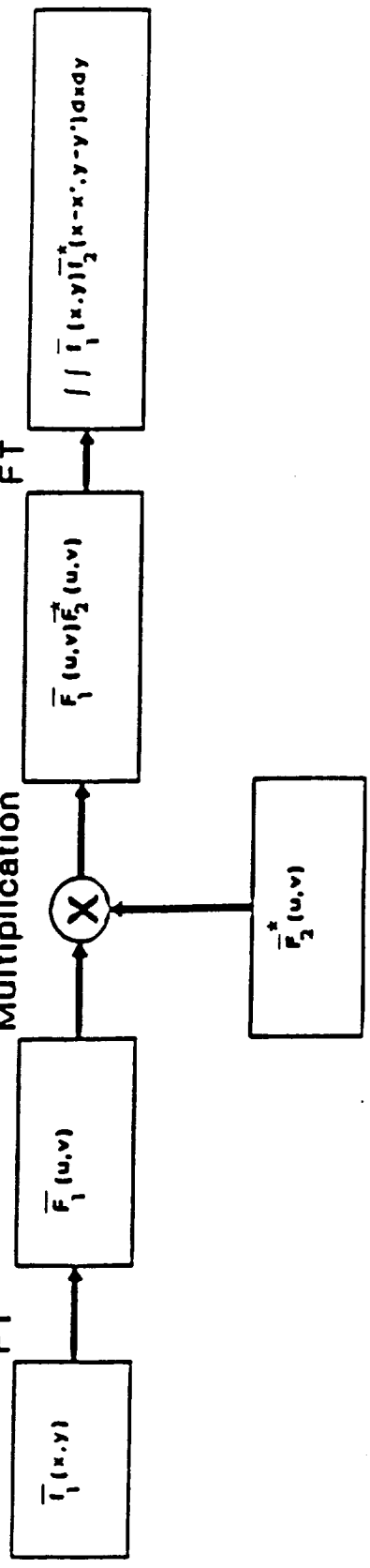

Figure 2.2. Basic Correlation Operation in Fourier Space

performance is quite acceptable when the background is a practical structural clutter or colored noise [22].

A classical optical correlation system for spatial filtering is shown in Figure 2.3. This system works as follows. The image of a test object $\bar{f}_1(x,y)$ is placed in plane P_1 in the form of a transparency and is illuminated by a plane wave of coherent light. The diffraction pattern formed is focused by a spherical lens L_1 which is placed at a distance f_L, equal to the focal length of the lens L_1, from the image plane. Lens L_1 produces the two-dimensional spatial FT of the pattern $\bar{f}_1(x,y)$ on plane P_2. Thus the light incident on plane P_2 is $\bar{F}_1(u,v)$. A transparency containing the optical filter $\bar{H}(u,v) = \bar{F}_2^*(u,v)$ produced from the reference object or pattern $\bar{f}_2(x,y)$ is positioned in the plane P_2. The interaction between the filter and FT of the input pattern produces the product of the two transforms. Thus, the light distribution leaving P_2 is $\bar{F}_1(u,v)\bar{F}_2^*(u,v)$. Finally, a second lens L_2 produces the inverse FT of the product yielding the correlation function onto the output plane P_3. $\bar{c}(x,y)$, the output in plane P_3, is given by

$$\begin{aligned} \bar{c}(x,y) &= \iint \bar{F}_1(u,v)\, \bar{F}_2^*(u,v) \exp\left[j2\pi\,(ux+vy)\right] du\,dv \\ &= \bar{f}_1(x,y) \otimes \bar{f}_2(x,y) \end{aligned} \tag{2.6}$$

where '$\otimes$' denotes the correlation operation. The spatial frequencies (u,v) of the input object are related to the distance in P_2 by:

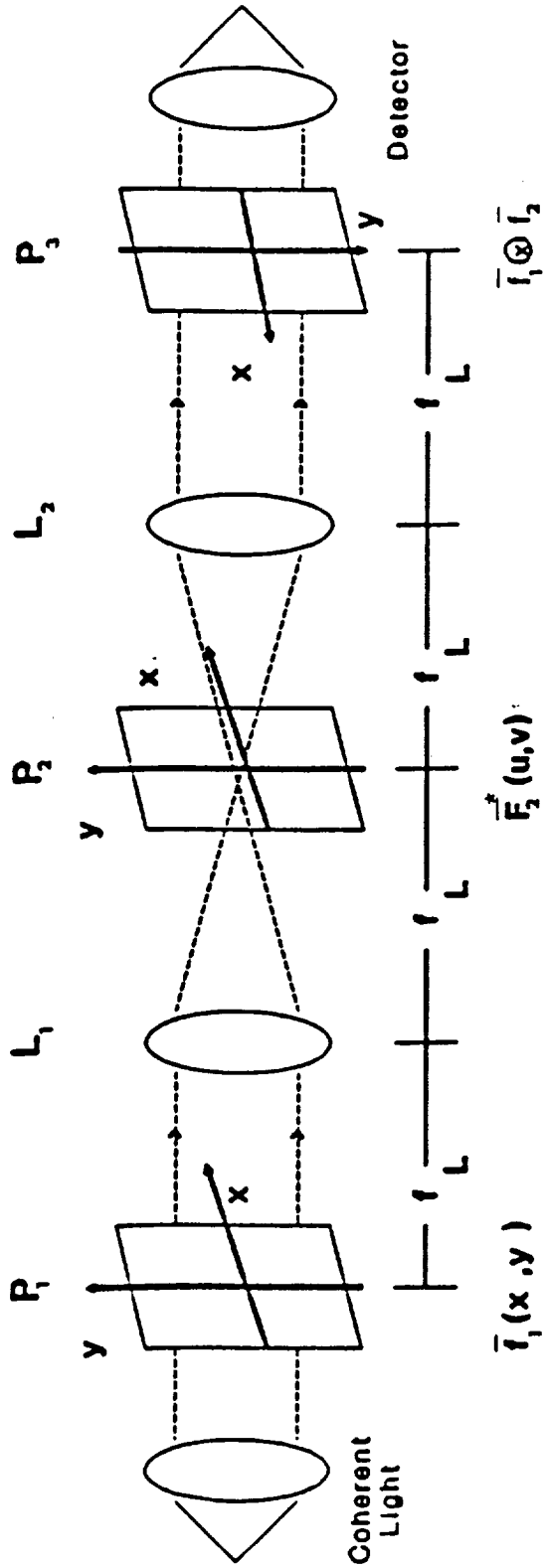

Figure 2.3. A Conventional Frequency Plane Correlator

$$(u,v) = \left(\frac{x}{\lambda f_L}, \frac{y}{\lambda f_L}\right) \qquad (2.7)$$

where λ is the wave length of the input light and f_L is the focal length of the lens. This system is called a frequency plane correlator or Fourier plane correlator because the correlation function is performed by the multiplication in the frequency plane. Hence, the matched filter represents exactly the function required to obtain the correlation by spatial filtering.

2.2. Correlation-Based Filters

As mentioned earlier, a common application of the correlation operation is in the recognition of objects in the input scene using a matched spatial filter (MSF). The MSF is given by

$$\bar{H}(u,v) = \overline{X^*}(u,v) \qquad (2.8)$$

where $\bar{H}(u,v)$ is the filter function and $\bar{X}(u,v)$ is the reference signal function in Fourier space and '*' indicates the conjugate operation. The MSF yields the highest signal to noise ratio (SNR) at the output when detecting known objects corrupted by additive white noise [6]. However, for the MSF the light efficiency defined as the ratio of the output light power to the input light power is poor [7]. This is because the filter gain is not uniform for all frequencies and so

certain frequency components in the input image are attenuated resulting in low light efficiency.

A pure phase correlation filter can have a light efficiency of 100 percent in an optical correlation system. It is given by [8]:

$$\overline{H_{POF}}(u,v) = \frac{\overline{H}(u,v)^*}{|\overline{H}(u,v)|}. \qquad (2.9)$$

However, the performance of these filters degrade considerably when the test objects are subjected to distortions such as geometric transformations and sensor variations.

There are mainly two classes of spatial filters designed to recognize distorted patterns. The first class of filters deal with deterministic distortions like scale changes, rotation, and view angle differences. These distortions can be represented by mathematical techniques using circular harmonic functions [13] and 2-D image transformations [23-24]. Using these, distortion invariant filters can be designed.

Such is not the case with other distortions like out of plane rotation and sensor variations. For these situations, a new class of filters, known as synthetic discriminant functions (SDFs), has been proposed. The SDF is similar to averaged filters [10,25], generalized Matched filters [26,27], and composite filters [28,29]. The philosophy behind this approach is as follows: a single composite filter is designed to match one or more of the possible input objects and thus obtain a suitable correlation function at the system output.

The training set or the number of reference images required must be sufficiently descriptive to include all possible expected distortions. For recognition, each test object is correlated with the composite filter. If the peak output correlation exceeds the predetermined threshold value then the object is recognized in the input scene, thereby requiring only one cross correlation per input object.

Since the introduction of SDF in 1980, several variations have been reported. Later sections of this chapter will summarize some of them.

2.2.1. Conventional SDF [11]

This is a generalized method to achieve a multi-object, shift invariant, and distortion invariant pattern recognition using correlators. This technique uses a SDF to form the filter for use in the correlator. That is, a single filter is constructed from a linear combination of weighted filters that are matched to the different objects in the training set. In this section the method of constructing the conventional SDF is given.

Before discussing the method, a few words about the notations used in this report are given. All image signals as well as filter functions are assumed to be in discrete domain and are represented either by vectors or by scalar functions. Boldface letters are used to denote vectors and matrices and lower case letters denote scalar quantities.

Let $\mathbf{x}_1, \mathbf{x}_2, \ldots\ldots, \mathbf{x}_N$ denote N column vectors of dimension d representing N images, each with d pixels in it; that is, $\mathbf{x}_i = [x_i(1), x_i(2), \ldots\ldots x_i(d)]^T$ denotes the i^{th} training signal obtained from the i^{th} image by a lexicographical ordering of the rows of the image. Also, let $\mathbf{h} = [h(1), h(2), \ldots h(d)]^T$ represent the filter function.

The conventional SDF filter vector $\mathbf{h}$, which is a weighted linear combination of the training vectors is given by

$$\boldsymbol{h} = \sum_{i=1}^{N} a_i \boldsymbol{x}_i \qquad (2.10)$$

where the coefficients a_i's of the linear combination are chosen to satisfy the following deterministic constraints:

$$c_j(0) = u_j, \qquad j=1,2,\ldots\ldots,N \qquad (2.11)$$

where c_j is the vector representation of the output of the filter for the input image $\mathbf{x}_j$. The above can be rewritten as

$$\boldsymbol{h}^T \boldsymbol{x}_j = u_j, \qquad j=1,2,\ldots\ldots,N. \qquad (2.12)$$

The superscript 'T' denotes the transpose operation and u_j is the desired response of the filter at the origin for the training image x_j. As an example, when all training images belong to a single class, then all u_j values will be equal. On the other hand u_j will take two different values for a two class problem.

To determine the coefficients a_i's, Eq. (2.10) can be substituted into Eq. (2.12) as:

$$\sum_{i=1}^{N} a_i (\boldsymbol{x}_i^T \boldsymbol{x}_j) = u_j, \qquad j=1,2,.....,N. \qquad (2.13)$$

The vector inner product $\mathbf{x}_i^T\mathbf{x}_j$ is the cross correlation at zero shift between the i^{th} and j^{th} training images and is denoted by

$$R_{ij} = \boldsymbol{x}_i^T \boldsymbol{x}_j, \qquad i,j=1,2,.....,N. \qquad (2.14)$$

Then Eq. (2.13) can be expressed as:

$$\boldsymbol{R}\boldsymbol{a} = \boldsymbol{u} \qquad (2.15)$$

where $\mathbf{a} = [a_1,a_2,.....,a_N]^T$ is a (N×1) unknown coefficient vector and $\mathbf{u} = [u_1,u_2,.....,u_N]^T$ is the (N×1) output constraint vector. **R** is the (N×N) symmetric vector inner product (VIP) matrix with R_{ij} as its $(i,j)^{th}$ element. If the VIP matrix **R** is invertible, then vector '**a**' can be obtained as:

$$\boldsymbol{a} = \boldsymbol{R}^{-1}\boldsymbol{u}. \qquad (2.16)$$

It is necessary that **R** be a matrix of full rank for it to be invertible. **R** will be of full rank if and only if the original N training images $\mathbf{x}_1,\mathbf{x}_2,.....,\mathbf{x}_N$ form a linearly independent set of vectors [11].

Let $\mathbf{X}_s$ denote a matrix with d rows and N columns with its i^{th} column as $\mathbf{x}_i$: $\mathbf{X}_s = [\mathbf{x}_1,\mathbf{x}_2,....,\mathbf{x}_N]$. In terms of this space domain data matrix $\mathbf{X}_s$, the SDF composite vector **h** is given as:

$$\boldsymbol{h} = \boldsymbol{X}_s\boldsymbol{a} \qquad (2.17)$$

where the coefficient vector 'a' must satisfy

$$(X_s^T X_s)\, a = u. \qquad (2.18)$$

Substituting Eq. (2.18) into Eq. (2.17) the expression for the conventional SDF can be obtained as:

$$h = X_s (X_s^T X_s)^{-1} u. \qquad (2.19)$$

2.2.1.1. Intra-Class SDF The objective of an intra-class SDF is to select **h** such that it has the same correlation value at the origin with all N input training images. That is,

$$h = X_s (X_s^T X_s)^{-1} u \qquad (2.20)$$

where $\mathbf{u} = [c,c,\ldots,c]^T$, and c is a constant. Thus, the filter **h** in Eq. (2.20) is capable of recognizing objects of a particular class. It is also known as equal correlation peak (ECP) filter. The same idea can be extended for an inter-class pattern recognition problem.

2.2.1.2. Inter-Class SDF Consider an inter-class pattern recognition problem where M different objects belong to M different classes. So it is required to synthesize M different filters, $\mathbf{h}_1, \mathbf{h}_2, \ldots\ldots, \mathbf{h}_M$ such that

$$h_j^T x_i = c\,\delta_{ij}, \qquad i,j=1,2,\ldots\ldots,M. \qquad (2.21)$$

Thus for a particular input image only one of the M SDFs yields an output of c whereas all (M-1) other SDFs yield zero output. The filter with the output of c determines the class of the input object.

Each of the M SDFs can be described as a different weighted linear combination of all M training set images:

$$\begin{aligned} h_1 &= \sum_{i=1}^{M} a_{1i} x_i \\ h_2 &= \sum_{i=1}^{M} a_{2i} x_i, \ldots \end{aligned} \qquad (2.22)$$

By combining Eqs. (2.21) and (2.22), the following equations are obtained:

$$\begin{aligned} R a_1 &= u_1 = [c, 0, \ldots . 0]^T, \\ R a_2 &= u_2 = [0, c, \ldots . 0]^T, \\ &\ldots\ldots\ldots \\ R a_M &= u_M = [0, 0, \ldots . c]^T. \end{aligned} \qquad (2.23)$$

Thus, the filter $\mathbf{h}_1$ yields an output c for the image $\mathbf{x}_1$ and zero for all the other images and so on. The filter vectors $\mathbf{h}_i$, i =1,2,....M, is given by

$$h_i = X_s (X_s^T X_s)^{-1} u_i \qquad (2.24)$$

where $\mathbf{u}_i$ is a vector of size M, with c as its i^{th} element and zeros elsewhere.

2.2.1.3. Inter-Class-Intra-Class SDF This is a combination of intra-class ECP SDF and the inter-class SDF. Consider the case of M different classes with N objects in each of them. Then it is required to have M filter vectors to satisfy,

$$\boldsymbol{x}_{ki} \otimes \boldsymbol{h}_j = c_i \delta_{kj}, \quad i=1,2,....N, \quad j,k=1,2,....M. \quad \textbf{(2.25)}$$

The SDFs can be obtained as:

$$\begin{aligned} \boldsymbol{h}_1 &= \boldsymbol{X}_s (\boldsymbol{X}_s^T \boldsymbol{X}_s)^{-1} \boldsymbol{u}_1 \\ \boldsymbol{h}_2 &= \boldsymbol{X}_s (\boldsymbol{X}_s^T \boldsymbol{X}_s)^{-1} \boldsymbol{u}_2, \quad \textit{and so on} \end{aligned} \qquad \textbf{(2.26)}$$

where $\mathbf{u}_i$'s are vectors of size MN given as:

$\mathbf{u}_1 = [c_1,c_1,....,c_1:0,0,....,0:.....:0,0,....,0]^T$,

$\mathbf{u}_2 = [0,0,....,0:c_2,c_2,....,c_2:.....:0,0,....,0]^T$,

.....

and

$\mathbf{u}_M = [0,0,....,0:0,0,....,0:.....:c_M,c_M,....,c_M]^T$.

Riggins and Butler [30] implemented the above conventional SDF using a computer generated hologram encoding and reported positive results. However, there are some practical problems in using this filter for OPR. First, the conventional SDF assumes that the filter function is a linear combination of the training images (as in Eq. (2.10)). This assumption is useful when SDFs are synthesized in an optical laboratory using multiple exposure techniques. However,

nowadays the SDFs are synthesized on digital computers. Thus, filters can be designed by removing this unnecessary restriction. Also, the original SDF design does not consider noise in the input. In the presence of noise the output values will not be exactly the required values even for training images. Thus, filters capable of tolerating input noise are necessary. These have led to the development of Minimum Variance Synthetic Discriminant Function (MVSDF) [14] which is designed to maximize noise tolerance. This is discussed in the next section.

Second, the conventional SDF controls the output at only one point, the origin, in the correlation output. Correlators are attractive because they can detect as well as locate an object, in the input scene. If the input object is shifted by a certain unknown distance from the origin, the peak correlation output is also shifted by that distance. The values at the origin thus moved by the unknown distance. However, in the presence of noise, other values in the output correlation plane may produce larger peaks. Hence, it is impossible to locate the shifted origin in the presence of even small amounts of noise. Thus, it is desirable to produce correlation peaks that are extremely sharp. In this chapter SDFs designed with this goal are also discussed.

2.2.2. Minimum Variance Synthetic Discriminant Function [14]

The Minimum Variance Synthetic Discriminant Function (MVSDF) is synthesized by minimizing the output variance due to noise in the input [14]. Consider the situation when the image $\mathbf{x}_i$ being tested is corrupted by an additive noise vector $\mathbf{n}$. Then the correlation output value is given by

$$\begin{aligned} v &= \boldsymbol{h}^{\dagger}(\boldsymbol{x}_i + \boldsymbol{n}) \\ &= u_i + \boldsymbol{h}^{\dagger}\boldsymbol{n} \\ &= u_i + y, \qquad i=1,2,.....N \end{aligned} \tag{2.27}$$

where $\mathbf{h}$ is designed to satisfy Eq. (2.11). The output v is the desired output u_i, corrupted by the random variable $\mathbf{h}^T\mathbf{n}$ which is denoted by y. The MVSDF attempts to design $\mathbf{h}$ such that the variance in the output due to input noise is minimized while satisfying the constraints in Eq. (2.12).

Let $\mathbf{n}$ be a zero mean noise vector with a d×d covariance matrix $\mathbf{R}_n$. Then

$$\mathbf{E\{y\} = 0}$$

and

$$\begin{aligned} Var\{y\} &= E\{(\boldsymbol{h}^{\dagger}\boldsymbol{n})^2\} \\ &= E\{\boldsymbol{h}^{\dagger}\boldsymbol{n}\boldsymbol{n}^{\dagger}\boldsymbol{h}\} \\ \sigma_y^2 &= \boldsymbol{h}^{\dagger}\boldsymbol{R}_n\boldsymbol{h}. \end{aligned} \tag{2.28}$$

A small σ_y^2 will ensure that the output values are close to the desired values even in the presence of noise. Minimizing

σ_y^2 in Eq. (2.28) subject to the constraints in Eq. (2.12) leads to the following MVSDF [14],

$$h_{MVSDF} = R_n^{-1} X_s (X_s^T R_n^{-1} X_s)^{-1} u. \qquad (2.29)$$

For the special case of white noise, $R_n = \sigma^2 I_d$, where I_d is an identity matrix of size d×d and σ^2 is the power of the white noise. Then Eq. (2.29) reduces to Eq. (2.19). Thus the conventional SDF achieves the smallest output variance when the input noise is white. But for other types of noise, the conventional SDF is not the optimal SDF. Vijaya Kumar [31] considered the special case of input Markov noise. For this special case, R_n is a Toeplitz matrix and can be easily inverted.

The minimal achievable output noise variance can be obtained by substituting Eq. (2.29) into Eq. (2.28). The resulting variance is given by

$$\begin{aligned} \sigma_{min}^2 &= [R_n^{-1} X_s (X_s^T R_n^{-1} X_s)^{-1} u]^T R_n [R_n^{-1} X_s (X_s^T R_n^{-1} X_s)^{-1} u] \\ &= u^T (X_s^T R_n^{-1} X_s)^{-1} u. \end{aligned} \qquad (2.30)$$

It is interesting to see that the minimal achievable variance depends on the constraint vector **u**. It has been shown that the output noise variance can further be reduced by selecting the phase values of the constraint in an optimal manner [32]. When these filters are used in the optical correlator, the output intensities are used for detection

purposes. Thus suitable phase choices can be made without affecting the magnitudes but minimizing the noise variance.

2.2.3. Minimum Average Correlation Energy (MACE) Filter [15]

The MVSDF is optimal from the noise tolerance considerations; however, the MVSDF controls the response at only one point in the output correlation plane. Thus, large sidelobes in the correlation may degrade its performance. For good detection and location accuracy, the filters must be capable of producing sharp peaks. The MACE filter is designed to produce sharp correlation peaks which allow easy detection [15]. The MACE filter is designed in the discrete frequency domain.

Let the two-dimensional discrete Fourier Transform (DFT) of the i^{th} image $\bar{x}_i$ be $\bar{X}_i$, given by

$$\overline{X_i}(k_1,k_2) = \sum_{n_1=1}^{M}\sum_{n_2=1}^{M} \overline{x_i}(n_1,n_2)\exp\{\frac{-2j\pi((k_1-1)(n_1-1)+(k_2-1)(n_2-1))}{M}\} \qquad 1\le k_1,k_2\le M. \tag{2.31}$$

Let the d dimensional vectors $\mathbf{X}_i$, i = 1,2,...,N, denote the one-dimensional equivalence of the images $\bar{X}_i$ and the vector $\mathbf{H}$ of size d denote the filter function $\bar{H}$ in the discrete frequency domain. The output of the i^{th} image $\bar{X}_i$ with the filter $\bar{H}$ is given by,

$$\overline{g_i}(n_1,n_2) = IDFT\{\overline{X_i}(k_1,k_2)\,\bar{H}(k_1,k_2)\}, \qquad i=1,2,.....N.$$

To achieve good detection, it is necessary to reduce the output level at all points in the correlation plane except at the origin where the necessary constraint must be met. This is equivalent to minimizing the correlation plane energy while simultaneously satisfying the constraint at the origin:

$$\overline{g_i}(0,0) = \frac{1}{M^2}\sum_{k_1=1}^{M}\sum_{k_2=1}^{M}\overline{X_i}(k_1,k_2)\,\overline{H}(k_1,k_2)$$

$$= \frac{1}{M^2}\sum_{k=1}^{M^2} X_i(k)\,H(k)$$

$$= \frac{1}{M^2}\boldsymbol{X_i^T H}, \qquad i=1,2,.....N$$

where the superscript 'T' denotes the transpose operation. If $\mathbf{X_i}^{\mathbf{T}}\mathbf{H}$ is required to be u_i, then

$$\boldsymbol{X_i^T H} = M^2\,\overline{g_i}(0,0) = u_i, \qquad i=1,2,....,N.$$

Now combining the condition for i = 1,2,...,N,

$$\boldsymbol{X^T H} = \boldsymbol{u} \tag{2.32}$$

where $\mathbf{X} = [\mathbf{X_1},\mathbf{X_2},.....\mathbf{X_N}]$ is the frequency domain data matrix and **u** is the output vector defined earlier.

The average correlation plane energy is,

$$E_{av} = \frac{1}{N}\sum_{i=1}^{N}\frac{1}{d}\sum_{k=1}^{d} |H(k)|^2 |X_i(k)|^2 = \frac{1}{N}\sum_{i=1}^{N} H^+ D_i H \qquad (2.33)$$

where D_i is a d×d diagonal matrix with elements

$$D_i(k,k) = |X_i(k)|^2/d$$

and the superscript '+' denotes the conjugate transpose operation.

Let

$$D = \frac{1}{N}\sum_{i=1}^{N} D_i.$$

Then Eq. (2.33) reduces to

$$E_{av} = H^+ D H. \qquad (2.34)$$

Minimizing E_{av} in Eq. (2.34) subject to the constraints in Eq. (2.32) leads to the filter:

$$H_{MACE} = D^{-1} X (X^T D^{-1} X)^{-1} u. \qquad (2.35)$$

It has been found that MACE filters are more sensitive to the non-training image views than other composite filters [33]. This is perhaps due to the fact that MACE filters favor producing sharp correlation peaks thereby emphasizing the high frequencies. A filter designed to produce broad Gaussian-

shaped correlation peaks rather than a sharp delta function reduces this problem of MACE filters [34]. In addition, MACE filters have not been designed to have low noise tolerance.

When correlation is performed using DFT, the output is a circular correlation rather than linear correlation [16]. However, in a practical implementation using optical lenses, linear correlation rather than circular correlation is performed and so the energy of the linear correlation output needs to be minimized for optimal filter design. In the next section the design of MACE filter in the space domain (SMACE) in order to minimize directly the linear correlation energy is discussed.

2.2.4. SMACE Filter [16]

This filter is designed to minimize the average correlation energy in the space domain while satisfying the output constraints in Eq. (2.12). Let $\mathbf{h}$ denote the SMACE filter in the space domain. The size of the image is assumed to be M×M and M^2 = d. The convolution of the training image $\mathbf{x}_i$ with $\mathbf{h}$ is given by the $K = (2M - 1)^2$ dimensional vector as

$$g_i = S_i h, \qquad i=1,2,.....N, \qquad (2.36)$$

where $\mathbf{S}_i$ is a real matrix of size K×d obtained from the signal $\mathbf{x}_i$ as

$$S_i = \begin{bmatrix} 0 & \dots & 0 & \psi_i^1 \\ 0 & \dots & \psi_i^1 & \psi_i^2 \\ \vdots & \ddots & \vdots & \vdots \\ \psi_i^1 & \psi_i^2 & \dots & \psi_i^M \\ \psi_i^2 & \dots & \psi_i^M & 0 \\ \vdots & \ddots & \vdots & \vdots \\ \psi_i^M & 0 & \dots & 0 \end{bmatrix}, \qquad i = 1,2,\dots\dots,N. \tag{2.37}$$

The real matrices Ψ_i^l, $l = 1,2,\dots.(2M-1)$ are given by

$$\psi_i^l = \begin{bmatrix} 0 & \dots & 0 & x_i(M(l-1)+1) \\ 0 & \dots & x_i(M(l-1)+1) & x_i(M(l-1)+2) \\ \vdots & \ddots & \vdots & \vdots \\ x_i(M(l-1)+1) & x_i(M(l-1)+2) & \dots & x_i(M(l-1)+M) \\ x_i(M(l-1)+2) & \dots & x_i(M(l-1)+M) & 0 \\ \vdots & \ddots & \vdots & \vdots \\ x_i(M(l-1)+M) & 0 & \dots & 0 \end{bmatrix},$$

$$i = 1,2,\dots\dots,N. \tag{2.38}$$

The energy in the i^{th} response output is given by $g_i^T g_i$. Then the average energy is given by,

$$\begin{aligned} E_{av} &= \frac{1}{N}\sum_{i=1}^{N} h^T S_i^T S_i h \\ &= h^T R_s h \end{aligned} \tag{2.39}$$

where

$$R_s = \frac{1}{N} \sum_{i=1}^{N} S_i^T S_i. \qquad (2.40)$$

When E_{av} in Eq. (2.40) is minimized subject to the constraints in Eq. (2.11), the space domain filter function can be computed as [16]:

$$h_{SMACE} = R_s^{-1} X_s \left(X_s^T R_s^{-1} X_s \right)^{-1} u \qquad (2.41)$$

where $\mathbf{X_s}$ is the data matrix in space domain.

The $\mathbf{R_s}$ matrix in Eq. (2.41) in general is not a diagonal matrix, whereas the **D** matrix in the frequency domain MACE filter is a diagonal matrix. Thus the computational complexity in finding the inverse of $\mathbf{R_s}$ is higher. But the special block Toeplitz structure of the matrix $\mathbf{R_s}$ may be used to reduce the complexity of the inversion.

Both frequency and space domain MACE filter designs, however, do not take noise tolerance into consideration. This led to the subsequent development of an improved filter [16] discussed next.

2.2.5. MVSDF-MACE Filter [16]

The MVSDF is designed to maximize noise tolerance, whereas the MACE filter maximizes the peak sharpness. In reality both these criteria are important. A compromise measure between these two can be written from the noise variance σ^2 in Eq. (2.28) and the average correlation plane energy E_{av} in Eq. (2.39) as:

$$C_M = \alpha_1 E_{av} + \alpha_2 \sigma^2$$
$$= \alpha_1 \boldsymbol{h}^T \boldsymbol{R}_s \boldsymbol{h} + \alpha_2 \boldsymbol{h}^T \boldsymbol{R}_n \boldsymbol{h} \qquad (2.42)$$
$$= \boldsymbol{h}^T (\alpha_1 \boldsymbol{R}_s + \alpha_2 \boldsymbol{R}_n) \boldsymbol{h}$$

where α_1 and α_2 are nonnegative constants which are to be chosen such that a compromise between the relative importance of noise tolerance and the sharp correlation peak is achieved. For large values of α_2/α_1, C_M is dominated by $\alpha_2\sigma^2$ and noise tolerance will be emphasized. For small α_2/α_1 values, $\alpha_1 E_{av}$ dominates C_M and the peak sharpness will be maximized. For other values of α_2/α_1 the filter response will be in between the two extremes.

Minimization of C_M in Eq. (2.42) subject to the usual constraints in Eq. (2.12) leads to the improved filter:

$$\boldsymbol{h}_{IMPROVED} = (\alpha_1 \boldsymbol{R}_s + \alpha_2 \boldsymbol{R}_n)^{-1} \boldsymbol{X}_s \{\boldsymbol{X}_s^T (\alpha_1 \boldsymbol{R}_s + \alpha_2 \boldsymbol{R}_n)^{-1} \boldsymbol{X}_s\}^{-1} \boldsymbol{u}. \qquad (2.43)$$

When $\alpha_2 \rightarrow 0$, $\mathbf{h}$ approaches $\mathbf{h}_{SMACE}$ in Eq. (2.41) and as $\alpha_2 \rightarrow \infty$, $\mathbf{h}$ approaches $\mathbf{h}_{MVSDF}$ in Eq. (2.29).

An extension of the conventional SDF, namely correlation SDF [35], has also been reported. This filter is designed to control the sidelobe levels and the shape of the output correlation as well as its peak intensity. Bahri and Vijaya Kumar proposed a generalized SDF which completely characterizes all the possible solutions to the conventional SDF problems [36]. A general $\mathbf{h}$ capable of satisfying Eq. (2.12) is given as follows [34]:

$$h = X_s (X_s^T X_s)^{-1} u + \{I_d - X_s (X_s^T X_s)^{-1} X_s^T\} z \qquad (2.44)$$

where I_d is a d×d identity matrix and z is column vector with d entries. It can be verified that when z = 0, the solution vector in Eq. (2.44) is the conventional SDF. Also, two popular variations of the conventional SDF, namely MVSDF and MACE filters can be seen as special cases of the generalized SDF [36]. Sudharsanan, Mahalanobis, and Sundareshan proposed a method for the selection of optimal output constraint values by minimizing the probability of error (POE) in detection [37].

Much of the discussion so far is focused on the use of single composite filter. It is unrealistic to expect a single filter, however well designed, to give the necessary performance. With ever increasing speeds of the SLMs and output detectors, it should be possible to test an input object against multiple filters in real-time. Hence, the design of multiple filters for a multi-class pattern recognition problem or multistage high order filters for specific output results would be valuable. References [38-42] discuss the design of multiple filters for pattern recognition.

The importance of being able to design partial information (e.g., phase-only and binary phase-only) SDFs is well recognized and several attempts have been made to design such filters. In Reference [43], Vijaya Kumar briefly outlines some of this work.

2.3. Summary

The discussion in this chapter was focused on different correlation-based composite filters for pattern recognition and parameter estimation. In this report the development of real filters for the same purpose is studied. In the following chapter, the development of real MACE filter, its properties, together with the comparison of its performance with the complex MACE and the conventional filters are discussed.

CHAPTER 3

Real-Valued MACE Filter

In the past, several methods have been suggested to introduce distortion tolerance in the filter design. The most well-known method is the use of the synthetic discriminant function [11] (SDF) and its variations [14-16]. The conventional SDF has been shown to achieve distortion invariance; however, this filter results in large sidelobe levels in the correlation plane. This is due to the fact that the input object usually has cross correlation with the images in the training set. But, for good detection and location accuracy, the filters should be capable of producing sharp correlation peaks. The minimum average correlation energy (MACE) filter is designed to achieve this objective. In this chapter the development of real-valued MACE filters and its performance are presented.

3.1. Need for Real-Valued MACE Filter

The MACE filter usually has complex-valued frequency response. For realizing complex functions holograms are required. Two types of holograms are commonly used. They are optically produced holograms and computer generated holograms. Optically produced holograms cannot generate the desired phase variation. Hence most often, the only alternative is to use some form of computer generated holograms. Many different

methods for encoding a complex function onto a computer generated mask have been devised [44]-[45]. In all these cases the space-bandwidth product available is limited by the display or plotting device used to produce the computer generated holograms. In addition real-time applications, such as landmark identification, require cycling of multiple filters through the correlators at very high speeds. Hence, it might be impractical to design holograms on-line for portable optical systems.

The advent of spatial light modulators (SLMs), which could be interfaced with digital computers, has made it possible to correlate an input object with a large number of filters at video rates. However, most commonly available optical spatial light modulators (SLMs) cannot encode fully complex functions. Instead, they can accommodate phase-only, amplitude-only, or phase-mostly functions. But optical setups that use two SLMs to encode complex functions has been under the investigation. Hence, by designing real filters, currently available SLMs can be used to encode the filters without the use of holographic techniques. Hence, it is proposed in this research to develop the theory of real-valued MACE filters and study their performance.

3.2. Theoretical Development

In this section, mathematical notations and terminology used in the design of RMACE filters are presented. Then, the

filter design problem is formulated and its solution discussed.

3.2.1. Notation

The RMACE filter, like the MACE filter, is synthesized in the discrete frequency domain. Let $\bar{X}_i$ be the two-dimensional discrete Fourier transform (DFT) of the i^{th} training image $\bar{x}_i$ of size M×M for i = 1,2,....,N. Then $\bar{X}_i$ is given by

$$\overline{X_i}(k_1,k_2) = \sum_{l_1=1}^{M}\sum_{l_2=1}^{M} \overline{x_i}(l_1,l_2)\cdot \exp\left\{\frac{-j2\pi((l_1-1)(k_1-1)+(l_2-1)(k_2-1))}{M}\right\}, \quad k_1,k_2=1,2,..,M. \tag{3.1}$$

The training images are represented in the discrete frequency domain by vectors $\mathbf{X}_i$, i=1,2,....,N with the subscript denoting the training image number. The set of all training vectors $\mathbf{X}_i$, i = 1,2,...,N, form the data matrix $\mathbf{X}$ with $\mathbf{X}_i$ arranged as the columns of $\mathbf{X}$. Let the real function $\bar{H}$ represent the response of the filter in the frequency domain.

The correlator output of the i^{th} image with the filter function $\bar{H}$ is given by

$$\overline{g_i}(n_1,n_2) = IDFT\{\overline{G_i}(k_1,k_2)\} \tag{3.2}$$

where $\bar{G}_i(k_1,k_2)$ represents the discrete Fourier transform (DFT) of the response function, and is given by

$$\overline{G_i}(k_1,k_2) = \overline{X_i}(k_1,k_2)\,\overline{H}(k_1,k_2). \tag{3.3}$$

The energy of the correlation output for the image $\bar{x}_i$ is then given by

$$E_i = \sum_{n_1=1}^{M} \sum_{n_2=1}^{M} |\overline{g_i}(n_1, n_2)|^2 = \frac{1}{M^2} \sum_{k_1=1}^{M} \sum_{k_2=1}^{M} |\overline{G_i}(k_1, k_2)|^2. \quad (3.4)$$

Substituting Eq. (3.3) into Eq. (3.4), the energy of the output corresponding to the i^{th} image $\bar{x}_i$ is obtained as:

$$E_i = \frac{1}{M^2} \sum_{k_1=1}^{M} \sum_{k_2=1}^{M} [\overline{H}(k_1, k_2)]^2 |\overline{X_i}(k_1, k_2)|^2 = \frac{1}{d} \sum_{k=1}^{d} [H(k)]^2 |X_i(k)|^2 \quad (3.5)$$

where $\mathbf{H}$ and $\mathbf{X}_i$ are the one-dimensional vectors representing the filter $\bar{H}$ and the image $\bar{X}_i$. Then, using vector-matrix notation, Eq. (3.5) can be written as:

$$E_i = \boldsymbol{H}^T D_i \boldsymbol{H} \quad (3.6)$$

where D_i is a diagonal matrix of size d×d such that

$$D_i(k,k) = \frac{1}{d} |\boldsymbol{X}_i(k)|^2, \qquad k=1,2,\ldots,d, \quad (3.7)$$

and

$$D_i(k_1, k_2) = 0, \qquad k_1 \neq k_2,\ 1 \leq k_1 \leq d,\ 1 \leq k_2 \leq d. \quad (3.8)$$

3.2.2. Problem Definition

The objective of the pattern recognition problem under consideration is to design a real-valued filter that results in sharp correlation peaks while meeting the constraints on the correlation peak values and retaining the shift invariance property. To achieve a good detection, filters should produce sharp and easily detectable correlation peaks and small sidelobes. Hence, it is necessary to reduce the correlation plane values at all the points except at the origin of the correlation plane, while the value of the correlation function must be at a user specified value at the origin. This is equivalent to minimizing the energy of the correlation function while satisfying the intensity constraint at the origin.

In vector notation, the correlation intensity constraint at the origin is given as

$$\overline{g_i}(0,0) = \frac{1}{M^2} \boldsymbol{X_i^T H}$$
$$M^2 \overline{g_i}(0,0) = \boldsymbol{X_i^T H} = u_i, \qquad i=1,2,.....,N \tag{3.9}$$

where u_i is the user specified value of the i^{th} correlation function at the origin. Taking all the images into account, Eq. (3.9) can be written as

$$\boldsymbol{X^T H} = \boldsymbol{u} \tag{3.10}$$

where $\mathbf{u} = [u_1, u_2, ..., u_N]^T$ is an N dimensional vector.

The problem is to determine the frequency domain real vector **H** which minimizes $\mathbf{H}^T\mathbf{D}_i\mathbf{H}$ for all i = 1,2,.....N, while satisfying the peak constraints in Eq. (3.10). When the filter **H** is required to be real, the constraints in Eq. (3.10) can be written as

$$(X_R + jX_I)^T H = u. \tag{3.11}$$

That is,

$$(X_R^T + jX_I^T)\, H = u \tag{3.12}$$

where $\mathbf{X}_R$ and $\mathbf{X}_I$ are the real and imaginary parts of **X**, respectively. In general **u** can be complex. Then for a real filter response **H**, Eq. (3.12) can be written as

$$X_R^T H + j\, X_I^T H = u_R + j\, u_I \tag{3.13}$$

where $\mathbf{u}_R$ and $\mathbf{u}_I$ are the real and imaginary parts of **u**. By equating the real and imaginary parts of Eq. (3.13) the following pair of constraints is obtained:

$$X_R^T H = u_R \tag{3.14}$$

and

$$X_I^T H = u_I. \tag{3.15}$$

The simultaneous constrained minimization of all E_i, i = 1,2,...,N, is not possible. So the problem is reformulated to minimize the average value of E_i in Eq. (3.6) while meeting

the constraints in Eqs.(3.14) and (3.15). The average correlation plane energy is

$$\begin{aligned} E_{av} &= \frac{1}{N}\sum_{i=1}^{N} E_i = \frac{1}{N}\sum_{i=1}^{N} \boldsymbol{H}^{\boldsymbol{T}} D_i \boldsymbol{H} \\ &= \boldsymbol{H}^{\boldsymbol{T}}\{\frac{1}{N}\sum_{i=1}^{N} D_i\}\boldsymbol{H} \\ &= \boldsymbol{H}^{\boldsymbol{T}}\boldsymbol{D}\boldsymbol{H} \end{aligned} \tag{3.16}$$

where **D** is defined as:

$$\boldsymbol{D} = \frac{1}{N}\sum_{i=1}^{N} D_i. \tag{3.17}$$

3.3. RMACE Filter Solution

In this section, the solution of the RMACE filter is developed. It is required to minimize the average correlation plane energy $\mathbf{H^TDH}$ subject to the linear constraints $\mathbf{X^TH = u}$. Using the method of Lagrangian multipliers, the function to be minimized can be written as

$$\begin{aligned} \phi = \boldsymbol{H}^{\boldsymbol{T}}\boldsymbol{D}\boldsymbol{H} &- 2\lambda_1(\boldsymbol{H}^{\boldsymbol{T}}\boldsymbol{X}_{R1} - u_{R1}) - \ldots\ldots\ldots - 2\lambda_N(\boldsymbol{H}^{\boldsymbol{T}}\boldsymbol{X}_{RN} - u_{RN}) \\ &- 2\beta_1(\boldsymbol{H}^{\boldsymbol{T}}\boldsymbol{X}_{I1} - u_{I1}) - \ldots\ldots\ldots - 2\beta_N(\boldsymbol{H}^{\boldsymbol{T}}\boldsymbol{X}_{IN} - u_{IN}). \end{aligned} \tag{3.18}$$

Setting the gradient of ϕ with respect to **H** equal to **0**(zero vector), the following equation is obtained:

$$\boldsymbol{D}\boldsymbol{H} = \lambda_1 \boldsymbol{X}_{1R} + \ldots + \lambda_N \boldsymbol{X}_{NR} + \beta_1 \boldsymbol{X}_{1I} + \ldots + \beta_N \boldsymbol{X}_{NI}. \tag{3.19}$$

As **D** is a diagonal matrix, if $D(k,k) \neq 0$ for all k, then **D** will be invertible and $D^{-1}(k,k) = 1/D(k,k)$ and $D^{-1}(k,l) = 0$, for $k \neq l$. **D** will become noninvertible if $D(k,k) = 0$ for some k. $D(k,k) = 0$ means that the reference images have zero energy at the frequency corresponding to k. Hence, it is desirable to make the filter to have zero response at this frequency so that any noise in the test image at this frequency does not contribute to the output. This can be accomplished by making $D^{-1}(k,k) = 0$ where $D(k,k) = 0$ and $D^{-1}(k,k) = 1/D(k,k)$ where $D(k,k) \neq 0$. Then, from Eq. (3.19), **H** is obtained as

$$H = D^{-1} \sum_{i=1}^{N} (\lambda_i X_{iR} + \beta_i X_{iI}) = D^{-1} X_R \lambda + D^{-1} X_I \beta \qquad (3.20)$$

where the vectors λ and β are defined as

$$\lambda = [\ \lambda_1, \lambda_2, \ldots . \lambda_N\ ]^T,$$

and $$\beta = [\ \beta_1, \beta_2, \ldots . \beta_N\ ]^T.$$

Substituting Eq. (3.20) into Eqs.(3.14) and (3.15), the constraint equations become

$$X_R^T (D^{-1} X_R \lambda + D^{-1} X_I \beta) = u_R, \qquad (3.21)$$

$$X_I^T (D^{-1} X_R \lambda + D^{-1} X_I \beta) = u_I. \qquad (3.22)$$

Letting

$$\begin{aligned} A &= X_R^T D^{-1} X_R \\ B &= X_R^T D^{-1} X_I \\ C &= X_I^T D^{-1} X_I. \end{aligned} \qquad (3.23)$$

Eqs.(3.21) and (3.22) can be written as

$$A\lambda + B\beta = u_R \tag{3.24}$$

$$B^T\lambda + C\beta = u_I. \tag{3.25}$$

Eqs.(3.24) and (3.25) can be solved for λ and β as

$$\begin{aligned} \lambda &= (A - BC^{-1}B^T)^{-1}(u_R - BC^{-1}u_I) \\ \beta &= (C - B^TA^{-1}B)^{-1}(u_I - B^TA^{-1}u_R). \end{aligned} \tag{3.26}$$

Then substituting for λ and β from Eq. (3.26) into Eq. (3.20), the final expression for **H** is found as

$$H = D^{-1}\left[\{X_R - X_IC^{-1}B^T\}\{A - BC^{-1}B^T\}^{-1}u_R + \{X_I - X_RA^{-1}B\}\{C - B^TA^{-1}B\}^{-1}u_I\right]. \tag{3.27}$$

The real vector **H** in Eq. (3.27) minimizes $\mathbf{H}^T\mathbf{D}\mathbf{H}$ while simultaneously satisfying the constraint $\mathbf{X}^T\mathbf{H} = \mathbf{u}$.

3.4. RMACE Filter for Real Signals

Often the test objects are real as input to the correlator. Hence, the RMACE filter for real test objects is first considered. Since the filter is synthesized in the frequency domain, the odd and even symmetry properties of the Fourier transform (FT) of real signals may be used to simplify the filter function derived in the previous section. The FT of a real image $\bar{x}(n_1,n_2)$ has the following symmetry property:

$$\bar{X}(k_1,k_2) = \overline{X^*}(M+2-k_1, M+2-k_2) \tag{3.28}$$

where

$$\overline{X}(k_1, k_2) = F\{\overline{x}(n_1, n_2)\}$$

and '*' denotes the complex conjugate operation. Eq. (3.28) can be rewritten as

$$\overline{X_R}(k_1, k_2) = \overline{X_R}(M+2-k_1, M+2-k_2), \qquad (3.29)$$

and

$$\overline{X_I}(k_1, k_2) = -\overline{X_I}(M+2-k_1, M+2-k_2). \qquad (3.30)$$

The odd symmetry in Eq. (3.30)results in

$$\boldsymbol{B} = \boldsymbol{X}_R^T \boldsymbol{D}^{-1} \boldsymbol{X}_I = \boldsymbol{0}.$$

Substituting this condition into Eq. (3.27), the purely real filter function for real signals is obtained as

$$\boldsymbol{H} = \boldsymbol{D}^{-1}\left[\boldsymbol{X}_R(\boldsymbol{X}_R^T \boldsymbol{D}^{-1} \boldsymbol{X}_R)^{-1} \boldsymbol{u}_R + \boldsymbol{X}_I(\boldsymbol{X}_I^T \boldsymbol{D}^{-1} \boldsymbol{X}_I)^{-1} \boldsymbol{u}_I\right]. \qquad (3.31)$$

For the case when **u** is real, i.e., $\mathbf{u}_I = \mathbf{0}$, the solution in Eq. (3.31) reduces to

$$\boldsymbol{H} = \boldsymbol{D}^{-1} \boldsymbol{X}_R(\boldsymbol{X}_R^T \boldsymbol{D}^{-1} \boldsymbol{X}_R)^{-1} \boldsymbol{u}. \qquad (3.32)$$

It should be noted that only $\mathbf{X}_R$, the real part of the matrix **X** is needed for the design of the filter function. Hence, the RMACE filter in Eq. (3.32) needs less memory and computation

time. Unless otherwise stated all the results presented in this chapter refers to the RMACE filter in Eq. (3.32).

3.5. The Symmetry Property of the RMACE Filter

When the input objects $\bar{x}_i$, i= 1,2,.....,N, are real, the two-dimensional DFTs $\bar{X}_i$ possess centro conjugate symmetry as:

$$\overline{X_i}(k_1, k_2) = \overline{X_i^*}(M+2-k_1, M+2-k_2), \quad 1 \le k_1, k_2 \le M \qquad (3.33)$$

where M×M is the size of the object. This can be used to reduce the number of filter coefficients to be determined. Since $\mathbf{X}_i$ is the one-dimensional equivalence of $\bar{X}_i$, this condition can be written in terms of $\mathbf{X}_i$ as

$$\boldsymbol{X}_i = \boldsymbol{J}_c \boldsymbol{X}_i^*, \qquad i=1,2,....,N \qquad (3.34)$$

where $\mathbf{J}_c$ is a dxd matrix given by

$$\boldsymbol{J}_c = \begin{bmatrix} \boldsymbol{Y}_{M\times M} & \boldsymbol{Z}_{M\times(M-2)M} & \boldsymbol{Z}_{M\times M} \\ \boldsymbol{Z}_{M\times(M-2)M} & \boldsymbol{Z}_{M\times M} & \boldsymbol{Y}_{M\times M} \\ \boldsymbol{Z}_{M\times(M-2)M} & \boldsymbol{Y}_{M\times M} & \boldsymbol{Z}_{M\times M} \\ \vdots & \vdots & \vdots \\ \boldsymbol{Z}_{M\times M} & \boldsymbol{Y}_{M\times M} & \boldsymbol{Z}_{M\times(M-2)M} \end{bmatrix} \qquad (3.35)$$

where $\mathbf{Z}_{M\times M}$ is a M×M matrix of zero entries and

$$Y_{M\times M} = \begin{bmatrix} 1 & 0 & 0 & \dots & 0 & 0 \\ 0 & 0 & 0 & \dots & 0 & 1 \\ 0 & 0 & 0 & \dots & 1 & 0 \\ \vdots & \vdots & \vdots & \dots & \vdots & \vdots \\ 0 & 1 & 0 & \dots & 0 & 0 \end{bmatrix}. \qquad (3.36)$$

That is, from Eq. (3.34)

$$J_c X_{iR} = X_{iR}$$
$$J_c X_{iI} = -X_{iI}, \qquad i = 1, 2, \dots, N.$$

Since **D**, a diagonal matrix, has its diagonal elements the samples of the average power spectrum of the training images, it satisfies the following condition:

$$J_c D^{-1} J_c = D^{-1}. \qquad (3.37)$$

The same matrix J_c can be used to show the symmetry property of the filter **H** as follows: The filter from Eq. (3.31) is

$$H = D^{-1}\{X_R A^{-1} u_R + X_I C^{-1} u_I\}. \qquad (3.38)$$

Noting that $J_c J_c = I$, identity matrix, $J_c H$ is obtained as

$$\begin{aligned} J_c H &= J_c\left[D^{-1}\{X_R A^{-1} u_R + X_I C^{-1} u_I\}\right] \\ &= \{J_c D^{-1} J_c\}\{J_c X_R A^{-1} u_R + J_c X_I C^{-1} u_I\} \qquad (3.39) \\ &= D^{-1}\{X_R A^{-1} u_R - X_I C^{-1} u_I\}. \end{aligned}$$

If **u** is restricted to be real, u_I is zero, then $J_c H = H$. Thus the filter possesses centrosymmetry and the corresponding impulse response is real. If **u** is imaginary, u_R is zero, then $J_c H = -H$. That is, **H** possesses centro anti symmetry and the

impulse response is imaginary. Then for M even, it is only required to determine $M^2/2 + 2$ filter coefficients. This would save computer memory and CPU time in filter design. If **u** is complex the filter **H** does not possess any symmetry.

3.6. Properties of the RMACE Filter when u is Real

The RMACE filter for the case of real signals and for the real output was derived in Section 3.4. This section discusses two noteworthy properties of this filter. Section 3.6.1 discusses the filter performance and Section 3.6.2 discusses the structure of this filter.

3.6.1. Single Training Image

Consider the case where the number of training images N is equal to one. Let **X** represent the DFT of the single training image. Then the diagonal elements of **D** are given by

$$\boldsymbol{D}(k,k) = |\boldsymbol{X}(k)|^2, \qquad k=1,2,.....d. \tag{3.40}$$

Thus, the quadratic term **A** is given by

$$\begin{aligned} \boldsymbol{A} &= \boldsymbol{X}_R^T \boldsymbol{D}^{-1} \boldsymbol{X}_R \\ &= \sum_{i=1}^{d} X_R^T(i)\, X_R(i)\, D^{-1}(i,i) \end{aligned} \tag{3.41}$$

where X(i) denotes the i^{th} element of the vector **X**. Since **D** is diagonal, Eq. (3.40) can be substituted into Eq. (3.41) to obtain

$$\boldsymbol{X}_R^T \boldsymbol{D}^{-1} \boldsymbol{X}_R = \sum_{i=1}^{d} \frac{X_R^T(i)\, X_R(i)}{|X(i)|^2} = \alpha \qquad (3.42)$$

where α is a constant. For this special case, Eq. (3.32) reduces to

$$\boldsymbol{H} = \boldsymbol{D}^{-1} \boldsymbol{X}_R \boldsymbol{u}' \qquad (3.43)$$

where $\mathbf{u}' = \mathbf{u}/\alpha$. That is,

$$H(k) = \frac{\boldsymbol{u}' X_R(k)}{|X(k)|^2}. \qquad (3.44)$$

Note that the RMACE filter of Eq. (3.32) with a single training image under a suitable scaling is the real part of an inverse filter defined in Reference [46] as

$$H_{INVERSE}(k) = \frac{X^*(k)}{|X(k)|^2}. \qquad (3.45)$$

3.6.2. Structure of the RMACE filter

The RMACE filter of Eq. (3.32) can be interpreted as a cascade of two stages as in the case of MACE filter [15]. For the special case where **D** is an identity matrix, the filter function of Eq. (3.32) reduces to the real-valued conventional SDF and is given by

$$\boldsymbol{H}_{RSDF} = \boldsymbol{X}_R (\boldsymbol{X}_R^T \boldsymbol{X}_R)^{-1} \boldsymbol{u}. \qquad (3.46)$$

All the terms in Eq. (3.46) refer to quantities in the discrete frequency domain. Therefore, the expression in Eq. (3.46) represents the real-valued conventional SDF filter in the frequency domain.

Using this real conventional SDF filter, the RMACE filter can be considered as the cascade of two separate stages as described below. The RMACE filter is given by

$$H = D^{-1} X_R (X_R^T D^{-1} X_R)^{-1} u.$$

The diagonal elements of D are equal to the samples of the average power spectrum of the training images. Hence, the diagonal elements of D^{-1} are reciprocals of the corresponding elements of the average power spectrum. Let $D^{-1/2} = P$, i.e., P is a diagonal matrix with its diagonal elements being the reciprocal square root of the diagonal elements of D. Then

$$H = P(PX_R)(X_R^T PPX_R)^{-1} u. \qquad (3.47)$$

Let $PX_R = Y_R$. Then Eq. (3.47) can be written as

$$H = P Y_R (Y_R^T Y_R)^{-1} u. \qquad (3.48)$$

The term $Y_R\{Y_R^T Y_R\}^{-1}u$ is the real conventional SDF denoted by H^Y_{RSDF}. Then

$$H = P H^Y_{RSDF}. \qquad (3.49)$$

Thus, from Eq. (3.49) the filter function **H** in frequency domain may be seen as the cascade of a matrix **P** and the real conventional SDF. Eq. (3.49) can be described by the block diagram in Figure 3.1.

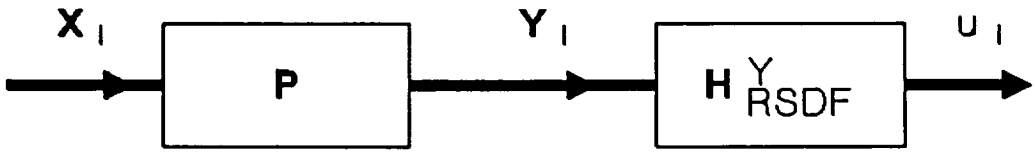

Figure 3.1. RMACE Filter as a Cascade of the Pre-whitener **P** and the Conventional SDF

As shown in Figure 3.1, the input data X_i is first filtered by **P** which may be viewed as a spectrum whitening filter and then by $\mathbf{H}^{\mathbf{Y}}_{\mathbf{RSDF}}$ which is based on the filtered data to obtain the output u_i.

From the above discussion the following alternate interpretations for the RMACE filter can be made:

1. The RMACE filter is a real conventional SDF filter operating on the preprocessed or filtered data, where the preprocessor forces the average power spectrum of the training images to become white.
2. The results in Reference [47] show that the optimal filter for a particular type of input noise is a cascade of a whitening filter and a conventional SDF operating on the transformed data. Hence, the RMACE filter is also

optimal in the presence of noise for which **P** is the whitening filter.

3.7. Algorithm for the Construction of RMACE Filter

An algorithm for the development of the RMACE filter of Eq. (3.32) for a real input object and real **u** specification is given below.

1. From the given training images $\bar{x}_i$, i=1,2,.....,N, compute the two-dimensional Fourier transform $\bar{X}_i$.
2. Obtain the column vectors $\mathbf{X}_i$, i = 1,2,.....,N, by a lexicographical ordering the rows of the image $\bar{X}_i$.
3. From the vector images $\mathbf{X}_i$, i = 1,2,....,N, find the diagonal matrix $\mathbf{D}_i$ as

$$D_i(k,k) = \frac{1}{d} \mid X_i(k) \mid^2.$$

4. Compute the matrix **D** as

$$\boldsymbol{D} = \frac{1}{N} \sum_{i=1}^{N} \boldsymbol{D}_i.$$

5. From the real part of the training images $\mathbf{X}_{Ri}$, find the data matrix $\mathbf{X}_R$ as

$$\boldsymbol{X}_R = [\boldsymbol{X}_{R1}, \boldsymbol{X}_{R2}, \ldots\ldots, \boldsymbol{X}_{RN}].$$

6. Obtain the matrix $\mathbf{A} = \{\mathbf{X}_R^T \mathbf{D}^{-1} \mathbf{X}_R\}^{-1}$.
7. Using the specified correlation output constraints u_i, i = 1,2,.....,N, and matrices **D** and **A** construct the RMACE filter as

$$H = D^{-1} X_R A^{-1} u.$$

3.8. RMACE Filter when the Specified u is Complex

The previously proposed RMACE filter maximizes the peak sharpness by minimizing the average output energy resulting in good performance. In this section, it is shown that this output correlation energy can be further reduced by selecting optimally the phase values of the output constraints **u**. Since only output intensity values are used by the detector for recognition, these phase choices do not affect the detector output.

3.8.1. Optimal Phase for Correlation Outputs at the Origin

In order to reduce the output correlation energy by the proper selection of the phases of the output constraints, the correlation output for the i^{th} image may be written as

$$\begin{aligned} u_i &= \mu_i \exp(j\theta_i) \\ &= \mu_i \cos\theta_i + j\mu_i \sin\theta_i, \qquad i=1,2,.....,N \end{aligned} \tag{3.50}$$

where μ_i ,i = 1,2,....,N, denotes the output constraint magnitude and Θ_i denotes its phase. As mentioned earlier, in a typical optical correlator, only the magnitude of the correlation outputs are available from the detectors and thus only μ_i, i=1,2,...,N, need to be specified. Hence the phases

θ_i, i=1,2,.....,N, can be chosen to reduce the correlation plane energy.

Substituting Eq. (3.50) into Eq. (3.9) the constraint at the origin can be obtained as

$$\boldsymbol{X}_i^T \boldsymbol{H} = \mu_i \cos\theta_i + j\,\mu_i \sin\theta_i, \qquad i=1,2,.....,N. \quad (3.51)$$

The above expression can be written in terms of the data matrix **X** as

$$\boldsymbol{X}^T \boldsymbol{H} = \mu \cos\theta + j\,\mu \sin\theta \quad (3.52)$$

where μ is an N×N diagonal matrix with diagonal elements as

$$\mu(k,k) = \mu_k, \quad (3.53)$$

$$\cos\theta = [\cos\theta_1, \cos\theta_2, ..., \cos\theta_N]^T$$

and

$$\sin\theta = [\sin\theta_1, \sin\theta_2, ..., \sin\theta_N]^T$$

are N dimensional vectors.

Comparing Eqs.(3.13) and (3.52) the following conditions may be obtained.

$$u_R = \mu \cos\theta \quad (3.54)$$

and

$$u_I = \mu \sin\theta. \quad (3.55)$$

Hence, for real signals, the new optimal filter $\mathbf{H_{opt}}$ is obtained from Eq. (3.31) as

$$\boldsymbol{H_{opt}} = \boldsymbol{D^{-1}}\{\boldsymbol{X_R A^{-1}}\,\mu\cos\theta + \boldsymbol{X_I C^{-1}}\,\mu\sin\theta\} \tag{3.56}$$

where

$$\boldsymbol{A} = \boldsymbol{X_R^T D^{-1} X_R} \tag{3.57}$$

and

$$\boldsymbol{C} = \boldsymbol{X_I^T D^{-1} X_I}. \tag{3.58}$$

Note that when $\mathbf{u}$ is real, i.e., $\theta_i = 0$ or π for i = 1,2,...N, Eq. (3.56) reduces to the original RMACE given in Eq. (3.32).

The output plane correlation energy resulting from the use of optimum RMACE filter can be computed from Eqs.(3.56) and (3.14) as

$$\begin{aligned} E_{opt} &= \boldsymbol{H_{opt}^T D H_{opt}} \\ &= [\boldsymbol{\cos\theta^T}\,\mu\,\boldsymbol{A^{-1}}\,\mu\cos\theta + \boldsymbol{\sin\theta^T}\,\mu\,\boldsymbol{C^{-1}}\,\mu\sin\theta]. \end{aligned} \tag{3.59}$$

Let a_{ij} and c_{ij} be the ij^{th} elements of the matrices $\mathbf{A^{-1}}$ and $\boldsymbol{C^{-1}}$, respectively. Then Eq. (3.59) can be obtained as

$$\begin{aligned} E_{opt} &= \sum_{i=1}^{N}\sum_{j=1}^{N} (\cos\theta_i\,\mu_i\,a_{ij}\,\mu_j\cos\theta_j \\ &\quad + \sin\theta_i\,\mu_i\,c_{ij}\,\mu_j\sin\theta_j) \\ &= \sum_{i=1}^{N}\mu_i^2(a_{ii}\cos^2\theta_i + c_{ii}\sin^2\theta_i) \\ &\quad + 2\sum_{i=1}^{N}\sum_{j=i+1}^{N}\mu_i\mu_j(a_{ij}\cos\theta_i\cos\theta_j + c_{ij}\sin\theta_i\sin\theta_j). \end{aligned} \tag{3.60}$$

The output correlation energy can be minimized by making Eq. (3.60) as small as possible by a proper choice of the phase values θ_i, i= 1,2,...,N. So the required optimization can be written as

$$\phi = Min_{\theta_1,\theta_2,\ldots,\theta_N}\left[\sum_{i=1}^{N}\mu_i^2(a_{ii}\cos^2\theta_i + c_{ii}\sin^2\theta_i) + 2\sum_{i=1}^{N}\sum_{j=i+1}^{N}\mu_i\mu_j(a_{ij}\cos\theta_i\cos\theta_j + c_{ij}\sin\theta_i\sin\theta_j)\right]. \quad (3.61)$$

The optimization of the trigonometric function in Eq. (3.61) can be performed to choose the optimal θ_i by setting the gradient of ϕ to zero:

$$\frac{\partial\phi}{\partial\theta_i} = 0, \qquad i=1,2,\ldots,N. \quad (3.62)$$

Combining Eqs.(3.61) and (3.62) leads to the following simultaneous equations in N variables and obtained:

$$\sin\theta_i\sum_{j=1}^{N}(a_{ij}\cos\theta_j) - \cos\theta_i\sum_{j=1}^{N}(c_{ij}\sin\theta_j) = 0, \quad i=1,2,\ldots\ldots,N. \quad (3.63)$$

For the given matrices **A** and **C** the above simultaneous equations may be solved using a nonlinear algorithm. These optimal phase values can then be used to obtain the required filter function in Eq. (3.56).

It may be noted that $\theta_i = 0$, i = 1,2,.....N, is one of the solutions to the above nonlinear set of equations, which corresponds to the original RMACE filter. The important fact to be noted is that the optimization in Eq. (3.63) is

independent of **H** itself and depends only on the constraint magnitudes μ_i, and the training vector $\mathbf{X}_i$. This permits a convenient de-coupling of the optimal correlation output constraint phase selection and the synthesis of the filter. An outline of the algorithm for the development of RMACE filter with optimal phase values is presented.

3.8.2. Algorithm for the Filter Construction

The steps in the synthesis of RMACE filter with proper selection of output phase values are summarized below.

1. From the vector matrix **X** find $\mathbf{A} = (\mathbf{X}_R^T \mathbf{D}^{-1} \mathbf{X}_R)$ and $\mathbf{C} = (\mathbf{X}_I^T \mathbf{D}^{-1} \mathbf{X}_I)$, where **D** is given by

$$D(k,k) = \frac{1}{N} \sum_{i=1}^{N} |X_i(k)|^2.$$

2. Using the elements of matrices $\mathbf{A}^{-1}$ and $\mathbf{C}^{-1}$ solve the non-linear set of equations given in Eq. (3.63) to obtain the optimal correlation output phase values θ_i, i = 1,2,....N.
3. Use these phase values along with the specified correlation output constraint magnitudes μ_i, i=1,2,....N, and the inverse of the matrices **A** and **C** to obtain the required optimal RMACE filter in Eq. (3.56).

Before giving the results of the simulation, a simple analytical example to illustrate the importance of this method is presented in the next section.

3.8.3. Example with N = 2

For this case the optimization problem in Eq. (3.63) is simplified to the following:

$$\begin{aligned} \sin\theta_1\cos\theta_1(a_{11}-c_{11}) + a_{12}\sin\theta_1\cos\theta_2 - c_{12}\cos\theta_1\sin\theta_2 = 0 \\ \sin\theta_2\cos\theta_2(a_{22}-c_{22}) + a_{21}\sin\theta_2\cos\theta_1 - c_{21}\cos\theta_2\sin\theta_1 = 0. \end{aligned} \tag{3.64}$$

If θ_1 is set arbitrarily to zero then, Eq. (3.64) reduces to

$$\sin\theta_2 = 0.$$

Thus, θ_2 can either take the value of zero or π. $\theta_1 = 0$ and $\theta_2 = 0$ corresponds to the RMACE filter discussed in Section 3.4 and the resulting output correlation plane energy is

$$E_{av} = \frac{1}{2}\left[\mu_1^2 a_{11} + \mu_2^2 a_{22} + 2\,\mu_1\mu_2 a_{12}\right]. \tag{3.65}$$

When $\theta_1 = 0$ and $\theta_2 = \pi$, the corresponding output plane energy is given by

$$E_{opt} = \frac{1}{2}\left[\mu_1^2 a_{11} + \mu_2^2 a_{22} - 2\,\mu_1\mu_2 a_{12}\right]. \tag{3.66}$$

From Eqs.(3.65) and (3.66) it can be seen that if a_{12} is positive then a reduction in correlation plane energy may result from the phase optimization of the constraint.

Consider the special case where the two training vectors having the following 2×2 vector inner product matrix

$$X_R^T X_R = \begin{bmatrix} 1 & \rho \\ \rho & 1 \end{bmatrix} \qquad (3.67)$$

where $|\rho| < 1$. For this choice of vector inner product and unit diagonal matrix **D**, the elements of the inverse of the matrix **A** can be obtained as

$$a_{11} = a_{22} = \frac{1}{1-\rho^2}$$
$$a_{12} = a_{21} = \frac{-\rho}{1-\rho^2}. \qquad (3.68)$$

Thus $\theta_1 = 0$ and $\theta_2 = \pi$ is the optimal choice compared to the case where $\theta_1, \theta_2 = 0$, only when a_{12} is positive; i.e., for negative ρ values. Hence, the above example shows that there is potential for a reduction in the output correlation plane energy when the training images are negatively correlated.

3.9. Simulation Results

In this section the distortion tolerance properties of the RMACE filter for real u are studied using computer simulations. The RMACE filter was synthesized to discriminate between two objects of images of the landscape of Mars, referred to as mars1 (Class 1) and mars2 (Class 2) as shown in Figures 3.2 and 3.3. Both mars1 and mars2 are 64×64 pixel sized images padded with zeros to generate the 128×128 pixel sized images, with the image located at the origin.

The database used to test the RMACE filter performance consisted of thirteen images of each object class. Thirteen images were obtained by rotating the base image through angles

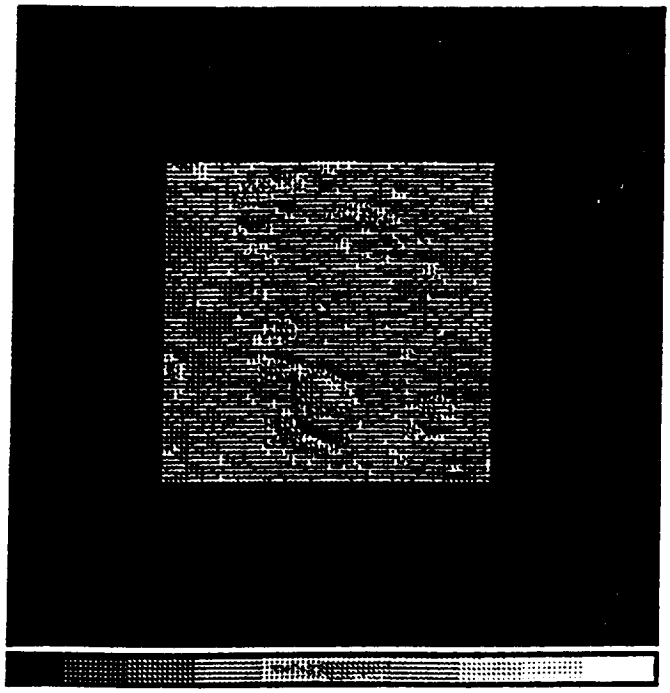

Figure 3.2. Image mars1

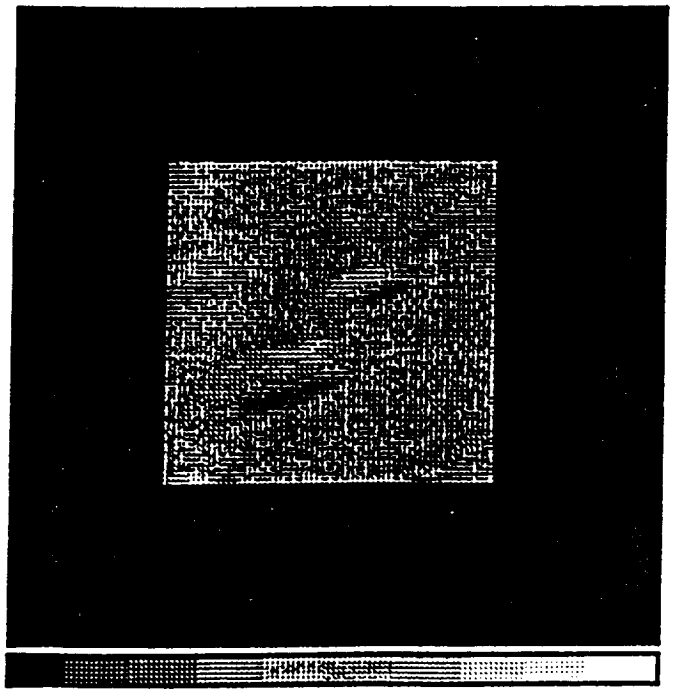

Figure 3.3. Image mars2

one through thirteen degrees. The rotation was carried out using a computer algorithm. The training set data used in the construction of the filter was evenly spaced in the range of the angle of rotation. The parameters used in the test to describe the sharpness of the correlation peak were the peak-to-side-lobe ratio (PSR) in the correlation plane and the average correlation plane energy E.

The threshold used for discriminating the two classes of objects was obtained as

$$T = 0.2\,u_1 + 0.8\,u_2 \qquad \textbf{(3.69)}$$

where u_1 and u_2 are the specified peak correlation outputs for the images mars1 and mars2, respectively. Since by choice $u_1 > u_2$, the weight for u_1 was kept low. Generally no peak higher than u_2 for mars2 images or u_1 for mars1 images occurs. Hence, by choosing a low weight for u_1, the threshold value can be kept very close to u_1, thereby improving the rate of detection.

Section 3.9.1. discusses the results of the computer simulation to show the distortion tolerance capacity of the RMACE filter. These tests were also implemented for the conventional SDF which is referred to as CSDF and for the MACE filter in order to compare the performance of the RMACE filter with their performances.

3.9.1. Distortion Test Results

The results of the computer simulations to evaluate the distortion tolerance of the RMACE filter against the MACE and the CSDF filters are presented. All three filters are correlated with both training and nontraining set images. The resulting correlation peak is measured and used for image classification.

In the following tests, the correlation peak values were compared to the fixed threshold T in Eq. (3.69) for target classification. The training set chosen in all the tests for the filter construction consisted of images evenly distributed through the range of rotation. Three types of filters were synthesized for the two class pattern recognition problem of mars1 and mars2. Tests were conducted on all thirteen images belonging to each class. The results of these tests are now discussed.

In the initial tests, the training set for the filter synthesis included three evenly spaced images for each of the two classes for a total of 6 training images. The images used were rotated through angles 1,7, and 13 degrees. Correlation peak amplitudes of 20 and 10 were arbitrarily specified for images mars1 and mars2, respectively.

The RMACE filter was synthesized according to the algorithm given in the previous section. The MACE and CSDF filters were also synthesized for the same training set images. The average correlation energy of the training images

is an indication of the filter performance. A low average correlation energy implies sharper correlation peak, higher PSR and more sensitivity to distortion.

The average correlation energy $E_{av} = \mathbf{H}^T\mathbf{D}\mathbf{H} = 0.1743$ was achieved for the RMACE filter. This is relatively small compared to the energy of 29.89 obtained for the same set of training images with the CSDF filter. The energy of 0.0856 was achieved with the MACE filter, which is smaller than that of RMACE filter, however, the reduction is not much. A poor recognition rate is suggested by the higher average correlation energy. However, when the correlation plane energy is small resulting in sharper peaks, the filter is more sensitive to noise and distortion. Since the correlation plane energy of the RMACE filter is higher than that of the MACE filter, the distortion tolerance of RMACE filter would be better. Further, since the energy is much lower than that of the CSDF filter, the quality of the correlation plane is expected to be good with low side lobe levels. The data presented in this section confirm the trends predicted on the basis of the average correlation plane energy values.

A typical three-dimensional plot of the output correlation plane for the RMACE filter is shown in Figure 3.4. The sharpness of the correlation peak is excellent, and the sidelobes are very low. For comparison, the three-dimensional plots for MACE filter and CSDF filter are shown in Figures 3.5 and 3.6. Comparing Figures 3.4 and 3.5, no significant

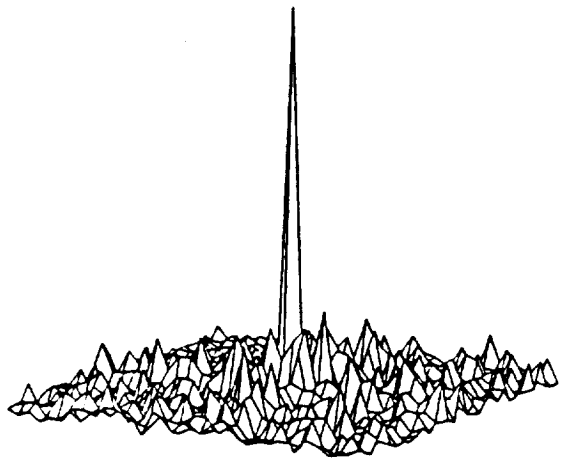

Figure 3.4. Correlation Plane Output Intensity with the RMACE filter

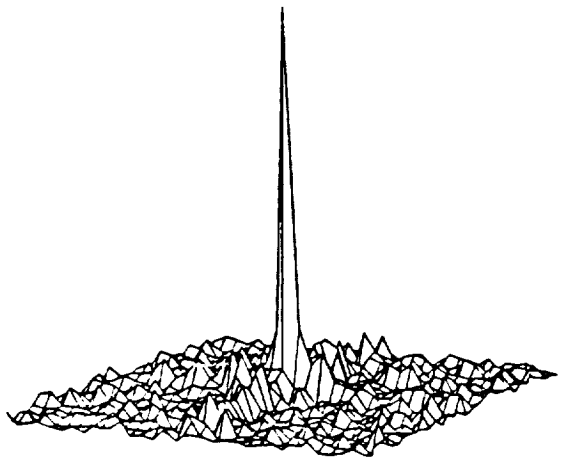

Figure 3.5. Correlation Plane Output Intensity with the MACE filter

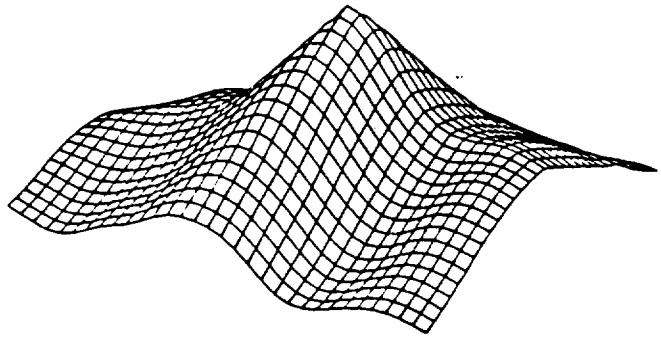

Figure 3.6. Correlation Plane Output Intensity with the CSDF filter

difference in performance between the RMACE filter and the MACE filter can be seen. Both filters have very sharp correlation peaks and very low sidelobes. From Figure 3.6 the correlation peak sharpness of the CSDF can be seen as being very low.

All three filters were then tested against the 13 images of mars1 and mars2 in the database. . Table 3.1 lists the statistics for Class 1 and Class 2 training data for the RMACE filter. These data include test image, the intensity at the origin, the highest and the second highest peak anywhere in the correlation plane, plus the two measures of sharpness of the correlation peak namely, average correlation plane energy E for the test image and PSR, the peak to sidelobe ratio. Pixel (1,1) is the origin at which the value is specified as 20 and 10 for mars1 and mars2 images, respectively.

It can be seen from Table 3.1 that all six correlation peaks obtained from the images used in the filter construction satisfied the imposed constraints at the origin. The peak at the center is also the largest peak and has a reasonably high PSR and low E measures indicating sharp peaks. The same statistics for the MACE and CSDF filters are given in Tables 3.2 and 3.3, respectively. As expected the performance of the RMACE filter is similar to that of the MACE filter.

Table 3.1. Correlation Plane Statistics for RMACE Filter

Image	Specified Intensity at the Origin	Intensity at the Origin	Largest Peak	PSR	Average Energy
mars1.1	20.0	20.0	20.0	5.13	0.173
mars1.7	20.0	20.0	20.0	3.91	0.186
mars1.13	20.0	20.0	20.0	4.58	0.193
mars2.1	10.0	10.0	10.0	3.51	0.160
mars2.7	10.0	10.0	10.0	3.01	0.168
mars2.13	10 0	10.0	10.0	3.01	0.167

Table 3.2. Correlation Plane Statistics for MACE Filter

Image	Specified Intensity at the Origin	Intensity at the Origin	Largest Peak	PSR	Average Energy
mars1.1	20.0	20.0	20.0	9.14	0.086
mars1.7	20.0	20.0	20.0	7.47	0.092
mars1.13	20.0	20.0	20.0	7.99	0.094
mars2.1	10.0	10.0	10.0	5.31	0.078
mars2.7	10.0	10.0	10.0	5.25	0.082
mars2.13	10 0	10.0	10.0	3.88	0.082

Table 3.3. Correlation Plane Statistics for CSDF Filter

Image	Specified Intensity at the Origin	Intensity at the Origin	Largest Peak	PSR	Average Energy
mars1.1	20.0	20.0	20.0	1.02	37.37
mars1.7	20.0	20.0	20.0	1.00	37.39
mars1.13	20.0	20.0	20.0	1.02	37.38
mars2.1	10.0	10.0	12.60	1.00	22.40
mars2.7	10.0	10.0	12.64	1.00	22.41
mars2.13	10 0	10.0	12.53	1.00	22.41

From Table 3.3 it can be seen that the largest peak obtained using CSDF for Class 2 images are not at the center of the correlation plane. The energy scatter of the individual correlation energy levels with the average correlation plane energy of 29.89 is much higher in comparison to that of both RMACE and MACE filters. Also, the PSR values are much lower. However, the variation in PSR and E values over all the test images is greater for both RMACE and MACE filters than for CSDF filter. Thus, RMACE and MACE filters are more sensitive to distortions than the CSDF filter.

The test results of the RMACE filter for both training and nontraining images along with those for the MACE and CSDF filters are summarized in Table 3.4a as tests 1, 2, 3, 4, 5, and 6. A fixed threshold of T = 12.0 was used for classification. If the largest peak anywhere in the

correlation plane was found to exceed this threshold, the input image was classified as belonging to Class 1, otherwise to Class 2. While the training set images are easily recognized, the nontraining images are often misclassified.

The plots of the largest peak anywhere on the correlation plane versus the test image number for mars1 (represented by •) and the test image number for mars2 (represented by *) are shown in Figures 3.7, 3.8, and 3.9 for RMACE, MACE, and CSDF filters, respectively. Figure 3.7 shows six mars1 images below T = 12 and zero mars2 images above this threshold. Thus, the RMACE filter was able to achieve recognition rates of 54 percent and 100 percent for mars1 and mars2 images, respectively. Figure 3.8 is similar to Figure 3.7. However, Figure 3.9 shows all mars1 and mars2 images above the threshold. Hence, the detection rates of 100 percent and 0 percent for mars1 and mars2 images were achieved. However, if the threshold was set to T = 15, then 100 percent detection rates for both mars1 and mars2 images may be obtained.

On the basis of tests 1-6, it can be concluded that, while the sidelobe suppression is acceptable, the RMACE filter does not provide good distortion tolerance. One method to achieve better distortion tolerance is to increase the number of training set images. Tests 1-6 were repeated with the number of class 1 images increased to seven, each spaced two degrees apart in the angle of rotation. The number of class 2 training images were kept at three per object. The results

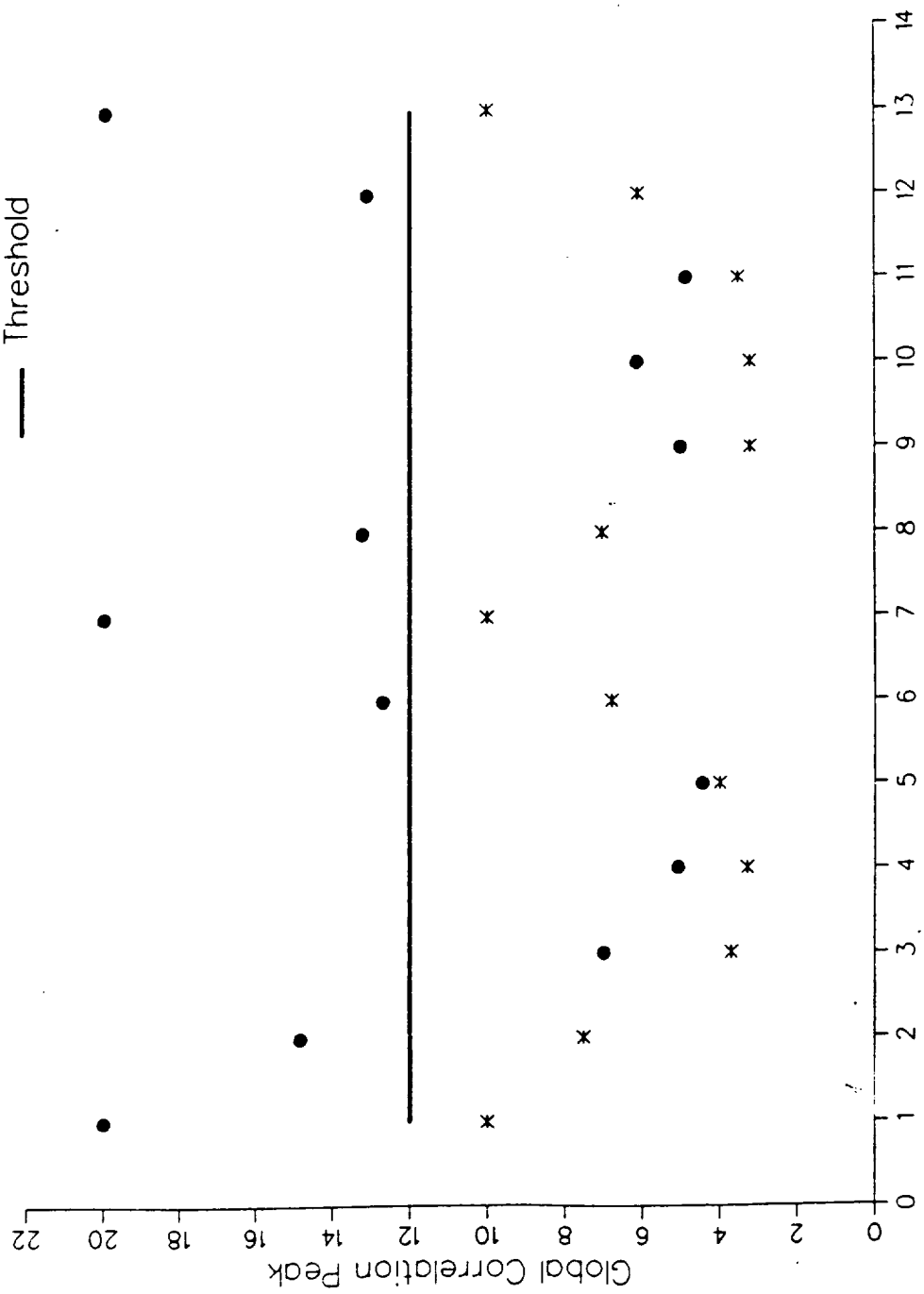

Figure 3.7. Response (at the origin) of the RMACE Filter Constructed with Image Numbers 1, 7, & 13

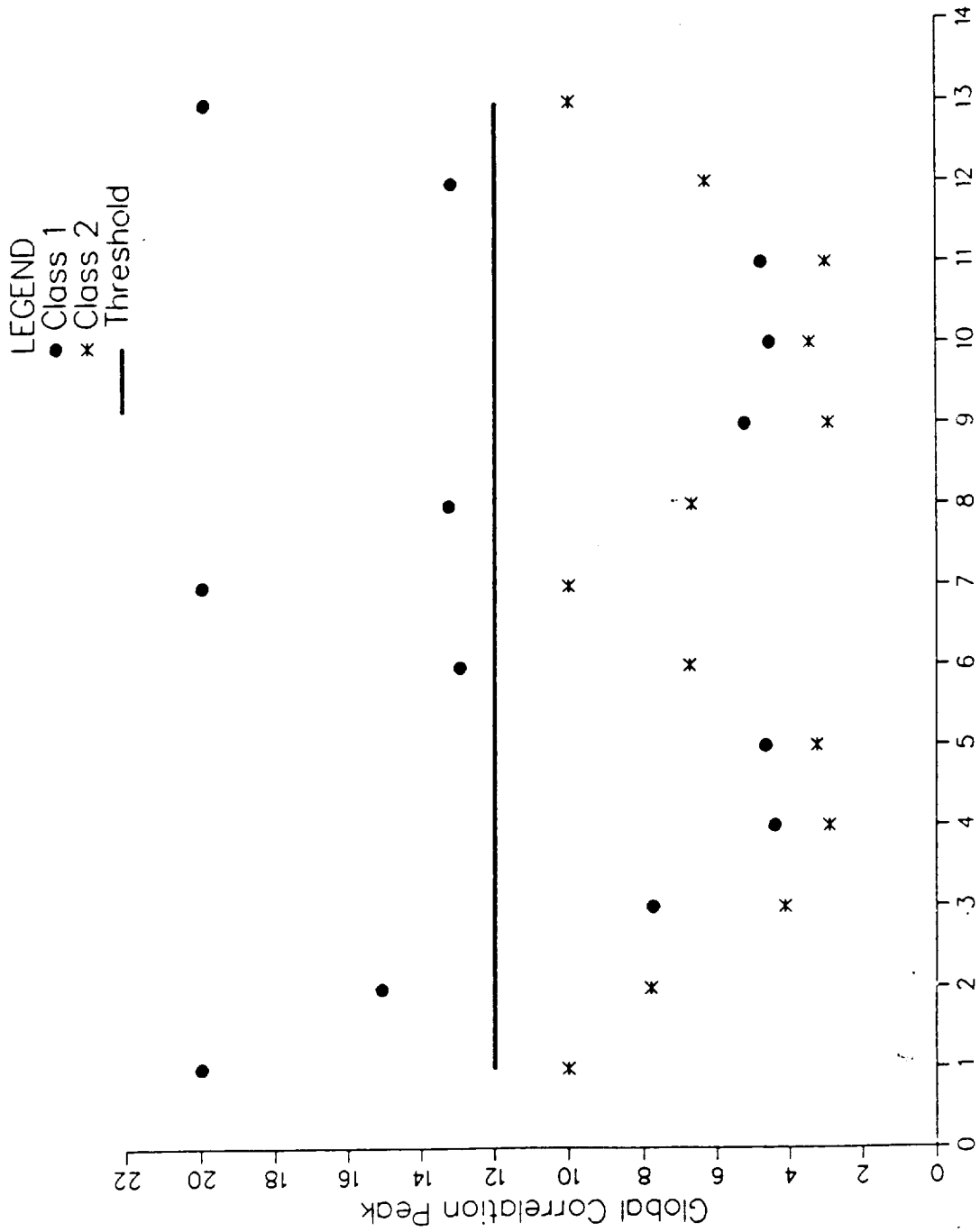

Figure 3.8. Response (at the origin) of the MACE Filter Constructed with Image Numbers 1, 7, & 13

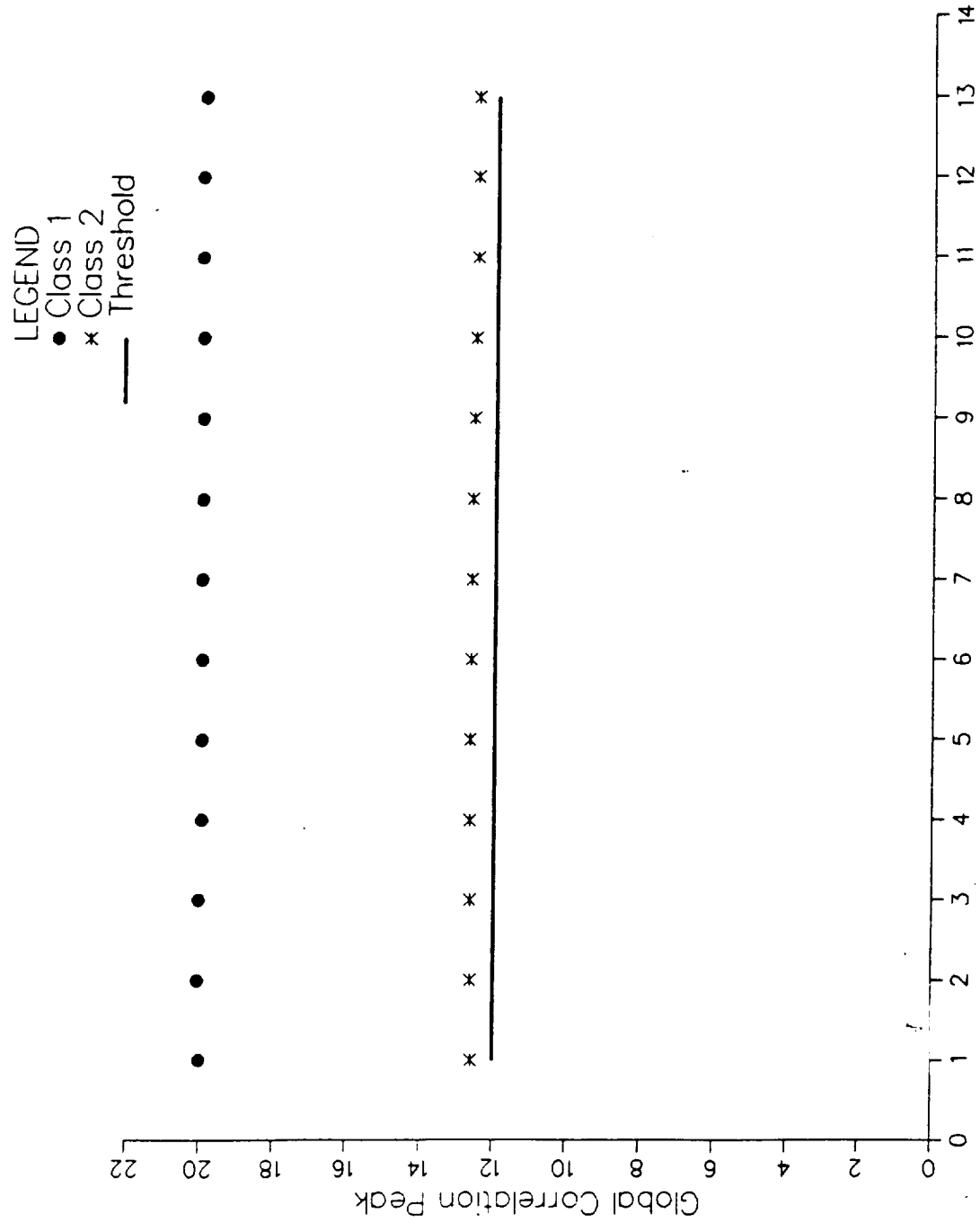

Figure 3.9. Response (at the origin) of the CSDF Filter Constructed with Image Numbers 1, 7, & 13

of these tests (tests 7-12) are summarized in Table 3.4b. It can be observed that the Class 1 recognition rate improved by 46%. Also, the average PSR values increased from 2.67 to 4.21. However, the PSR values for class 2 images have decreased.

To avoid this, the class 2 training set images were also increased to 7 images per class and the same tests (tests 13-18) were repeated and tabulated in Table 3.4c. As can be noted, the effect of increasing the number of training images is to increase the average correlation energy and broaden the correlation peaks.

Table 3.4a. Filter Performance for Three Training Images per Object Class

Test Number	Filter	Object Class	Percent Correct	Average PSR	Average Energy
1	RMACE	mars1	54%	2.67	0.234
2	RMACE	mars2	100%	1.94	0.225
3	MACE	mars1	54%	3.69	0.119
4	MACE	mars2	100%	2.58	0.112
5	CSDF	mars1	100%	1.01	37.38
6	CSDF	mars2	0%	1.00	22.41

Table 3.4b. Filter Performance for Seven Class 1 and Three Class 2 Training Images

Test Number	Filter	Object Class	Percent Correct	Average PSR	Average Energy
7	RMACE	mars1	100%	4.21	0.281
8	RMACE	mars2	100%	1.70	0.323
9	MACE	mars1	100%	4.19	0.140
10	MACE	mars2	100%	2.12	0.156
11	CSDF	mars1	100%	1.01	37.45
12	CSDF	mars2	0%	1.00	22.45

Table 3.4c. Filter Performance for Seven Training Images per Object Class

Test Number	Filter	Object Class	Percent Correct	Average PSR	Average Energy
13	RMACE	mars1	100%	3.84	0.301
14	RMACE	mars2	100%	2.10	0.291
15	MACE	mars1	100%	3.76	0.150
16	MACE	mars2	100%	2.48	0.139
17	CSDF	mars1	100%	1.00	37.45
18	CSDF	mars2	0%	1.00	22.44

3.9.2. Observations

On the basis of the results of the previous section, it can be concluded that the distortion tolerance of the RMACE filter may be easily improved by increasing the number of training set images with distortion. The correlation plane PSR would then be reduced but it is still sufficiently high to facilitate easy detection. Unlike the CSDF, the average correlation plane energy is much lower for the RMACE filter. Though the RMACE filter produces slightly larger correlation energy than that of the MACE filter, it does not provide high sidelobes. Narrow correlation peaks provide better location of the target but make the filter's distortion invariance poor and its noise performance worse. Thus, reducing the requirements on the sharpness of the correlation peak is attractive.

3.10. Noise Test Results

The ability of RMACE filters to recognize the object was tested under the following conditions:

1. When the intensity levels of the input images are varied by multiplying it with a constant factor.
2. When the input images are corrupted by a zero mean white noise.
3. When the intensity of each pixel of the input image is affected by a random bias term.

3.10.1. Input Image Intensity Correction

The peak correlation at the origin depends on the intensity of the input image. For example, if the intensity of the test image is multiplied by a factor α then the correlation peak is also multiplied by the same factor α. This problem may be overcome by normalizing the output. The normalizing technique used here is the normalization using the average value of the image.

In order to make the filter robust against any intensity scaling, the correlation peak output constraints at the origin in Eq. (3.8) is modified to obtain the normalized output as

$$\frac{\boldsymbol{X}_i^{\dagger}\boldsymbol{H}}{\alpha_i} = u_i, \qquad i = 1,2,.....N \tag{3.70}$$

where α_i is the average value of the test image $\mathbf{X}_i$. Hence, to avoid correlation peak variation due to intensity scaling the new constraints in Eq. (3.70) are imposed during the filter synthesis. The performance of the filter synthesized using normalization was found to remain independent of the scale factor, unlike the response of the filter without normalization.

The performance of normalized RMACE filter is also examined in the presence of noise. The effect of zero mean white noise on the performance of the filter is studied by observing the degradation of the filter output with increasing

noise power. Since the noise is zero mean, the response of the normalized filter is expected to be good.

The normalized RMACE filter was synthesized with seven images of mars1 and mars2. As before the correlation peak output was specified to be 20 and 10 for all the images in Class 1 and Class 2, respectively. White, zero-mean, Gaussian noise of different signal to noise ratio (SNR) values were added to all the images in the database (all 26 images). Then, the normalized filter was applied on all the images.

The peak correlation value, the PSR, and the energy of the correlation plane were noted and averaged over all the images. The results of the test are summarized in Table 3.5 for various SNR values between 20 dB and 0 dB.

The average behavior of the global correlation peak over ten Class 1 and Class 2 images for SNR of 20 dB, 15 dB, 10 dB, 5 dB, and 0 dB was considered. The global peak intensity and the true peak were observed to drop steadily for SNR values between 20 dB and 5 dB and increased for the SNR of 0 dB. From the average PSR values it can be seen from Table 3.5 that for SNR > 5 dB sharp peak occurred. Also, it was observed that the global correlation peak occurred away from the origin of the correlation plane for SNR value < 5 dB. For higher SNR values, the global correlation peak always occurred at the center of the correlation plane. However, for lower SNR values (SNR < 5 dB), the global correlation peak occurred at

points away from the center of the correlation plane, and detection errors were encountered.

The object recognition rates achieved by the filter in the presence of noise is also summarized in Table 3.5. It can be noted that the recognition rate remains well above 90 percent even for SNR of 15 dB. This demonstrates the enhanced noise tolerance of the RMACE filter. From these tests it can be concluded that the RMACE filter can tolerate a significant amount of noise (SNR = 10 dB) before the sidelobes dominate the correlation peak at the origin. Also, it can be seen from the table that the PSR of the correlation peak slowly degrades with increasing noise.

Table 3.5. RMACE Filter Performance with Noise

SNR in dB.	% Recognition		PSR	
	mars1	mars2	mars1	mars2
20	100%	100%	3.40	1.75
15	100%	92%	3.00	1.51
10	100%	70%	2.09	1.17
5	100%	0%	1.25	1.08
0	100%	0%	1.07	1.05

3.10.2. Input Image Bias Correction

Another practical issue associated with filter synthesis is the effect of input bias. A random bias term can be considered as a constant noise term added uniformly to the

entire input image. This bias term results in the degradation of correlation plane PSR.

To avoid this, it is required that the output of the filter for a random but spatially constant bias signal be zero. If this condition is satisfied, uniform bias terms at the input will not affect the correlation plane PSR. So the required filter must satisfy

$$\sum_{i=1}^{M} \sum_{j=1}^{M} \bar{h}(i,j) = 0. \qquad (3.71)$$

Thus, to ensure invariance to uniform bias signals, the filter should satisfy the condition $H(0) = 0$. This condition may be easily imposed on the filter synthesis by including a constant image in the training set and setting the corresponding output to zero.

An example to demonstrate the effectiveness of the proposed scheme for protecting PSR degradation resulting from input bias is given below. RMACE and MACE filters (denoted by h_{R1} and h_{M1}) for a single training image were synthesized from one of the set of mars1 images. A second set of filters, both RMACE and MACE (denoted by h_{R2} and h_{M2}), were also synthesized for the same training image with the additional constraint in Eq. (3.71). The desired output correlation peak values for all four filters were specified to be 20. Four filters were then correlated with ten biased versions of the training

image. The bias levels, the correlation plane PSR values for all four filters are indicated in Table 3.6.

From Table 3.6, it can be seen that the performance of the MACE filter h_{M1} synthesized without imposing the zero mean condition is clearly affected by the bias levels. However, the performance of the zero mean MACE filter h_{M2} is not affected by any bias added to the input image. On the other hand, the performance of both zero mean RMACE h_{R1} and the

Table 3.6. Filter Performance with Input Bias Levels

	Correlation Plane PSR Values			
	RMACE		MACE	
Bias	Filter h_{R1} with no Bias Correction	Filter h_{R2} with Bias Correction	Filter h_{M1} with no Bias Correction $\times 10^3$	Filter h_{M2} with Bias Correction $\times 10^3$
10	13.51	13.54	43.60	16.38
20	13.49	13.54	14.55	16.38
30	13.47	13.54	7.28	16.38
40	13.44	13.54	4.37	16.38
50	13.40	13.54	2.91	16.38
60	13.35	13.54	2.08	16.38
70	13.30	13.54	1.56	16.38
80	13.24	13.54	1.21	16.38
90	13.17	13.54	0.97	16.38
100	13.10	13.54	0.80	16.38

filter without the zero mean constraint. h_{R2} are quite similar. Thus, the RMACE filter without the additional constraint in Eq. (3.71) is not affected by the bias levels. Hence, it can

be concluded that the zero mean condition imposed during the filter synthesis is necessary to guarantee immunity for MACE filters against the random input bias levels. However, the RMACE filter preserves constant correlation plane PSR values against input bias levels even with no input bias correction.

3.11. Results of Phase Optimization

The performance of the filter, with phase optimization of the correlation output constraint discussed in Section 3.7, is presented here. The same two-class problem as before is considered. For various θ_1 and θ_2 values, the average energy per training image was evaluated and summarized in Table 3.7. It can be seen that the proposed phase optimization procedure reduces the output correlation plane energy from 0.1119 (θ_1 = 0 and θ_2 = 0) to 0.1096 when θ_1, $\theta_2 = \pi/2$. This represents an energy reduction of 2.1 percent. Even though the reduction is not much it shows the potential improvement in performance by proper selection of the correlation output constraint.

Hence the proposed method for the selection of the phases of the correlation output constraints leaves the magnitudes values unaffected while reducing the output correlation energy. This improves the detection/discrimination performance of the filter. The exact amount of reduction in energy depends on the training images used.

Table 3.7. Correlation Plane Energy for Phase Optimization

θ_1	θ_2	Correlation Plane Energy
0	0	0.1119
0	π	0.1207
$\pi/2$	$\pi/2$	0.1096
$\pi/2$	$3\pi/2$	0.1233

3.12. Summary

In this chapter the development of a real filter that produces sharp output correlation peak with a controlled peak value was presented. Also, it was shown that the energy in the output correlation plane may be further reduced by the proper selection of the phases of the correlation output constraint. The performance of the RMACE filter was examined for distortion and noise tolerance. It was shown that the distortion tolerance of the filter can be improved by increasing the number of training set images. The RMACE filter was thus shown to have many attractive features and properties useful for pattern recognition.

CHAPTER 4

Real-Valued MVSDF-MACE Filter

Recent developments in the field of distortion invariant pattern recognition using synthetic discriminant functions include the minimum variance synthetic discriminant function (MVSDF) and minimum average correlation energy (MACE) filters. MVSDF filters are designed to minimize the output noise variance due to input noise whereas MACE filters are designed to maximize the correlation peak at the origin. In Chapter 3, the design of real MACE filters was considered and their performance studied. In this chapter, the design of real filters which minimize a performance measure which is a linear combination of output correlation energy and output variance due to noise is considered. This filter is referred to as improved real-valued MVSDF-MACE filters. Simulation studies are presented to illustrate the performance improvements that result from the MVSDF-MACE filter.

4.1. Motivation for the Real-Valued MVSDF-MACE Filter

In simulation studies of previous chapters, real MACE filters designed to minimize the average correlation plane output energy were found to produce impressive easily detectable sharp correlation peaks. However, MACE filter have two drawbacks. First, since the MACE filter design does not explicitly include noise effects, it has poor noise

performance. Second, MACE filters are sensitive to non-training images. Since the MACE filter produces sharp correlation peaks, which is an indication of edge enhancement, the distortion tolerance of this filter is poor. That is, narrow correlation peaks provide easy detection but make the filter more sensitive to distortions and noise. Thus, broader correlation peaks would improve the filter's distortion and noise tolerance.

MVSDF filters overcome these problems of MACE filters. The MVSDF filter is designed to minimize the output noise variance due to input noise while satisfying the specified output at the origin of the correlation plane. However, the resulting correlation peak may not be sharp enough for easy detection. Hence, efforts were directed to develop filters that provided both acceptable noise and distortion tolerance and easily detectable sharp correlation peaks at the origin.

Sudharasanan, Mahalanobis, and Sundareshan [16] proposed an improved synthetic discriminant function in the space domain which gives sharp correlation peaks and better noise performance simultaneously. The frequency response of this filter is a complex function. In this chapter, real-valued MVSDF-MACE filter which provide better noise and distortion tolerance than the RMACE filters while providing sharp correlation peaks is developed.

The real-valued improved MVSDF-MACE filter is developed in the discrete frequency domain. The filter development is

discussed in the next section and simulation results are presented in the following sections.

4.2. Real-Valued MVSDF-MACE Filter Design

As mentioned earlier real-valued MVSDF-MACE filter is designed to satisfy the output constraints at the origin of the correlation plane while simultaneously minimizing the output variance due to noise as well as the correlation plane energy. The filter development in the discrete frequency domain follows that given in Reference [16] and is described below.

Let X_1, X_2, ..., X_N, denote N column vectors of dimension d representing N training images in the discrete frequency domain. Let the image under test be corrupted by a noise term n. Hence, the resulting test image can be written as

$$X_{it} = X_i + n. \tag{4.1}$$

The output of the filter with this test image is given by

$$\begin{aligned} H^T X_{it} &= H^T (X_i + n) \\ &= H^T X_i + H^T n \\ &= u_i + H^T n \end{aligned} \tag{4.2}$$

where H is a real filter vector in the frequency domain and u_i is the specified output for the test image X_i. Let the noise vector n be a zero-mean additive, stationary random variable. Then the mean of the random component $H^T n$ in the output is zero. The variance of this term is given by

$$\begin{aligned} var\{H^T n\} &= E\{H^T n n^T H\} \\ &= H^T E\{n^T n\} H \\ \sigma^2 &= H^T R_n H \end{aligned} \qquad (4.3)$$

where R_n is a dxd covariance matrix of the noise vector n.

The objective of the improved MVSDF-MACE filter is to minimize the output noise variance in Eq. (4.3) and the average correlation place output energy. The average correlation plane energy from Chapter 3 is given by

$$E_{av} = H^T D H \qquad (4.4)$$

where D is a diagonal matrix with diagonal elements equal to the samples of the average power spectrum of the training images. Hence, the compromise measure between the noise tolerance and the sharpness of the correlation peak can be written as

$$\begin{aligned} C_H &= \alpha_1 E_{av} + \alpha_2 \sigma^2 \\ &= H^T (\alpha_1 D + \alpha_2 R_n) H \end{aligned} \qquad (4.5)$$

where α_1 and α_2 are nonnegative constants chosen to trade-off between the output noise variance and the output correlation energy. Hence, minimization of C_H minimizes both correlation energy $H^T D H$ as well as noise variance $H^T R_n H$ and would yield filters with improved noise performance and sharp correlation peaks. For $\alpha_1 = 0$ and $\alpha_2 > 0$, C_H is equal to $\alpha_2 \sigma^2$ and noise tolerance will be maximized. On the other hand, for $\alpha_1 > 0$

sharpness will be maximized. For other α_1 and α_2 values a compromise between these two extremes is obtained.

Hence, the problem is to minimize C_H in Eq. (4.15) subject to the constraint given by

$$X^T H = u \tag{4.6}$$

where $X = [X_1, X_2, \ldots, X_N]^T$ is a dxN data matrix, 'T' denotes the transpose operation, and u is assumed to be a real N dimensional output vector. For real training images, the real-valued improved MVSDF-MACE filter solution vector may be found using the method of Lagrangian multipliers as was done in Chapter 3 as

$$H_{MM} = (\alpha_1 D + \alpha_2 R_n)^{-1} X_R \{X_R^T (\alpha_1 D + \alpha_2 R_n)^{-1} X_R\}^{-1} u \tag{4.7}$$

where X_R is the real part of the data matrix X. When $\alpha_1 = 0$, H_{MM} becomes H_{RMVSDF}, is a real-valued frequency domain MVSDF filter, given by

$$H_{RMVSDF} = R_n^{-1} X_R \{X_R^T R_n^{-1} X_R\}^{-1} u. \tag{4.8}$$

When $\alpha_2 = 0$, H_{MM} becomes H_{RMACE} given in Eq. (3.32).

For the special case of white noise, the matrix R_n can be written as

$$R_n = \sigma_n^2 I_d \qquad (4.9)$$

where σ_n^2 is the variance of the white noise and I_d is an identity matrix. For this special case, the real-valued improved filter in Eq. (4.7) may be reduced to

$$H_{MM} = D_c^{-1} X_R \{X_R D_c^{-1} X_R\}^{-1} u \qquad (4.10)$$

where

$$D_c = \alpha_1 D + \alpha_2 \sigma_n^2 I_d \qquad (4.11)$$

is a diagonal matrix. Hence, the matrix inversion in Eq. (4.10) is relatively easy. Next section discusses the distortion tolerance characteristics of the improved MVSDF-MACE filter.

4.3. Distortion Tolerance Results

The performance characteristics of the real-valued improved MVSDF-MACE filter were evaluated using computer simulation results. As before, two sets of 23 images of MARS Landscape, Class 1 and Class 2, rotated through angles 1-13 degrees were used to test the filter performance. The images were of size 128x128 pixels. The rotated images were obtained using a computer algorithm. For the filter construction, four images from each of Class 1 and Class 2, rotated through angles 1, 5, 9, and 13 degrees were used. The improved MVSDF-MACE filter in Eq. (4.7) with different α_1 and α_2 values were synthesized. White Gaussian noise with a variance of 1.0 which represents a signal-to-noise ration (SNR) of 33 dB was

used in the filter synthesis. The required correlation output values were specified as 20 for Class 1 images and 10 for Class 2 images arbitrarily.

The average correlation plane energy $E = H^T DH$ and the output noise variance $\sigma^2 = \sigma_n^2(H^T H)$ were indicative of filter's the performance. A low average correlation energy with the specified peak value corresponds to sharper correlation peaks, a higher correlation plane peak-to-side-lobe ratio (PSR), and ratio more sensitivity to distortions. On the other hand, lower output noise variance implies higher tolerance to distortion and noise with lower correlation plane PSR values. Table 4.1 presents the average correlation energy (E) and the output noise variance (σ^2) for 8 different α_1 and α_2 combinations.

From the table it can be seen that the real-valued minimum average correlation energy (RMACE) filter which corresponds to $\alpha_1 = 1$ and $\alpha_2 = 0$ achieved the smallest average correlation plane energy of 0.064 with the output variance of 75.53, whereas the real-valued minimum variance synthetic discriminant function (RMVSDF) filter, that is, for $\alpha_1 = 0$ and $\alpha_2 = 1$ achieved the smallest output noise variance of 0.66 with the average correlation energy of 32.0. For other values of α_1 and α_2 the correlation energy and the output noise variance lie in between these extreme values.

Table 4.1. Real-Valued MVSDF-MACE Filter Performance for SNR of 33 dB and Desired Output Values at the Origin: 20 for Class 1 and 10 for Class 2

α_1	α_2	Average Energy	Variance of the Output at the Origin
1.00	0.0	0.064	75.53
1.00	1.0	0.065	58.98
1.00	10.0	0.070	38.34
1.00	100.0	0.113	19.17
1.00	1000.0	0.360	7.21
0.10	1000.0	1.264	2.62
0.01	1000.0	4.118	1.15
0.00	1.0	32.000	0.66

For performance comparison of the real-valued improved MVSDF-MACE filter with that of RMACE and RMVSDF filters, $\alpha_1 = 1.0$ and $\alpha_2 = 100$ referred to as MM1 and $\alpha_1 = 1.0$ and $\alpha_2 = 1000$ referred to as MM2 were considered. Figures 4.1, 4.2, 4.3, and 4.4 present three-dimensional plots of the output correlation plane intensity with RMACE, MM1, MM2, and RMVSDF filters, respectively. As can be seen from the plots, the RMACE filter produces sharp correlation peak at the origin of the correlation plane with an output noise variance of 75.53. Though the RMVSDF filter achieves the lowest output noise variance of 0.66 the correlation plane output of Figure 4.4 shows that the peak is not sharp enough for easy detection.

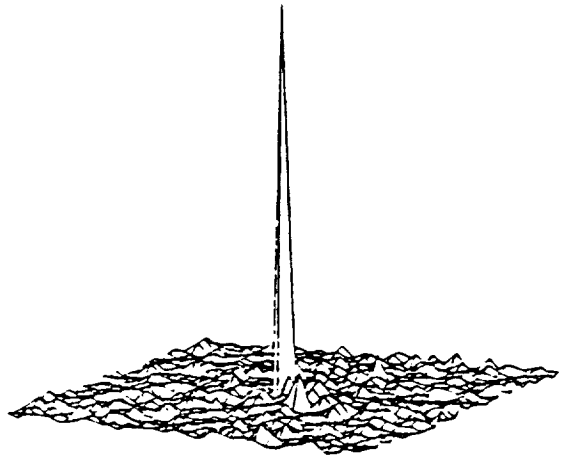

Figure 4.1. Correlation Plane Output Intensity with the RMACE Filter

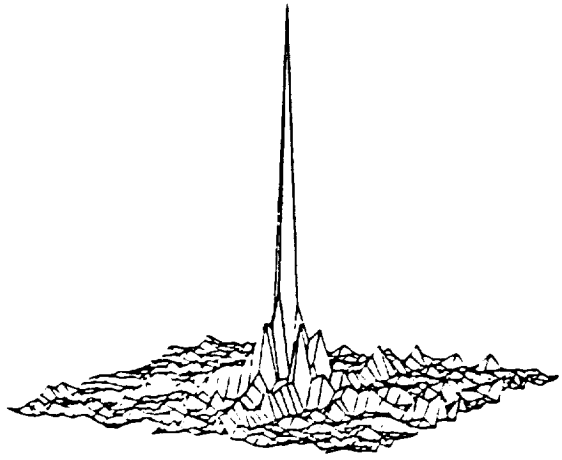

Figure 4.2. Correlation Plane Output Intensity with the MM1 Filter

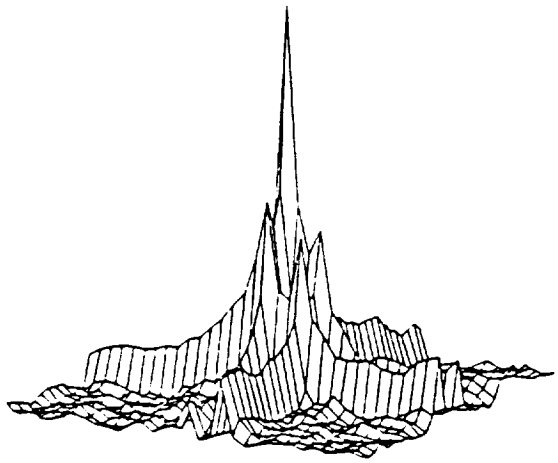

Figure 4.3. Correlation Plane Output Intensity with the MM2 Filter

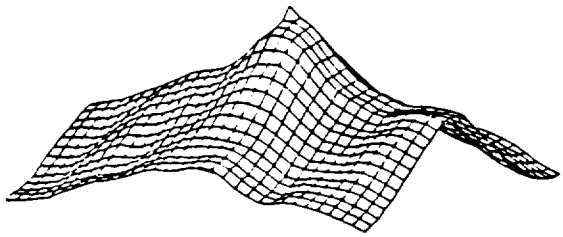

Figure 4.4. Correlation Plane Output Intensity with the RMVSDF Filter

From Figures 4.2 and 4.3 it can be seen that the improved MVSDF-MACE filters MM1 and MM2 produce reasonably sharp peaks with acceptable output variances of 19.17 and 7.21 and average correlation energies of 0.1132 and 0.3597, respectively. Thus, the improved MVSDF-MACE filter reduces the output noise variance considerably while still maintaining easily detectable sharp correlation peaks with low sidelobes.

To compare further the RMACE, MM1, MM2, and RMVSDF filters with respect to distortion tolerance, these filters were tested against all 26 images for discrimination. As a measure of the sharpness of the correlation peak, the smallest slope magnitude of the correlation response between the peak response and the response at an adjacent pixel and the average correlation plane energy were found and tabulated. Tables 4.2, 4.3, 4.4, and 4.5 list the correlation plane statistics for the training images with RMACE, MM1, MM2, and RMVSDF filters, respectively. It may be seen that all the training images when filtered through the RMACE, MM1, and MM2 filters produced the specified correlation peak output of 20 for Class 1 and 10 for Class 2 images at the origin of the correlation plane. The correlation peak at the origin was also the largest peak anywhere in the correlation plane. However, even though the RMVSDF filter yielded the specified correlation output at the origin, the largest peak occurred always off from the center of the plane.

Table 4.2. Correlation Plane Statistics with the RMACE Filter

Image	Specified Output	Peak at Origin	Global Peak	Average Energy	Slope Near Peak
mars1.1	20.00	20.00	20.00	0.21	17.97
mars1.5	20.00	20.00	20.00	0.23	17.17
mars1.9	20.00	20.00	20.00	0.24	16.63
mars1.13	20.00	20.00	20.00	0.24	18.00
mars2.1	10.00	10.00	10.00	0.19	7.20
mars2.5	10.00	10.00	10.00	0.21	6.90
mars2.9	10.00	10.00	10.00	0.20	7.35
mars2.13	10.00	10.00	10.00	0.21	7.25

Table 4.3. Correlation Plane Statistics with the MM1 Filter

Image	Specified Output	Peak at Origin	Global Peak	Average Energy	Slope Near Peak
mars1.1	20.00	20.00	20.00	0.35	12.12
mars1.5	20.00	20.00	20.00	0.35	11.19
mars1.9	20.00	20.00	20.00	0.36	10.40
mars1.13	20.00	20.00	20.00	0.35	12.13
mars2.1	10.00	10.00	10.00	0.28	4.60
mars2.5	10.00	10.00	10.00	0.26	4.53
mars2.9	10.00	10.00	10.00	0.26	4.74
mars2.13	10.00	10.00	10.00	0.27	5.34

Table 4.4. Correlation Plane Statistics with the MM2 Filter

Image	Specified Output	Peak at Origin	Global Peak	Average Energy	Slope Near Peak
mars1.1	20.00	20.00	20.00	0.76	7.17
mars1.5	20.00	20.00	20.00	0.77	5.40
mars1.9	20.00	20.00	20.00	0.79	4.15
mars1.13	20.00	20.00	20.00	0.81	6.00
mars2.1	10.00	10.00	10.00	0.50	2.99
mars2.5	10.00	10.00	10.00	0.44	2.23
mars2.9	10.00	10.00	10.00	0.45	2.23
mars2.13	10.00	10.00	10.00	0.52	2.77

Table 4.5. Correlation Plane Statistics with the RMVSDF Filter

Image	Specified Output	Peak at Origin	Global Peak	Average Energy	Slope Near Peak
mars1.1	20.00	20.00	20.04	48.03	0.04
mars1.5	20.00	20.00	20.47	51.94	0.03
mars1.9	20.00	20.00	20.62	51.93	0.03
mars1.13	20.00	20.00	20.00	46.96	0.23
mars2.1	10.00	10.00	14.09	27.31	0.03
mars2.5	10.00	10.00	14.02	27.30	0.06
mars2.9	10.00	10.00	14.05	27.28	0.02
mars2.13	10.00	10.00	14.11	27.45	0.01

As can be expected, the average correlation plane energy of the output of the RMACE filter was lower and the correlation peak slope value higher compared to those of other filters. Both improved filters were found to yield reasonably lower correlation energies and higher peak slope values. Variation in correlation peak slope and average energy values for different images were much lower for the improved filters than for the RMACE filter. Thus, improved MVSDF-MACE filters exhibited more distortion tolerance capability.

As mentioned in Chapter 3, it is more likely that the peak occurs below the specified output value. Hence, for image classification a predetermined threshold value of $T = 12.0$ was used. If the correlation plane peak is above this value then the image was recognized as Class 1 and otherwise as Class 2. Figures 4.5 through 4.8 show the global correlation peak values versus the test image number for all four filters. It may be seen from Figure 4.5 that three images of Class 1 have output peak values lower than the threshold value of $T = 12.0$. Hence, the recognition rates with the RMACE filter were 76.9 percent for Class 1 images and 100 percent for Class 2 images. Figures 4.6 and 4.7 show 100 percent recognition rates for both classes of images with the improved MVSDF-MACE filters. Figure 4.8 shows the output peaks of all the images to be above the threshold value and, hence, the recognition rates were 100 percent and 0 percent for Class 1 and Class 2 images, respectively.

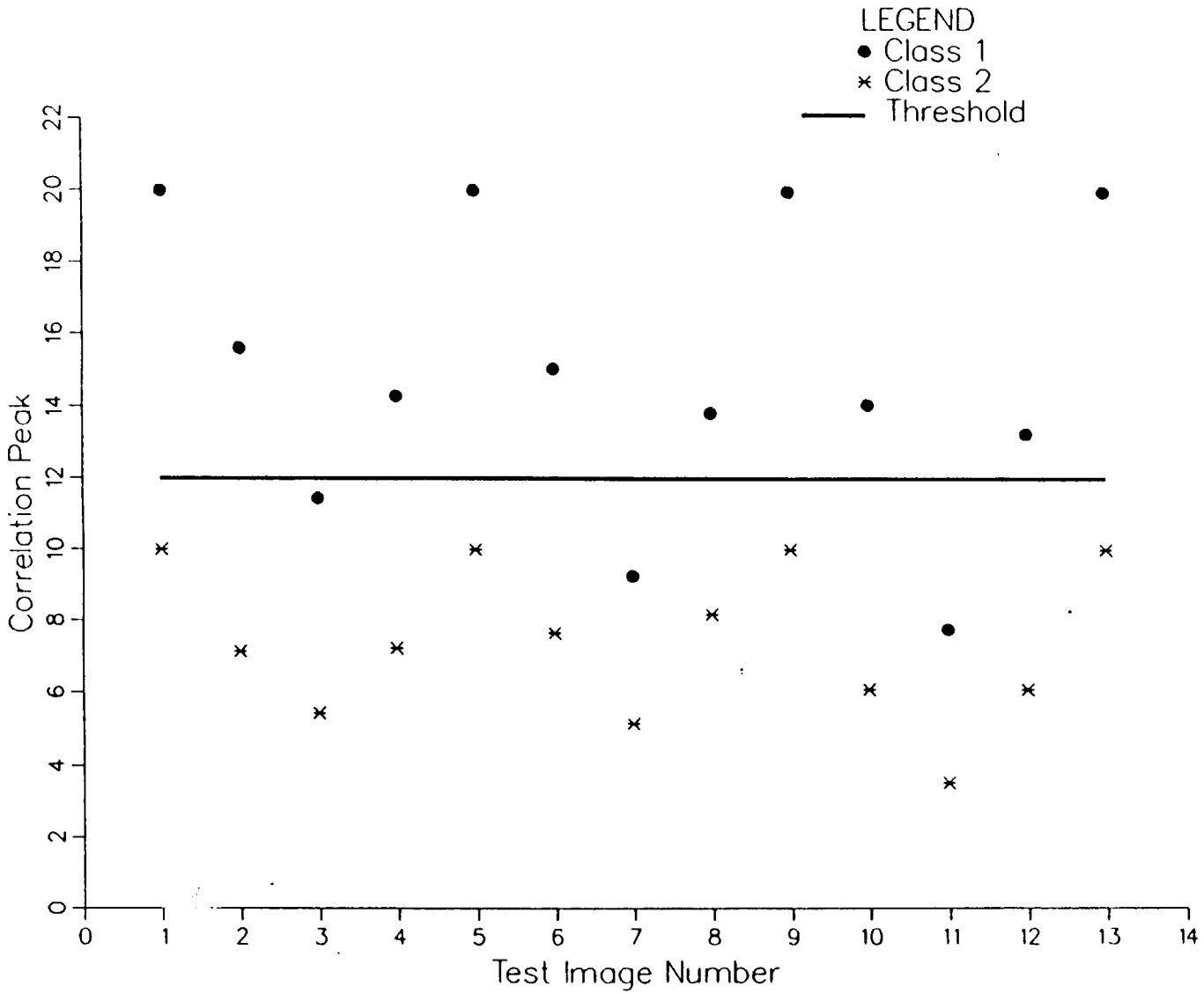

Figure 4.5. Response (at the origin) of the RMACE Filter Constructed with Image Numbers 1, 5, 9, & 13

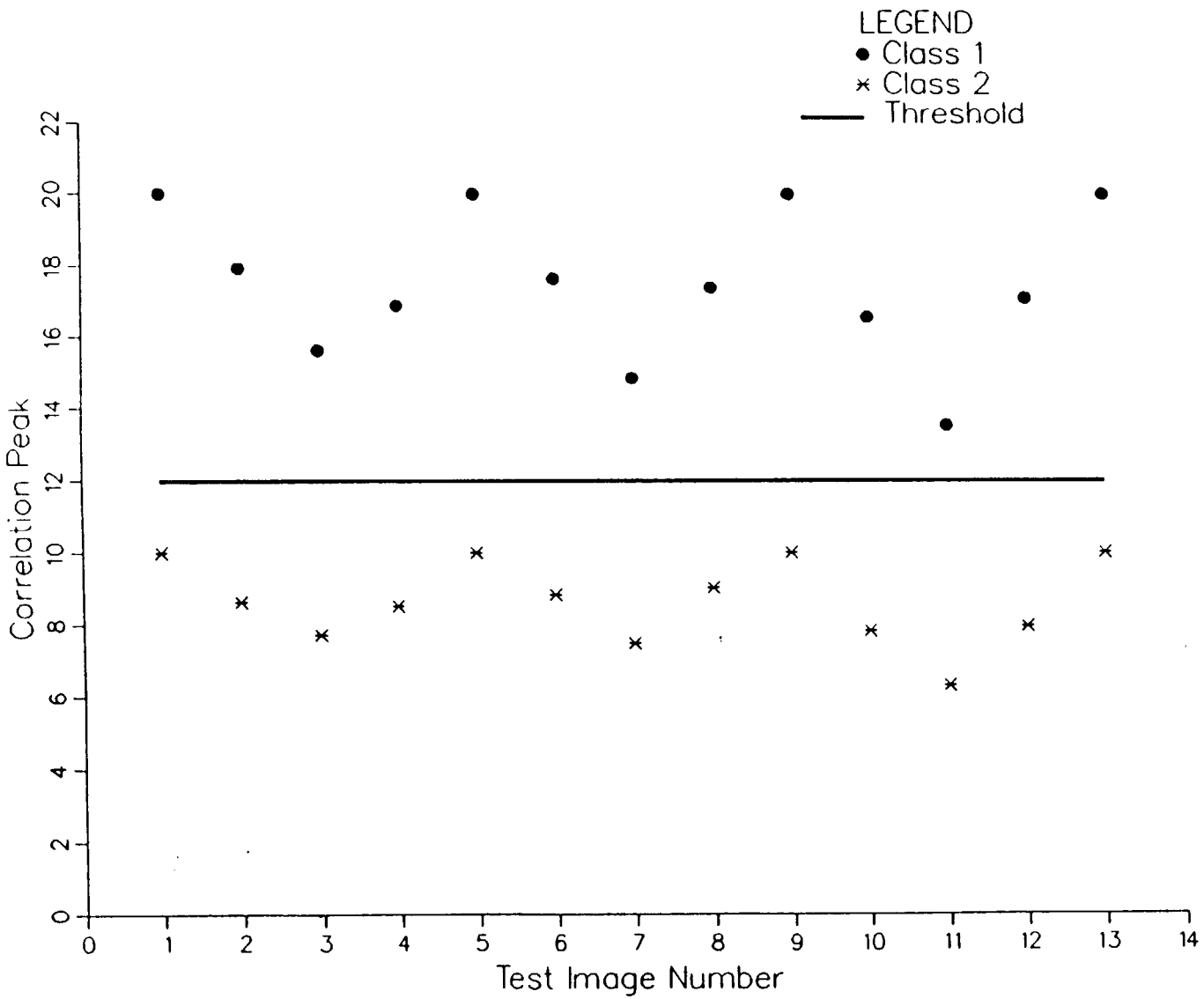

Figure 4.6. Response (at the origin) of the MM1 Filter Constructed with Image Numbers 1, 5, 9, & 13

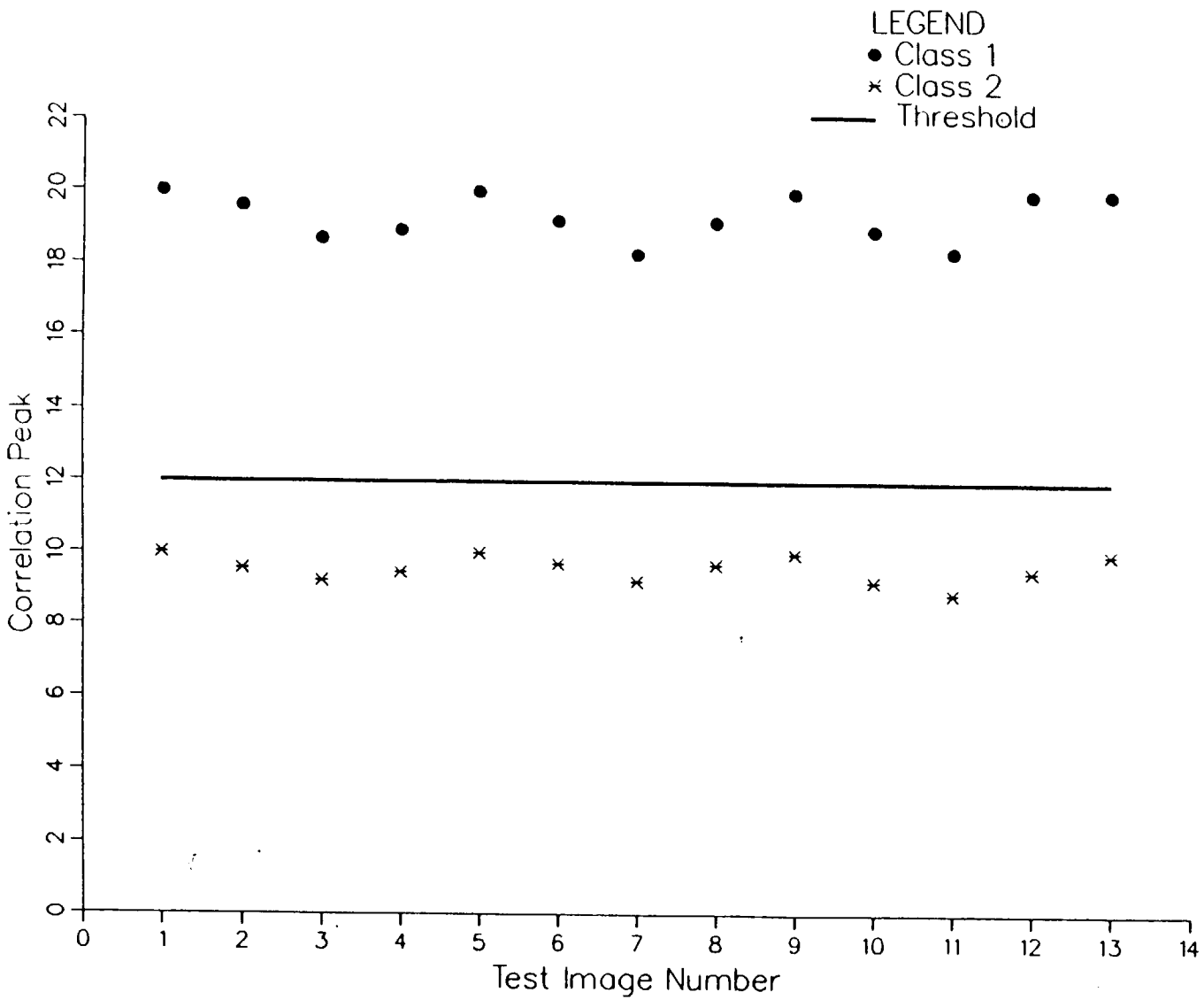

Figure 4.7. Response (at the origin) of the MM2 Filter Constructed with Image Numbers 1, 5, 9, & 13

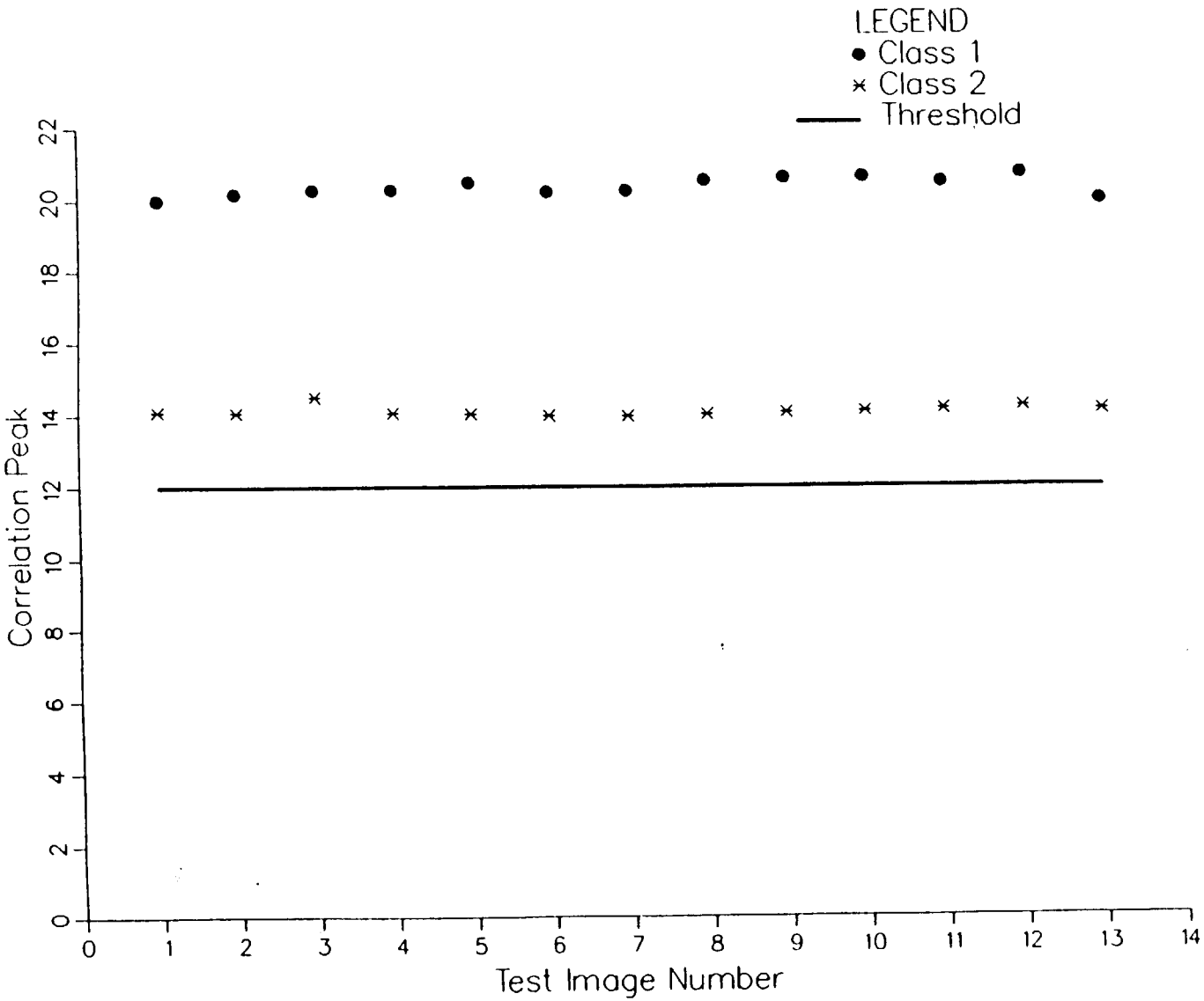

Figure 4.8. Response (at the origin) of the RMVSDF Filter Constructed with Image Numbers 1, 5, 9, & 13

From the results of the above tests, it can be concluded that an improved MVSDF-MACE filter designed with a proper choice for α_1 and α_2 will be capable of providing higher distortion tolerance than that of RMACE filters. The correlation sharpness near the peak is reduced, but is still high enough for easy detection. Thus, by reducing the sharpness requirements of the correlation peak, the filter's distortion invariance and noise performance can be improved. This can also be verified from the discussion of the noise analysis presented in the next section.

4.4. Noise Analysis

One of the practical issues related to filter synthesis is the effect of noise in input images. Hence it is necessary to study the effect of noise on the filter performance. In this section the performance of the improved MVSDF-MACE filters are compared with those of RMACE and RMVSDF filters in the presence of noise.

The effect of zero-mean, white Gaussian noise on the performance of the filters was investigated by studying the degradation of the filter output with increasing noise power. The same filters constructed in the previous section were used. Ten test images were constructed from the training images by adding white Gaussian noise to give signal to noise ratios (SNR) of 20 dB, 15 dB, 10 dB, 5 dB, and 0 dB each with two different seed values. The noisy images were then passed

through the RMACE, MM1, MM2, and RMVSDF filters for noise analysis.

Typical three-dimensional plots of the correlation plane output intensity of a noisy image with a signal to noise ratio of 10 dB are shown in Figure 4.9 through 4.12. Figure 4.9, the output of the RMACE filter, shows large sidelobes in comparison to the correlation plane output without noise as shown in Figure 4.1. However, comparing the correlation plane outputs of the improved MVSDF-MACE filter for noisy images (Figures 4.10 and 4.11) to those for noiseless images (Figures 4.2 and 4.3) it is noted that the changes are insignificant. This verifies the noise tolerance capability of the MVSDF-MACE filter.

The peak value at the origin, the largest peak in the correlation plane, slope near the correlation peak and average correlation energy were noted and averaged over all the training images of each class. The results are summarized in Tables 4.6, 4.7, 4.8, and 4.9 for RMACE, MM1, MM2, and RMVSDF filters, respectively.

For the RMACE filter the average correlation energy for Class 1 images increased from 0.724 to 10.778 and the correlation peak slope reduced from 17.05 to 5.17 when the noise power was increased such that SNR decreased to 0 dB from 20 dB. The same changes were noted for Class 2 images. However, in the case of the improved MVSDF-MACE filters these values did not vary significantly. That is, in the case of

the MM1 filter, for the same change in the noise power, the average correlation energy of Class 1 images varied from 0.458 to 4.711. Also, the correlation peak slope at 0 dB SNR with the MM1 filter was 5.67 compared to 5.17 with the RMACE filter. Similar results were achieved with the improved filter MM2. Thus, it shows that the performance of improved MVSDF-MACE filter in the presence of noise is better than that of RMACE filters.

Further, for the improved MVSDF-MACE filters, the global peaks in the correlation plans were found at the center of the correlation plane, whereas, the global peaks with the RMACE filter in the presence of noise occurred sometimes away from the center of the correlation plane. With the same threshold of $T = 12$, the training image recognition rates of the RMACE filter were 100 percent for Class 1 and 80 percent for Class 2 images, whereas, 100 percent training image recognition rates for both Class 1 and Class 2 images were obtained with the improved MVSDF-MACE filters.

It may be seen form Table 4.9 that when the noise to the test image was increased, the correlation plane energy and the peak slope in the outputs of the RMVSDF filter change very little. However, as mentioned before the peaks were not sharp.

Table 4.6. Noise Analysis with the RMACE Filter

Image Set	SNR in dB	Correlation Peak	Average Energy	Slope Near the Peak
Class 1	20	19.76	0.724	17.05
	15	19.43	1.726	16.45
	10	18.43	4.380	14.92
	5	16.44	10.060	11.86
	0	17.48	19.778	5.17
Class 2	20	9.31	0.480	6.33
	15	8.77	1.070	5.40
	10	9.00	2.751	4.02
	5	10.08	7.181	5.02
	0	15.34	16.637	7.13

Table 4.7. Noise Analysis with the MM1 Filter

Image Set	SNR in dB	Correlation Peak	Average Energy	Slope Near the Peak
Class 1	20	19.63	0.458	11.23
	15	19.19	0.681	10.80
	10	18.08	1.277	9.85
	5	15.84	2.564	8.05
	0	12.79	4.711	5.67
Class 2	20	9.60	0.321	4.41
	15	9.28	0.450	4.06
	10	8.68	0.826	3.43
	5	7.80	1.835	2.24
	0	8.45	3.988	3.40

Table 4.8. Noise Analysis with the MM2 Filter

Image Set	SNR in dB	Correlation Peak	Average Energy	Slope Near the Peak
Class 1	20	19.57	0.776	5.57
	15	18.97	0.804	5.43
	10	17.92	0.887	5.09
	5	15.59	1.225	4.39
	0	11.46	1.546	3.27
Class 2	20	9.69	0.475	2.38
	15	9.43	0.495	2.23
	10	8.93	0.568	1.97
	5	8.24	0.791	1.63
	0	7.16	1.298	1.11

Table 4.9. Noise Analysis with the RMVSDF Filter

Image Set	SNR in dB	Correlation Peak	Average Energy	Slope Near the Peak
Class 1	20	19.80	47.840	0.08
	15	19.29	45.210	0.08
	10	17.93	39.326	0.09
	5	15.62	29.621	0.08
	0	12.03	18.404	0.09
Class 2	20	13.74	26.542	0.03
	15	13.58	25.242	0.03
	10	12.92	23.648	0.03
	5	12.03	20.698	0.05
	0	10.44	15.591	0.05

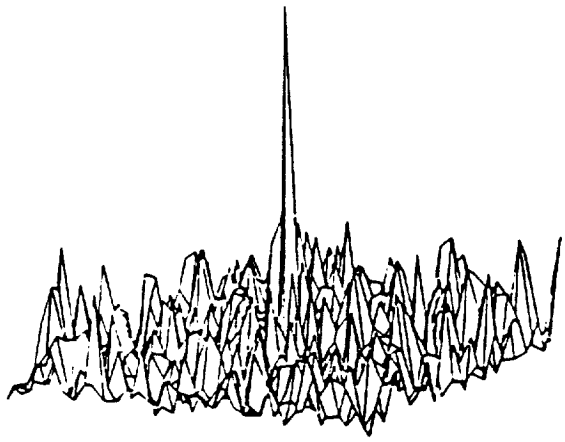

Figure 4.9. Correlation Plane Output Intensity with the RMACE Filter for SNR of 10 dB

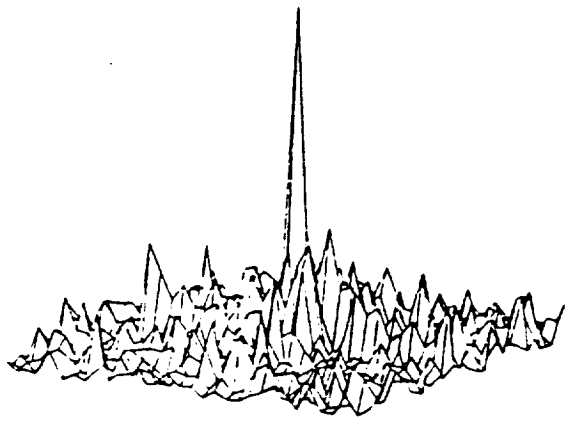

Figure 4.10. Correlation Plane Output Intensity with the MM1 Filter for SNR of 10 dB

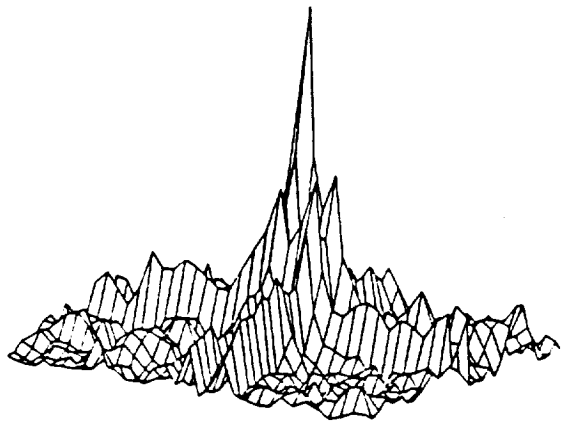

Figure 4.11. Correlation Plane Output Intensity with the MM2 Filter for SNR of 10 dB

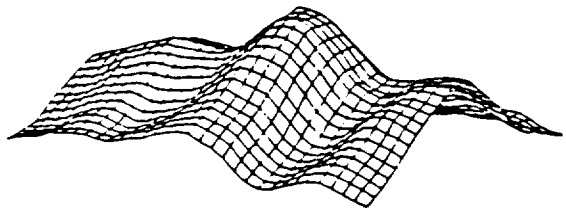

Figure 4.12. Correlation Plane Output Intensity with the RMVSDF Filter for SNR of 10 dB

4.5. Observations

From the results of the above simulation it is noted that the real-valued improved MVSDF-MACE filter has better performance in the presence of zero-mean, white Gaussian noise in comparison with that obtained with the RMACE filter.

CHAPTER 5

Real-Valued Space Domain MACE Filter

In previous chapters real-valued filters were developed in the discrete frequency domain and their performance studied using computer simulations. In this chapter a real-valued space domain MACE filter design is developed and its performance investigated.

5.1. Need for Real-Valued Space Domain MACE Filter

The MACE and RMACE filters are designed in the discrete frequency domain to minimize the average correlation energy of the filter so as to achieve sharp correlation peaks [15]. However, since they are designed in the discrete frequency domain, they minimize circular correlation energy rather than the linear correlation energy. That is, MACE and RMACE filters synthesized in the frequency domain minimizes the aliased version of the linear correlation energy. The commonly used technique, zero-padding, may be expected to remedy this aliasing problem. However, MACE filters designed with zero-padding for the image do not minimize the linear correlation energy because zero padding constraint is not used for the filter impulse response.

Sudharsanan, Mahalanobis, and Sundareshan [16] proposed the MACE filter design in the space domain (SMACE) to overcome this problem. In their design the linear correlation values

are computed in the space domain thereby reducing the linear correlation energy. Because of the powerful capability of optical lenses to generate the two-dimensional Fourier transform of an object, filters are generally implemented using frequency plane correlator. The frequency response of the SMACE filter is a complex function. As mentioned in the previous chapter complex filters are difficult to implement optically with currently available technology. Hence, a design procedure to synthesize a real-valued space domain MACE filter is proposed. Section 5.2 presents the development of the filter and the following sections discuss the results of computer simulations.

5.2. Filter Development

To facilitate easy implementation of MACE filter using currently available spatial light modulators, a real-valued space domain MACE (RSMACE) filter design is developed. For realizing purely real filter functions two types of methods are possible. The first method is to constrain the filter function to be purely real in the frequency domain. This approach is useful if the filter is synthesized in the frequency domain. The second method is to make use of the symmetry property of the two-dimensional fourier transform of an object. That is, the filter is designed in the space domain such that the two-dimensional filter coefficients posses centro conjugate symmetry with respect to the origin of the filter object. The RSMACE filter is designed using the

second method for realizing a filter with purely real frequency response.

In the development of the RSMACE filter the notations similar to those employed in Reference [16] are used. That is, the training set is assumed to contain N images each with d pixels. The i^{th} training image is denoted by a one dimensional vector $\mathbf{x}_i$ of size d×1, obtained by scanning the rows of the two-dimensional image given as:

$$\mathbf{x}_i = [x_i(1), x_i(2), \ldots, x_i(d)]^T.$$

The size of the image is assumed to be M×M and so $d = M^2$. Similarly the filter of the same size is denoted by a d×1 vector $\mathbf{h}$. The linear correlation image of the filter with the signal $\mathbf{x}_i$ will be of size $K = (2M-1)^2$. Let $\mathbf{g}_i$ be the K dimensional correlation vector obtained by correlating the filter $\mathbf{h}$ with the image $\mathbf{x}_i$. This may be expressed in matrix form as

$$g_i = S_i h \qquad (5.1)$$

where $\mathbf{S}_i$ is a real matrix of size K×d obtained from the signal $\mathbf{x}_i$ as

$$\mathcal{S}_i = \begin{bmatrix} 0 & \cdots & 0 & \psi^1_i \\ 0 & \cdots & \psi^1_i & \psi^2_i \\ \vdots & \ddots & \vdots & \vdots \\ \psi^1_i & \psi^2_i & \cdots & \psi^M_i \\ \psi^2_i & \cdots & \psi^M_i & 0 \\ \vdots & \ddots & \vdots & \vdots \\ \psi^M_i & 0 & \cdots & 0 \end{bmatrix}, \qquad i=1,2,\ldots,N, \tag{5.2}$$

with (2M-1)×M real matrices ψ^l_i, l = 1,2,.....,M, given by

$$\psi^l_i = \begin{bmatrix} 0 & \cdots & 0 & x_i(M(l-1)+1) \\ 0 & \cdots & x_i(M(l-1)+1) & x_i(M(l-1)+2) \\ \vdots & \ddots & \vdots & \vdots \\ x_i(M(l-1)+1) & x_i(M(l-1)+2) & \cdots & x_i(M(l-1)+M) \\ x_i(M(l-1)+2) & \cdots & x_i(M(l-1)+M) & 0 \\ \vdots & \ddots & \vdots & \vdots \\ x_i(M(l-1)+M) & 0 & \cdots & 0 \end{bmatrix}, \tag{5.3}$$

$$i=1,2,\ldots,N.$$

In order to synthesize a purely real filter function, the filter is constrained to have centro conjugate symmetry as described below. Let $\bar{h}(n_1,n_2)$ of size M×M be a two-dimensional inverse fourier transform of a real function $\bar{H}(f_1,f_2)$ as

$$\bar{h}(n_1,n_2) = F^{-1}\{\bar{H}(f_1,f_2)\}. \tag{5.4}$$

Since $\bar{H}(f_1,f_2)$ is constrained to be real, $\bar{h}$ will posses centro conjugate symmetry satisfying the following condition:

$$\bar{h}(n_1, n_2) = \overline{h^*}(M+2-n_1, M+2-n_2) . \qquad (5.5)$$

Figure 5.1 shows a two-dimensional image of size 4×4 which possess centro conjugate symmetry. The independent entries are enclosed by the dotted lines.

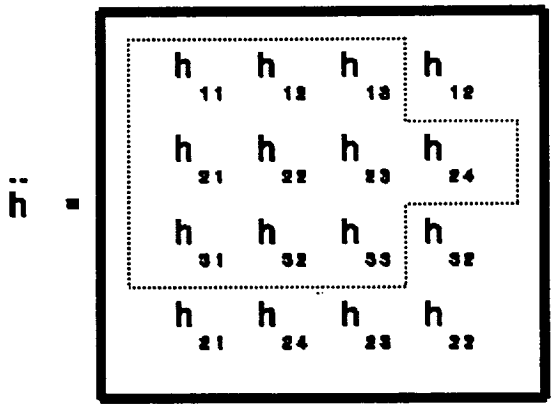

Figure 5.1. Centro Conjugate Symmetric Image

Let a two-dimensional array $\bar{h}_c$ be defined as shown in Figure 5.2.

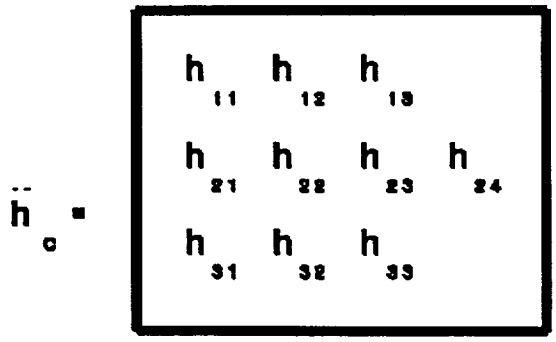

Figure 5.2. Image $\bar{h}_c$

Then from Eq.(5.5) and Figures (5.1) and (5.2) it is clear that the array $\bar{h}$ of size M×M can be constructed from the reduced size object $\bar{h}_c$. Let $\mathbf{h}'$ be a one-dimensional filter vector of size D, where for even values of M, D is given by

$$D = \frac{M^2}{2} + 2. \tag{5.6}$$

Then the independent vector $\mathbf{h}'$ is given by

$$\begin{aligned} \boldsymbol{h}' = [\, & h(1)\, h(2) \ldots\ldots\ldots h(\tfrac{M}{2}+1) \\ & h(M+1)\, h(M+2) \ldots\ldots h(M+M) \\ & \ldots\ldots\ldots \\ & h((\tfrac{M}{2}-1)M+1) \ldots\ldots h((\tfrac{M}{2}-1)M+M) \\ & h(\tfrac{M}{2}M+1)\, h(\tfrac{M}{2}M+2) \ldots\ldots h(\tfrac{M}{2}M+\tfrac{M}{2}+1)\,]^T. \end{aligned} \tag{5.7}$$

Using this symmetry property of $\mathbf{h}$, the correlation vector $\mathbf{g}_i$ in Eq.(5.1) can be written in terms of $\mathbf{h}'$ as

$$\boldsymbol{g}_i = \boldsymbol{S}_i' \boldsymbol{h}' \tag{5.8}$$

where $\mathbf{S}'_i$, i=1,2,....N, is a K×D matrix which may be obtained from Eq.(5.2) as follows. Let $\boldsymbol{\phi}_i$, i=1,2,....,d, be column vectors of $\mathbf{S}_i$ as

$$\boldsymbol{S}_i = [\phi_1\ \phi_2 \cdots \phi_d], \qquad i=1,2,\ldots,N. \tag{5.9}$$

Then $\mathbf{S}'_i$ of size K×D may be written as

$$S_i' = [\gamma_1\ \gamma_2\ \gamma_3\ \cdots\ \gamma_{M/2}\ \gamma_{M/2+1}], \qquad i=1,2,\ldots.N \tag{5.10}$$

where γ_1, is a matrix of size K×(M/2+1) given by

$$\gamma_1 = [\ \phi_1, (\phi_2+\phi_M), (\phi_3+\phi_{M-1}), \ldots, (\phi_{\frac{M}{2}}+\phi_{\frac{M}{2}+2}), \phi_{\frac{M}{2}+1}], \tag{5.11}$$

γ_i, i = 2,3,.....,M/2 are K×M sized matrices given by

$$\begin{aligned}\gamma_i = [&(\phi_{(i-1)M+1}+\phi_{(M+1-i)M+1}), (\phi_{(i-1)M+2}+\phi_{(M+1-i)+M}),\\ &(\phi_{(i-1)M+3}+\phi_{(M+1-i)M+M-1}, \ldots\ldots, (\phi_{(i-1)M+M}+\phi_{(M+1-i)M+2}]\end{aligned} \tag{5.12}$$

and $\gamma_{M/2+1}$ is a K×(M/2+1) size matrix given by

$$\begin{aligned}\gamma_{\frac{M}{2}+1} = [&\phi_{(\frac{M}{2})M+1}, (\phi_{(\frac{M}{2})M+2}+\phi_{(\frac{M}{2}+1)M}), (\phi_{(\frac{M}{2})M+3}+\phi_{(\frac{M}{2}+1)M-1}),\\ &\ldots. (\phi_{(\frac{M}{2})M+\frac{M}{2}}+\phi_{(\frac{M}{2})M+\frac{M}{2}+2}), \phi_{(\frac{M}{2})M+\frac{M}{2}+1}].\end{aligned} \tag{5.13}$$

The objective of the design is to find a space domain filter $\mathbf{h}'$ that minimizes the average correlation energy of the correlation plane. The correlation plane energy of the i^{th} image is given by

$$\begin{aligned}E_i &= \sum_{n=1}^{K} |\, g_i(n)\,|^2\\ &= h'^T S_i'^T S_i' h'.\end{aligned} \tag{5.14}$$

Hence, the average correlation energy over all training images $\mathbf{x}_i$, i=1,2,...,N, is given by

$$E_{av} = \frac{1}{N}\sum_{i=1}^{N} \boldsymbol{h}'^{T}\boldsymbol{S}_i'^{T}\boldsymbol{S}_i'\boldsymbol{h}' = \boldsymbol{h}'^{T}\boldsymbol{R}'\boldsymbol{h}' \tag{5.15}$$

where $\mathbf{R}'$ is a D×D symmetric matrix given by

$$\boldsymbol{R}' = \frac{1}{N}\sum_{i=1}^{N} \boldsymbol{S}_i'^{T}\boldsymbol{S}_i'. \tag{5.16}$$

The output constraint for the filter $\mathbf{h}$ is

$$\begin{aligned} \boldsymbol{x}_i^{T}\boldsymbol{h} &= u_i, \qquad i=1,2,\ldots,N \\ \boldsymbol{X}_s^{T}\boldsymbol{h} &= \boldsymbol{u} \end{aligned} \tag{5.17}$$

where $\mathbf{X}_s$ is a d×N data matrix in space domain and $\mathbf{u}$ is an N dimensional output vector. Let

$$\boldsymbol{X}_s^{T} = [\eta_1\ \eta_2\ \cdots\ \eta_d] \tag{5.18}$$

where η_i, i=1,2,...,d, are column vectors of size N. Also, let $\mathbf{\Pi}$ be a D×N data matrix defined as

$$\Pi^{T} = [\delta_1\ \delta_2\ \delta_3\ \cdots\ \delta_{M/2}\ \delta_{M/2+1}]. \tag{5.19}$$

where δ_1, is a matrix of size N×(M/2+1) given by

$$\delta_1 = [\ \eta_1, (\eta_2+\eta_M), (\eta_3+\eta_{M-1}), \ldots, (\eta_{\frac{M}{2}}+\eta_{\frac{M}{2}+2}), \eta_{\frac{M}{2}+1}], \tag{5.20}$$

δ_i, i = 2,3,.....,M/2 are N×M sized matrices given by

$$\delta_i = [(\eta_{(i-1)M+1}+\eta_{(M+1-i)M+1}), (\eta_{(i-1)M+2}+\eta_{(M+1-i)+M}), (\eta_{(i-1)M+3}+\eta_{(M+1-i)M+M-1}, \ldots\ldots, (\eta_{(i-1)M+M}+\eta_{(M+1-i)M+2}] \quad (5.21)$$

and $\delta_{M/2+1}$ is a N×(M/2+1) size matrix given by

$$\delta_{\frac{M}{2}+1} = [\eta_{(\frac{M}{2})M+1}, (\eta_{(\frac{M}{2})M+2}+\eta_{(\frac{M}{2}+1)M}), (\eta_{(\frac{M}{2})M+3}+\eta_{(\frac{M}{2}+1)M-1}), \ldots. (\eta_{(\frac{M}{2})M+\frac{M}{2}}+\eta_{(\frac{M}{2})M+\frac{M}{2}+2}), \eta_{(\frac{M}{2})M+\frac{M}{2}+1}]. \quad (5.22)$$

Then Eq.(5.17) can be written in terms of Π as

$$\Pi^T h' = u. \quad (5.23)$$

The real MACE filter **h′** which minimizes the average correlation energy E_{av} in Eq.(5.15) while satisfying the output constraints in Eq.(5.23) may be found using the method of Lagrangian multipliers. The solution vector **h′** is

$$h' = R'^{-1}\Pi(\Pi^T R'^{-1}\Pi)^{-1}u. \quad (5.24)$$

The SMACE filter solution vector from Reference [16] is given by

$$h_{SMACE} = R^{-1}X_s(X_s^T R^{-1}X_s)^{-1}u. \quad (5.25)$$

It may be noted from Eq.(5.25) that the size of the **R** matrix is d×d = $M^2 \times M^2$. On the other hand from Eq.(5.24), the size of the matrix **R′** is D×D = $(M^2/2+2)\times(M^2/2+2) \approx M^2/2 \times M^2/2$. The complexity of a matrix inversion is generally proportional to

the square of the size of the matrix. Hence, the complexity involved in the inversion of the matrix $\mathbf{R}'$ is much lower compared to that of $\mathbf{R}$. For example, when the images of size 16×16 are used the size of the $\mathbf{R}$ matrix is 256×256, whereas the $\mathbf{R}'$ matrix is only 130×130. Further, the number of RSMACE filter coefficients to be determined is $(M^2/2+2)$ whereas for SMACE filter it is M^2. Thus, like the RMACE filter, the realization of RSMACE filters in Eq.(5.24) will result in a substantial reduction in the complexity involved in the filter synthesis, thereby requiring less memory and cpu time.

5.3. Algorithm for the RSMACE Filter Synthesis

An algorithm for the RSMACE filter synthesis is summarized below.

1. From the given training vector images $\mathbf{x}_i$, i=1,2,...N, setup the matrix $\mathbf{S}_i$ from Eqs.(5.2) and (5.3).
2. Compute the matrix $\mathbf{S}_i'$ from Eqs.(5.9)-(5.13).
3. Obtain the matrix $\mathbf{R}'$ such that

$$R' = \frac{1}{N}\sum_{i=1}^{N} S'^{T}_{i} S'_{i}.$$

4. From the training images form the data matrix $\mathbf{X}_s$ as

$$\mathbf{X}_s = [\mathbf{x}_1, \mathbf{x}_2, \ldots\ldots, \mathbf{x}_N].$$

5. Obtain the reduced data matrix Π from Eqs.(5.18)-(5-22).

6. Using the specified correlation output vector $\mathbf{u}$, the inverse of the matrix $\mathbf{R}'$ and the matrix $\mathbf{\Pi}$, construct the RSMACE filter as

$$\boldsymbol{h}' = \boldsymbol{R}'^{-1}\mathbf{\Pi}(\mathbf{\Pi}^{T}\boldsymbol{R}'^{-1}\mathbf{\Pi})^{-1}\boldsymbol{u}.$$

5.4. Simulation Results

The new real-valued space domain MACE (RSMACE) filter was synthesized to discriminate between two images of the landscape of Mars, referred to as Class 1 and Class 2 images. Nine images of each class, rotated through one to nine degrees, totaling 18 images, were used to test the filter performance. Each image contained 16×16 pixels. The RSMACE filter was synthesized with five images of each class rotated through angles 1, 3, 5, 7, and 9. The correlation outputs at the origin were specified to be 20 and 10 for Class 1 and Class 2 images, respectively.

For this particular example, the number of SMACE filter coefficients were 256 and the cpu time required to synthesize the filter in VAX was 10 minutes. On the other hand for the RSMACE filter the number of filter coefficients were reduced to 130 and the cpu time was only 40 seconds. The performance of the RSMACE filter is demonstrated by the three-dimensional plot of the correlation plane output as shown in Figure 5.3. Even though the correlation plane contains side lobes, the peak at the origin is sharp enough for easy detection. For comparison, the SMACE filter in Eq.(5.21) was also synthesized

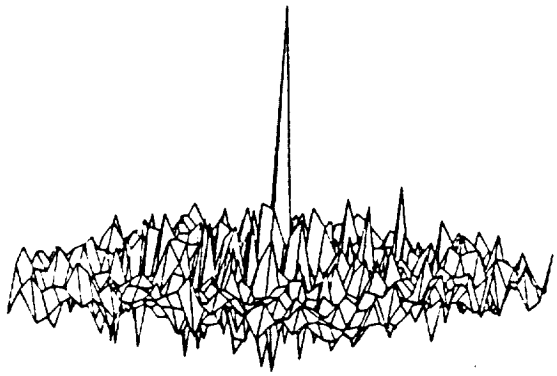

Figure 5.3. Correlation Plane Output Intensity with the RSMACE Filter

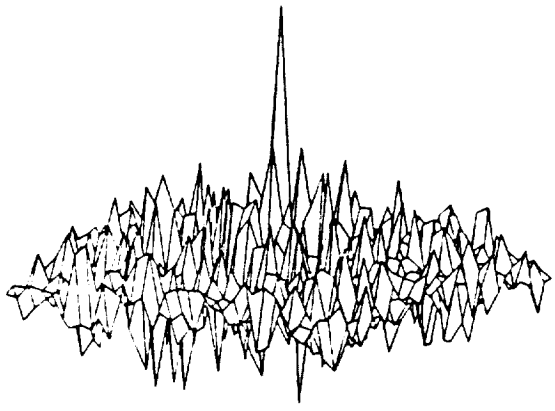

Figure 5.4. Correlation Plane Output Intensity with the SMACE Filter

using the same training images. The corresponding three-dimensional correlation plane output is shown in Figure 5.4. Comparing Figures 5.3 and 5.4, it can be seen that the sharpness of the correlation peak with the RSMACE filter is slightly less than that of the SMACE filter but is quite satisfactory for recognition purposes. The RSMACE filter produces more sidelobes in the correlation plane output compared to that obtained with the SMACE filter. However, there is a significant amount (93 percent) of saving in computation time required for the filter synthesis.

All the 18 images were then tested using both The RSMACE and SMACE filters for discrimination. Tables 5.1 and 5.2 show the simulation results for training images with RSMACE and SMACE filters respectively. As can be seen from the tables, for all ten training images the specified correlation peaks were achieved. For further comparison, the output correlation plane energies for all 18 images with both RSMACE filter, denoted by '+' and SMACE filter denoted by '×' is shown in Figure 5.5. From the figure it may be noted that the RSMACE filter results slightly higher energy in the correlation plane.

A fixed threshold T = 12 was chosen to classify images between classes 1 and 2. That is, if the correlation peak anywhere in the output correlation plane exceeds this threshold, the test object is classified as object that belongs to Class 1 otherwise Class 2. Plots of the highest

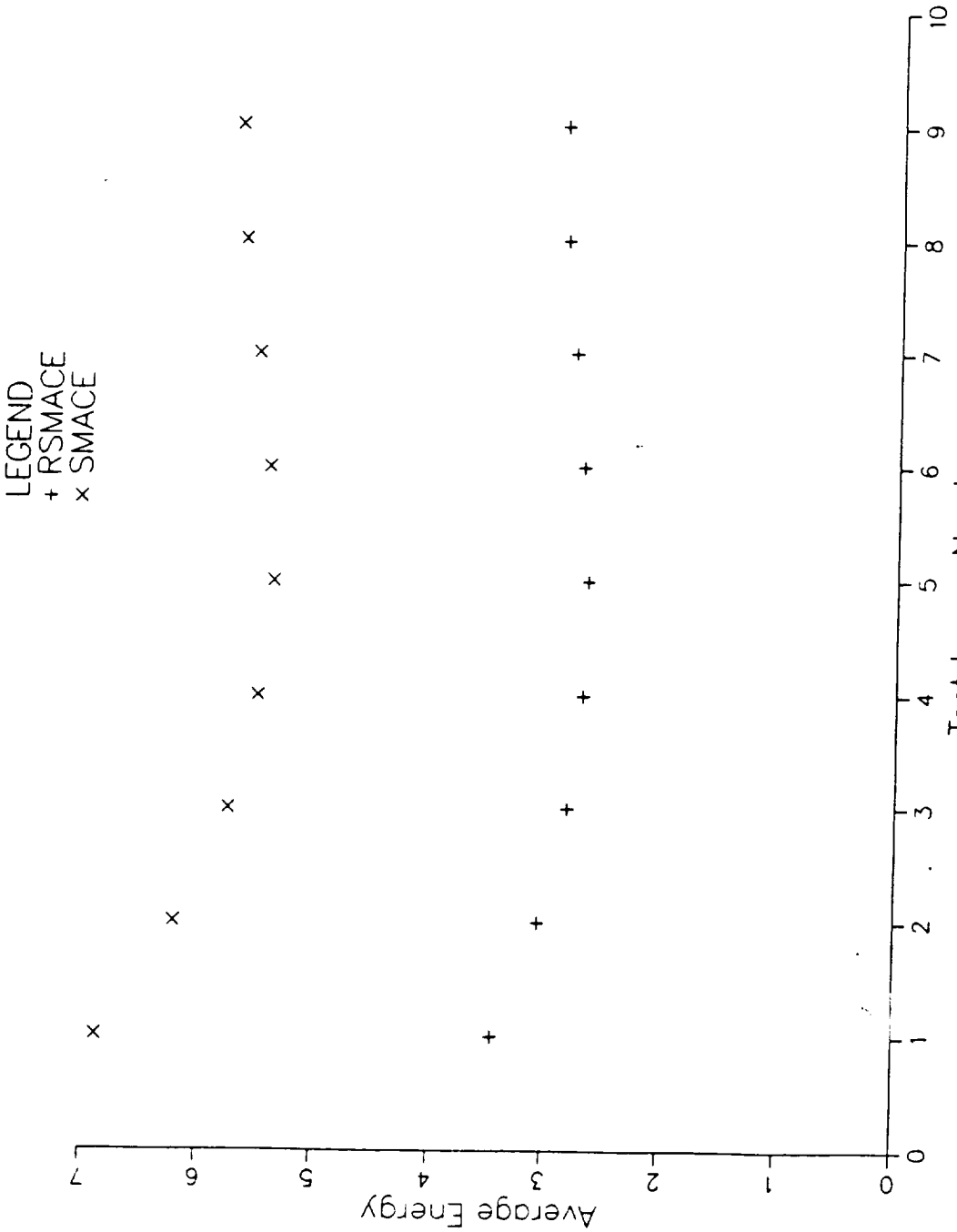

Figure 5.5. Correlation Plane Energies for Class 1 Images

Table 5.1. Correlation Plane Values with the RSMACE Filter

Image	Specified Output at the Origin	Intensity at the Origin	Largest Peak	Peak Location	Average Energy
mars1.1	20.00	20.00	20.00	(0,0)	6.88
mars1.3	20.00	20.00	20.00	(0,0)	5.76
mars1.5	20.00	20.00	20.00	(0,0)	5.39
mars1.7	20.00	20.00	20.00	(0,0)	5.55
mars1.9	20.00	20.00	20.00	(0,0)	5.74
mars2.1	10.00	10.00	10.00	(0,0)	3.68
mars2.3	10.00	10.00	10.00	(0,0)	2.98
mars2.5	10.00	10.00	10.00	(0,0)	2.77
mars2.7	10.00	10.00	10.00	(0,0)	2.90
mars2.9	10.00	10.00	10.00	(0,0)	2.98

Table 5.2. Correlation Plane Values with the SMACE Filter

Image	Specified Output at the Origin	Intensity at the Origin	Largest Peak	Peak Location	Average Energy
mars1.1	20.00	20.00	20.00	(0,0)	3.46
mars1.3	20.00	20.00	20.00	(0,0)	2.81
mars1.5	20.00	20.00	20.00	(0,0)	2.66
mars1.7	20.00	20.00	20.00	(0,0)	2.79
mars1.9	20.00	20.00	20.00	(0,0)	2.90
mars2.1	10.00	10.00	10.00	(0,0)	2.00
mars2.3	10.00	10.00	10.00	(0,0)	1.59
mars2.5	10.00	10.00	10.00	(0,0)	1.47
mars2.7	10.00	10.00	10.00	(0,0)	1.55
mars2.9	10.00	10.00	10.00	(0,0)	1.61

peak in the correlation plane versus the test image number are shown in Figures 5.6 and 5.7 for RSMACE and SMACE filters respectively. As can be seen from the figures, both RSMACE and SMACE filters achieved 100 percent recognition rates.

5.5. Observations

From the results of the tests it can be concluded that the performance of the RSMACE filter is almost as good as that of the SMACE filter. The frequency response of the RSMACE filter is purely real and, hence, currently available spatial light modulators can be used to optically implement the filter without the use of complicated holograms. Further the computation involved in the synthesis of the RSMACE filter is lower than 50 percent of that of the SMACE filter.

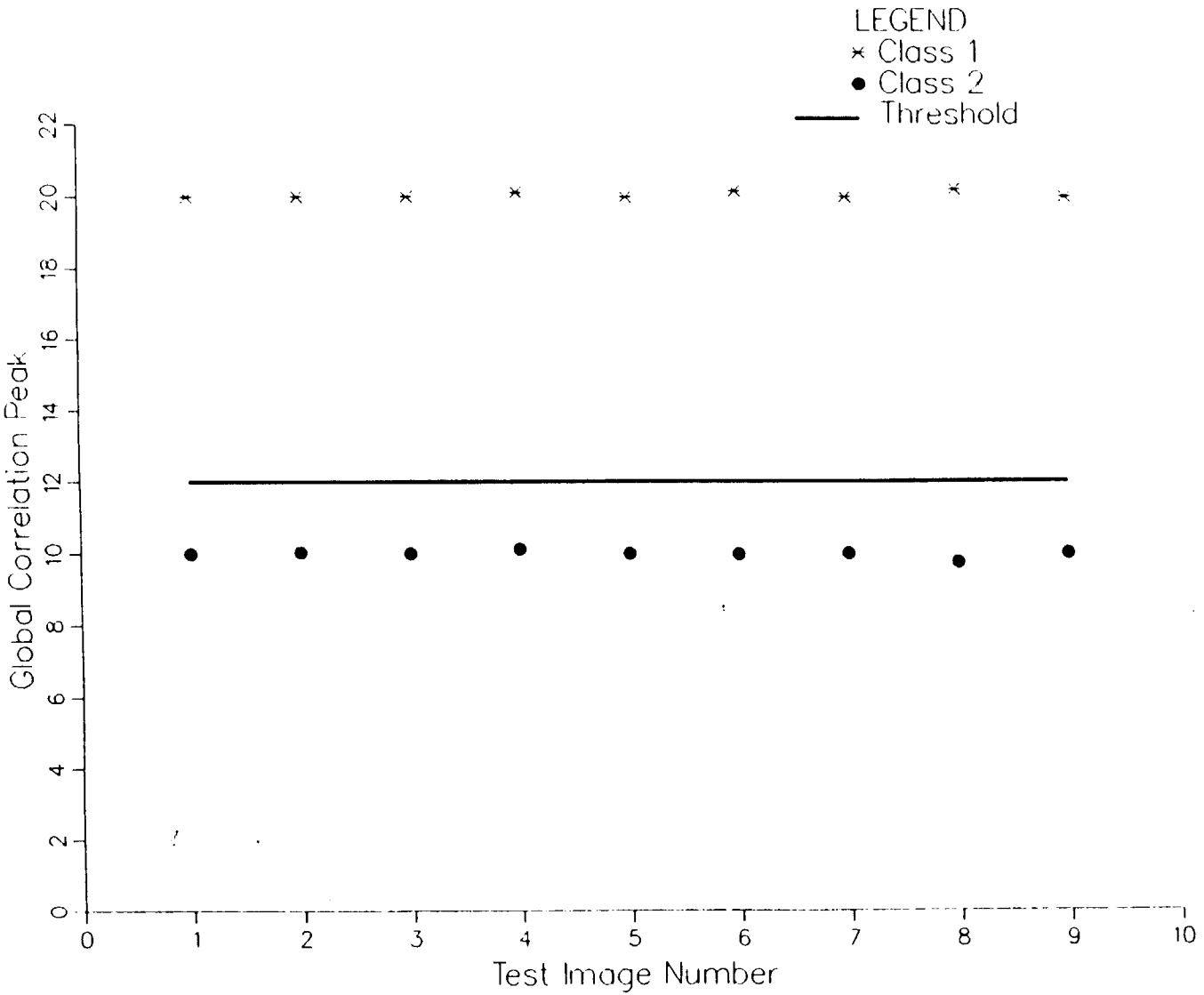

Figure 5.6. Response (at the origin) of the RSMACE Filter Constructed with Image Numbers 1, 3, 5, 7, & 9

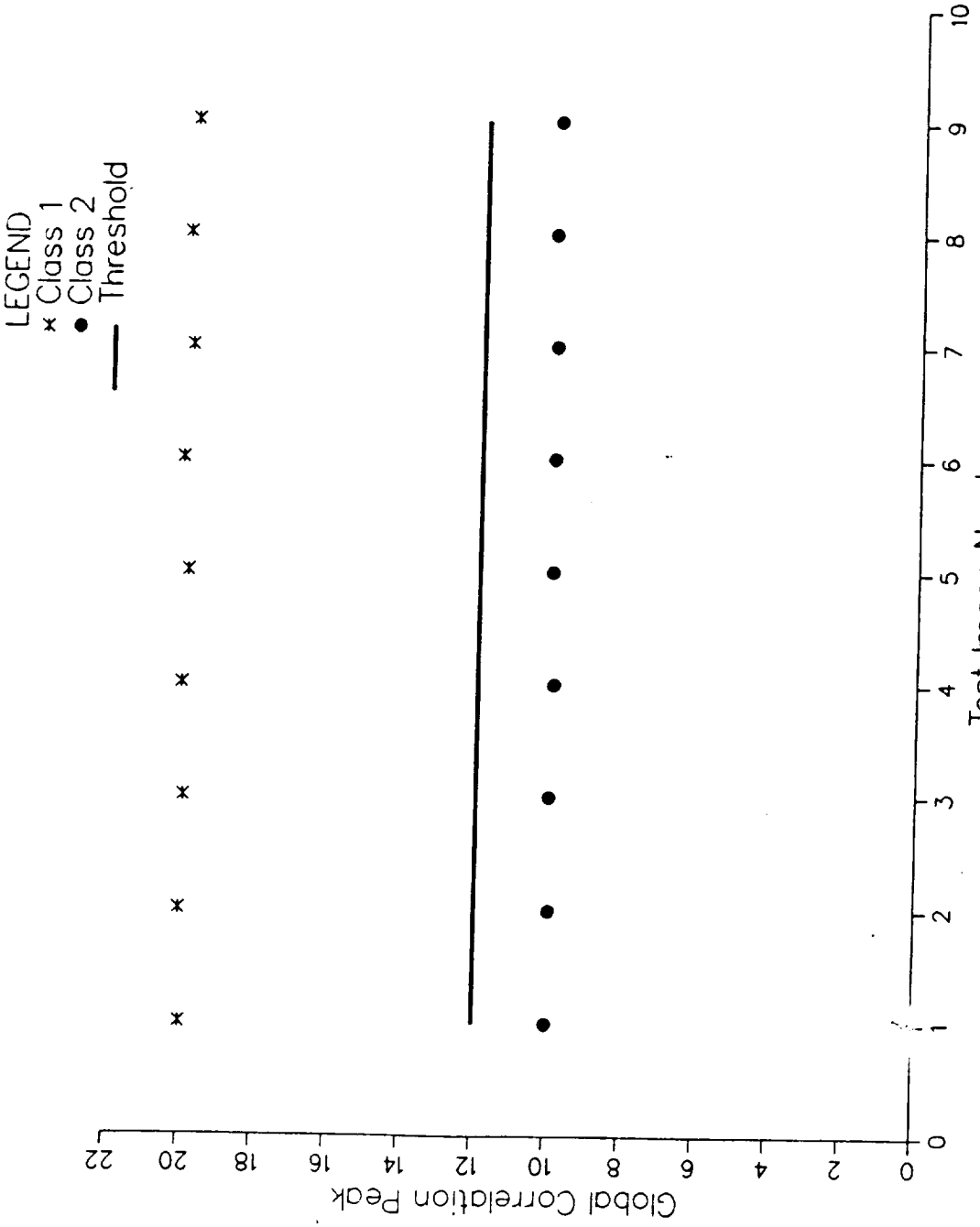

Figure 5.7. Response (at the origin) of the SMACE Filter Constructed with Image Numbers 1, 3, 5, 7, & 9

CHAPTER 6

Conclusions and Recommendations

The research leading to this report was concerned with the recognition of objects/patterns using optical correlators. The main objective was to develop real-valued filters for pattern recognition which could be implemented using currently available spatial light modulators.

6.1. Conclusions of this Research

A real-valued minimum average correlation energy (MACE) filter was developed. The performance of this filter was studied and compared with that of the MACE filter using computer simulations. It was found that the distortion tolerance of the real-valued MACE filter could be improved by choosing more number of training images in the filter synthesis. In comparison with the MACE filter, the real-valued MACE filter produces slightly smaller correlation peaks, however, the sharpness of the peak was good enough to facilitate easy detection.

In order to make the real-valued MACE filter robust against the intensity scaling, normalization by the average value of the test object was done. The performance of the normalized filter was found to be independent of the scaling factor. The performance of this filter was also studied when the test image is corrupted with white Gaussian noise. The

filter was found to tolerate significant amount of noise (SNR = 10 dB).

The real-valued MACE filter was tested on the effect of input bias. For the input bias correction, an additional constraint was needed to be imposed, namely, the filter coefficient at the origin should be zero. It was found that the input bias did not affect the output in the correlation plane of the real-valued MACE filter even with no input bias correction. The real-valued MACE filter for complex specified output values was developed. A procedure was formulated to choose optimally the phase of the output values such that the least correlation energy is obtained.

A design procedure for the real-valued improved minimum variance synthetic discriminant function (MVSDF)-MACE filter which minimizes both correlation plane energy and the output variance due to input noise was proposed. The simulation studies to compare this filter with the real-valued MVSDF and MACE filters were carried out. These studies exhibited that the real-valued MVSDF-MACE filter provides both tolerance to distortion and noise and sharp correlation peaks.

In order to minimize the linear correlation energy when the filter is implemented in continues frequency domain, the design of a real-valued space domain MACE (SMACE) filter was considered and its performance was compared with that of the SMACE filter. Though the correlation plane energy was slightly higher than that of the SMACE filter, it did not

produce high sidelobes. In addition it was shown that the synthesis of real SMACE filter was less computationally intensive than that of the complex SMACE filter with respect to the computation efficiency. Further, its real nature makes it easily implementable using available spatial light modulators.

6.2. Recommendations for Future Research

As mentioned above, real-valued filters are easily implementable using currently available spatial light modulators. In addition they give significant savings in the computation time and the computer memory as compared to that of complex filters. There are, however, certain limitations and possible extensions to this research. Some of them are described below.

Not all spatial light modulators are capable of providing real response. Many, such as deformable mirror devices, provide coupled magnitude-phase responses. Hence, the design of MACE filters to match the physical characteristics of the available spatial light modulators needs to be developed. When the specified output was complex, the real-valued MACE filter was shown to reduce the correlation plane energy further. But the reduction in the energy depends on the training images used in the filter construction. Hence, a systematic procedure for the selection of training images needs to be explored.

In a multi-class pattern recognition problem, the predetermined threshold values are used for pattern classification. However, the threshold values depend on the magnitude of the user specified output values. Thus, future work needs to be done for the selection of the output magnitudes by maximizing some criteria like signal-to-noise ratio.

Combining the concepts of minimum variance and minimum correlation energy, filters were designed to have acceptable tolerance to noise and distortions while providing sharp correlation peaks at the origin of the correlation plane. However, the performance of these filters critically depends on the constants, α_1 and α_2. More work needs to be done for the selection of these constants.

Recently much work has been carried out to design optical correlators to estimate the orientation of an object. Since MACE filters guarantee correlation peaks at the origin of the correlation plane, the ability of these filters for the positional parameter estimation needs to be evaluated.

REFERENCES

1. Francis, T. S. Yu, "Hybrid Optical Computing," Potentials IEEE, December 1987, pp. 34-37.

2. Casasent, D., "Pattern Recognition: A Review," IEEE Spectrum, March 1981, pp. 28-33.

3. Casasent, D., "Optical Signal Processing," Electro-Optical System Design, Vol. 12, No. 11, June 1981, pp. 39-47.

4. Horner, J. L., ed. Optical Signal Processing, London: Academic Press, Inc., 1987.

5. Casasent, D., "Hybrid Optical/Digital Image Pattern Recognition: A Review," Proc. of SPIE, Vol. 528, January 1985, pp. 64-82.

6. VanderLugt, A., "Signal Detection by Complex Matched Spatial Filtering," IEEE Trans. Inf. Theory, IT-10, 1964, pp. 139-145.

7. Horner, J. L., "Light Utilization in Optical Correlators," Applied Optics, Vol. 23, No. 16, March 1984.

8. Horner, J. L. and Gianino, P. D., "Phase-Only Matched Filtering," Applied Optics, Vol. 23, No. 16, March 1984.

9. Caulfield, H. J. and Maloney, W. T., "Improved Discrimination in Optical Character Recognition," Applied Optics, Vol. 8, 1969, pp. 2354-2356.

10. Hester, C. G. and Casasent, D., "Multivariant Technique for Multi-class Pattern Recognition," Applied Optics, Vol. 19, 1980, pp. 1758-1761.

11. Casasent, D., "Unified Synthetic Discriminant Function Computation Formulation," Applied Optics. Vol. 23, 1984, 1620-1627.

12. Gu, Z. and Lee, S. H., "Classification of Multi-class Stochastic Images Buried in Noise," J. Opt. Soc. Am. A., Vol. 3, 1986, pp. 1433-1442.

13. Hsu, Y. N. and Aresenault, H. H., "Optical Character Recognition using Circular Harmonic Expansion," Applied Optics, Vol. 21, 1982, pp. 4016-4019.

14. Vijaya Kumar, B.V.K., "Minimum Variance synthetic Discriminant Functions," J. Opt. Soc. Am. A., Vol. 3, 1986, pp. 1579-1584.

15. Mahalanobis, A., Vijaya Kumar, B.V.K., and Casasent, D., "Minimum Average Correlation Energy Filters," Applied Optics, Vol. 26, 1987, pp. 6633-6640.

16. Sudharsanan, S. I., Mahalanobis, A., and Sundareshan, M. K., "Unified Framework for the Synthesis of SDF with Reduced Noise Variance and Sharp Correlation Structure," Optical Engineering, Vol. 29, 1990, pp. 1021-1028.

17. Juday, R. D., Vijaya Kumar, B.V.K., and Rajan, P. K., "Optical Real Correlation Filters," Applied Optics, Vol. 30, 1991, pp. 520-522.

18. Mahalanobis, A. and Song, S., "Purely Real Filters," Proc. of SPIE, 1991.

19. Casasent, D., "Optical Feature Extraction," Optical Signal Processing, Horner, J. ed., New York: Academic Press, 1987.

20. Pepper, D. M., Au Yung, J., Feketę, D., and Yariv, A., "Spatial Convolution and Correlation of Optical Fields via Degenerate Four Wave Mixing," Optics Letters, Vol. 3, 1978, pp. 7-9.

21. Casasent, D., "Coherent Optical Pattern Recognition: A Review," Optical Engineering, Vol. 24, January 1985, pp. 26-32.

22. Vijaya Kumar, B.V.K. and Carroll, C., "Loss of Optimality in Cross Correlators," J. Opt. Soc. Am. A., Vol. 1, No. 4, 1984, pp. 392-397.

23. Casasent, D. and Psaltis, D., "New Optical Transforms for Pattern Recognition," Proc. IEEE, Vol. 65, 1977, pp. 77-84.

24. Casasent, D. and Krauss, D., "Polar Camera for Space-Variant Pattern Recognition," Applied Optics, Vol. 17, 1978, pp. 1559-1561.

25. Cheung, K. F., Atlas, J. A., Green, C. A., and Mareks II, R. J., "Conventional and Composite Matched Filters with Error Correction: A Comparison," Applied Optics, Vol. 26, 1987, pp. 4235-4239.

26. Caulfield, H. J., "Linear Combinations of Filters for Character Recognition: A Unified Treatment," Applied Optics, Vol. 19, No. 23, 1980, pp. 3877-3878.

27. Caulfield, H. J. and Weinberg, M. H., "Computer Recognition of 2-D Patterns Using Generalized Matched Filter," Applied Optics, Vol. 21, 1982, pp. 1699-1704.

28. Vijaya Kumar, B.V.K., "Efficient Approach for Designing Linear Combination Filters," Applied Optics, Vol. 22, 1983, pp. 1445-1448.

29. Caulfield, H. J., Haimes, R., and Horner, J., "Composite Matched Filter," Israel J. Tech, Vol. 18, 1980, pp. 263-267.

30. Riggins, J. and Butler, S., "Simulation of synthetic Discriminant Function Optical Implementations," Optical Engineering, Vol. 23, 1984, pp. 721-726.

31. Vijaya Kumar, B.V.K., Casasent, D., and Mahalanobis, A., "Correlation Filters for Target Detection in a Markvo Model Background Clutter," Applied Optics, Vol. 28, 1989, pp. 3112-3119.

32. Vijaya Kumar, B.V.K., Bahri, Z., and Mahalanobis, A., "Constraint Phase Optimization in Minimum Synthetic Discriminant Functions," Applied Optics, Vol. 27, 1988, pp. 409-413.

33. Mahalanobis, A. and Casasent, D., "Performance Evaluation of MACE Filters," Applied Optics, Vol. 30, No. 5, February 1991, pp. 561-572.

34. Casasent, D. and Ravichandran, G., "Modified MACE Filters for Distortion Invariant Recognition of Mobile Targets," Proc. of SPIE, Vol. 1156, 1989, pp. 177-187.

35. Casasent, D. and Chang, W. T., "Correlation Synthetic Discriminant Functions," Applied Optics, Vol. 25, 1986, pp. 2343-2350.

36. Bahri, Z. and Vijaya Kumar, B.V.K., "Generalized Synthetic Discriminant Functions," J. Opt. Soc. Am. A., Vol. 5, 1988, pp. 562-571.

37. Sudharsanan, S. I., Mahalanobis, A., and Sundareshan, M.K., "Selection of Optimum Output Correlation Values in Synthetic Discriminant Function Design," J. Opt. Soc. Am. A., Vol. 7, 1990, pp. 611-616.

38. Braunecker, B., Hauck, R. W., and Lohmann, A. W., "Optical Character Recognition Based on Non-Redundant Correlation Measurements," Applied Optics, Vol. 18, 1979, pp. 2746-2753.

39. Mui, J. K. and Fu, K. S., "Automated Classification of Nucleated Blood Cells Using a Binary Tree Classifier," IEEE Trans. on Patt. and Mach. Intell., Vol. 2, 1980, pp. 429-443.

40. Jared, D. A. and Ennis, D. J., "Learned Pattern Recognition Using SDF," Proc. of SPIE, Vol. 7, 1986.

41. Casasent, D., and Mahalanobis, A., "Rule-based Symbolic Processor for Object Recognition," Applied Optics, Vol. 26, 1987, pp. 4795-4797.

42. Gheen, G., "Maximum Mean Square Projection Filters," Proc. of SPIE, Vol. 1151, 1989, pp. 278-283.

43. Vijaya Kumar, B.V.K., "Tutorial Survey of Composite Filters for Optical Correlators," submitted to Applied Optics, December 1990.

44. Lohmann, A. W. and Paris, D. P., "Binary Fraunhofer Holograms, Generated by computer," Applied Optics, Vol. 6, No. 10, 1967, pp. 1739-1748.

45. Lee, W. H., "Binary Synthetic Holograms," Applied Optics, Vol. 13, No. 7, 1974, pp. 1677-1682.

46. Vijaya Kumar, B.V.K. and Hassebrook, L., "Performance Measures for Correlation Filters," Applied Optics, Vol. 29, No. 20, 1990, pp. 2997-3006.

47. Vijaya Kumar, B.V.K. and Mahalanobis, A., "Alternate Interpretation for Minimum Variance Synthetic Discrimination Functions," Applied Optics, Vol. 25, No. 15, 1986, pp. 2484-2485.